Politecnico di Torino

Master Degree in Automotive Engineering

Master Degree Thesis

EXPERIMENTAL AND NUMERICAL ANALYSIS OF RINGING AND DETONATION ON A SI NG ENGINE: CYCLE-TO-CYCLE VARIABILITY AND KNOCK PREDICTION

Supervisors:

Prof. Daniela Anna Misul

Prof. Mirko Baratta

Candidate:

Argese Marco

Academic Year 2017/2018

Index

Introduction

In the last decades, the problem of environmental pollution has become increasingly relevant. In the automotive field, more and more stringent international regulations are forcing carmakers to seek for practical answers with the primary goal of fuel consumption and noxious emissions reduction.

Some improvements have been obtained decreasing aerodynamic and rolling resistance, with innovations already on the market and still under study. The weight of cars has raised, due to additional functions implemented, increase of the average size and safety requirements, even if partly counterbalanced by the employment of lightweight materials.

From the propulsion point of view, this has pushed research interest towards innovative technical solutions, such as downsizing and turbocharging or the development of engines powered by alternative fuels. These targets can be reached improving the efficiency of the combustion process, but this requires an accurate study and knowledge of the evolution of the charge inside the combustion chamber.

The purpose of this work is the improvement of an existing combustion model, based on a fractal approach, able to predict combustion development inside the combustion chamber, always considering engine geometry and operating variables. This model has been implemented in a 0D-1D simulation software (GT-Power, developed by Gamma Technologies) in order to predict the behaviour of the actual engine. The predictive approach is useful in order to reduce time and cost of engine bench testing by means of computational simulation. Of course, this requires a great effort in terms of calibration of the model, starting from the analysis of experimental data.

This work of thesis is part of a project, named GasOn, promoted by CRF and AVL, consisting in the application the mentioned combustion model to a supercharged SI NG high performance mono-fuel engine and in the evaluation of its performances.

Great attention has been put in the prediction of knock onset; it is a phenomenon of abnormal combustion caused by the self-ignition of part of the mixture ahead of the flame front, causing a sharp increase of the in-chamber pressure and leading to serious mechanical failure if not kept under control. Knock is strictly related to cycle-to-cycle variability, in fact, even at constant operating points, local thermodynamic conditions inside the combustion chamber undergo cyclical variations and can promote knocking phenomenon appearance.

The work can be subdivided in two main parts:

- Analysis of experimental data;
- Simulation in GT-Power environment.

In the first part, a set of cycles are analysed using MatLab software in order to evaluate detonating cycles occurrence; obtained results are then compared with the actual values provided. Special care has been put in the distinction between ringing and knocking cycles.

In the second part, by means of GT-Power software, experimental conditions are reproduced simulating engine operation implementing the fractal combustion model, aiming to develop a predictive tool able to highlight knock occurrence once the cyclical dispersion model has been introduced.

1 Initial Concepts

Some topics necessary for better understanding and motivating the work done are now analysed and discussed.

1.1 From bi-fuel to mono-fuel engines

Nowadays on the market are present some examples of propulsion systems powered by natural gas, but these solutions are actually derivations of conventional spark ignition gasoline engines. They include all the features of the traditional SI engines, same architecture and combustion chamber design, with the addition of the subsystems necessary for NG running: a dedicates fuel tank for NG storage, additional pipes and injectors and a fuel switch able to shift between the two fuel supplies. Starting-up of the engine is always performed with gasoline, and after a while, the fuel supply can be switched to NG. This configuration shows some important limitations, in fact, when run by NG, the reachable efficiency is bounded by the relatively low compression ratio imposed by the gasoline employment, that shows a higher knock tendency respect to NG (RON around 130).

The possibility to switch to a pure mono-fuel NG engine allows to overcome the limits forced by gasoline, thus enabling to exploit the natural gas energy more efficiently with the design of small high-powered engines with increased compression ratio. Moreover, the presence of just one supply system promotes weight reduction. Higher peak firing pressure reached by an optimization of NG combustion process cannot be withstood by conventional gasoline engines, thus requiring a careful innovative design.

Obviously, this research represents only a preliminary step towards the new technology commercialisation, aiming for a higher diffusion of infrastructures and transportation systems able to support the spreading of NG powered cars, keeping in mind the lower vehicle range respect to conventional vehicles; natural gas in fact is stored in gaseous form, therefore its volumetric heating value is much lower than the gasoline and diesel oil ones. By the way, NG is the most promising alternative fuel, thanks to the abundance of its availability and low price, being ready to use and not requiring additional

processing. Furthermore, besides the increased combustion efficiency, thanks to its lower carbon content, it produces low carbon dioxide and no particulate emissions, thus promoting NG research interest.

1.2 Knock and autoignition model

Knock is the name given to the metallic noise transmitted by the engine structure in presence of an abnormal combustion phenomenon interesting part of the mixture inside the combustion chamber. When this portion of mixture meets a condition of high pressure and temperature, it can autoignite ahead of the flame front producing a sudden energy release that generates a high-pressure peak and strong pressure waves.

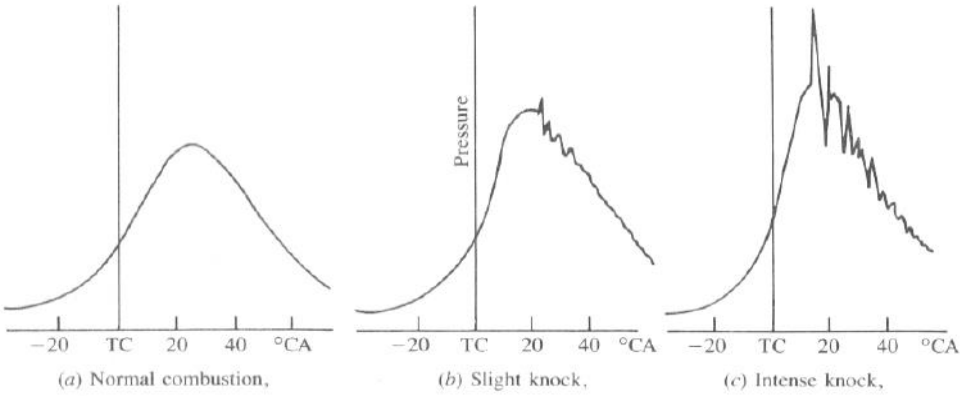

Figure 1.1 Knock effect on pressure cycle

Knock can have different severity: with slight knock, pressure waves fluctuation occurs late in the combustion process, while, with heavy knock, fluctuations of high amplitude develop around top dead centre; this is the most dangerous form of knocking, with severe consequences leading to mechanical fatigue failure.

Knocking is mainly promoted by the increase of compression ratio, the advance of the spark timing and is directly influenced by the fuel chemical composition.

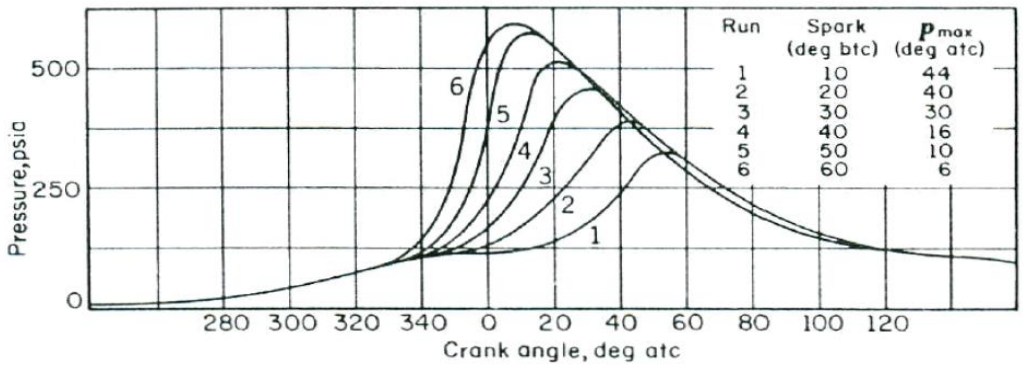

Figure 1.2 Spark advance effect on pressure cycle

It can be detected either by the analysis of the pressure cycles or experimentally by knock sensors mounted on the engine, accelerometers capable of capturing vibrations deriving from a detonation event; the engine Electronic Control Unit can optimize the spark advance in order to obtain the best cycle efficiency while avoiding knock.

Fuel tendency to knock is characterized by tests performed with a rapid compression machine; a mixture of air and fuel vapour is prepared and introduced in the cylinder, then the piston rapidly compresses the gas to a predetermined volume. At the start of combustion, the first reacting nucleus rapidly burns and propagates until all the charge is consumed. Charge evolution can be studied also changing the compression ratio. Pressure and temperature traces are collected and stored.

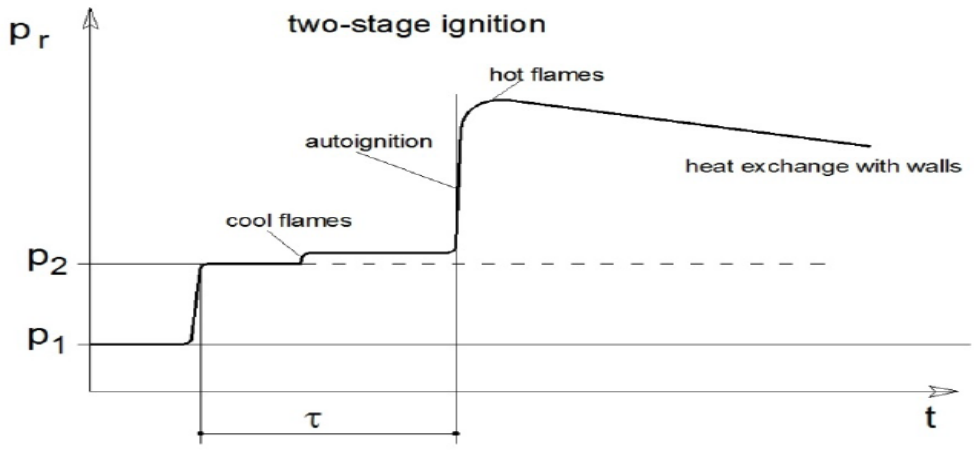

Figure 1.3 Rapid compression machine pressure trace

The autoignition process is composed by a period of slow reaction followed by a period of rapid reaction. τ represents the reaction time (or ignition delay), needed for the production of a sufficient number of highly reactive radicals that promote self-ignition. The autoignition theory states that autoignition occurs when

$$\sum \frac{\Delta t_i}{\tau_i} = 1 \quad so \quad \int \frac{dt}{\tau} = 1$$

and τ is defined as follows

$$\tau = c_1 p^{-c_2} e^{\frac{c_3}{T}}$$

It is function of instantaneous pressure and temperature in the unburnt zone and of the three parameters c_1, c_2 (fuel sensitivity to in-chamber pressure), c_3 (fuel sensitivity to the in-chamber temperature).

Unlike gasoline and diesel oil, which are blends of different chemical species, natural gas has a known chemical composition: it is a mixture of methane (about 85% in volume), propane, butane and ethane.

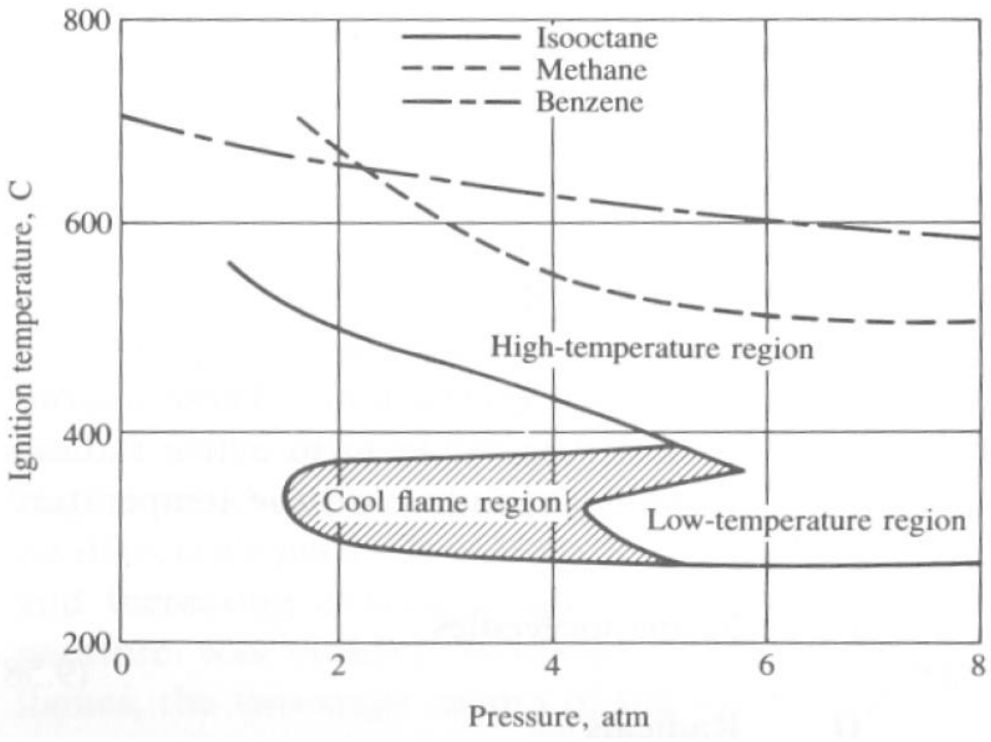

Figure 1.4 Autoignition temperature and pressure map

As shown in the figure, gasoline autoignition process does not develop at well-defined conditions, while for methane there are exact combinations of pressure and temperature for which the reaction will take place. Therefore, the outlined autoignition model is not accurate enough to describe gasoline behaviour, while it allows proper NG knocking behaviour evaluation.

During engine operation in firing condition, spark plug energizes only a small amount of cylinder charge so pressure rise will be initially small respect to motoring operation. When a higher portion of mixture will be involved in the combustion process, pressure in the combustion chamber will rise and the end gas will be compressed by the expanding burning gases. The last portion of unburnt gases is the most affected by the risk of detonation, being subjected for a longer time to high pressure and temperature. During piston expansion phase and due to thermal exchange with walls, combustion pressure and temperature will then decrease.

The knock model implemented in the simulation code considers a cycle as detonating when the aforementioned integral reaches a value equal to 1 before the combustion has finished, meaning that part of the mixture undergoes self-ignition before being reached by the flame front, producing a sudden pressure increase and high amplitude waves propagating in the chamber at high speed and transmitting vibrations to the engine structure, perceived as knock noise. Later, oscillations dissipate due to the gas viscosity.

1.3 Knock and cyclic dispersion

Cyclical dispersion has an important influence on knock occurrence. In a given stationary operating condition, defined by fixed control inputs, pressure cycles do not repeat identically cycle-by-cycle but are subjected to fluctuations reflected in local pressure and temperature differences. These variations are intrinsic in the combustion process and in the engine operation and are caused by different turbulence levels inside engine cylinder, amount of intake air and fuel injected, distribution of the charge, residual gas

content and so on. This phenomenon is accentuated in lean mixture condition and in presence of high EGR content.

From the analysis of experimental measurements in fixed operating point, knock, promoted by favourable local conditions for autoignition, has been detected only in a portion of cycles, thus strengthening the correlation between cyclical dispersion and detonation. Engine performances are strongly influenced by these irregularities.

Combustion speed is subjected to cycle-to-cycle variations, mainly affected by early combustion phase development, namely incubation phase, when the spark involves a really small amount of mixture, and by the rapid burning phase, due to charge and turbulence cyclical inhomogeneity. Faster cycles will produce higher pressure peaks with a major knocking tendency.

The parameter used to describe cyclical dispersion phenomenon is the Coefficient of Variation (CoV). It is a percentage defined as the ratio between standard deviation and mean value of the considered parameter.

$$CoV = \frac{\sigma_{(x)}}{\mu_{(x)}}$$

where:

- σ = standard deviation
- μ = mean value
- x = considered quantity

It is applied to the model under study in order to simulate the cyclical variability of the combustion speed with the introduction of CoV to describe the incubation and rapid burning phases variation.

1.4 Combustion and turbulence model

The combustion and turbulence models described in the following chapters have been compiled with FORTRAN programming code and implemented in the GT-Power engine model as a user-subroutine.

With the target of achieving good predictive capabilities, it is required that the simulation code could provide a correct estimation of heat-release, involving the evaluation of turbulence evolution inside the cylinder and flame front interaction with turbulence. This can be achieved with the application of reliable flame propagation models obtained with semi-empirical correlations involving geometrical and thermodynamic quantities obtainable by experimental analysis. The prediction of pressure evolution inside the combustion chamber needs the evaluation of Heat Release Rate, which in turn requires a correct estimation of the mass instantaneously trapped in the flame front and burnt.

The evaluation of mass fraction burnt can be performed by means of two different approaches: the first one models the combustion imposing a predefined combustion profile, while the second one includes the calculation of instantaneous flame front speed and flame front area.

The first approach approximates the experimental S-shaped burn profile with an equation characterized by parameters appropriately tuned, as in the case of Wiebe function:

$$x_b(\theta) = 1 - e^{\left[-a\left(\frac{\theta-\theta_0}{\Delta\theta}\right)^m\right]}$$

where:

- θ = crank angle
- θ_0 = start of combustion angle
- $\Delta\theta$ = combustion duration
- a, m = model tuning parameters

Actual mass fraction burnt profile are usually fitted with $a \approx 5$ and $m \approx 2$. It is important to remember that this kind of approach has no correlation with physical quantities and conditions affecting combustion, such as chamber geometry, in-cylinder turbulence and flame-turbulence interaction.

This is the reason why the second approach is more suitable to be applied to a predictive model. In this case combustion rate is computed considering both turbulent flame speed and flame front area; it is expressed by the following equation:

$$dx_b = \frac{1}{m}\rho_u A_{bf} S_b \frac{d\theta}{\omega}$$

where:

- m = trapped mass
- ρ_u = unburned gas temperature
- A_{bf} = flame front area
- S_b = turbulent flame speed
- ω = engine speed

This approach is implemented in a multizone combustion model to predict pressure and main combustion quantities evolution and includes a fractal geometry concept to describe the entrainment of fresh mixture in the flame front.

The model outlined in the following chapters can be used only to describe the rapid burning phase of combustion; in fact, it cannot be applied to the incubation phase, corresponding to the crank angle interval necessary to a reach a value of mass fraction burnt of 1% ($\Delta\theta_{0-1\%}$). For the evaluation of this first combustion phase, some correlations exist, but for the purpose of this work, $\Delta\theta_{0-1\%}$ has been computed from the values obtained from a Three Pressure Analysis, as it will be explained.

1.4.1 Combustion model

Combustion chamber content is subdivided into unburned and burned regions, this last additionally subdivided in a defined number of zones. These two regions are separated by the flame front. Different burned gas zones are generated at subsequent crank angles during combustion and no mixing is enabled between them in order to obtain a well-defined temperature gradient inside the chamber. Conventional approach including energy and mass conservation principles and perfect gas law is applied to the distinct zones. Basic equations are written in differential form referring to the time interval

$$\mathrm{dt} = \frac{d\theta}{\omega}$$

where:

- $d\theta$ = crank angle interval
- ω = engine speed

At any time, the sum of volumes of unburned and burned zones must be equal to the instantaneous chamber volume

$$dV_u + \sum_{i=1}^{n-1} V_{b,i} + dV_{b,n} = dV$$

where:

- dV_u = volume variation of unburned zone
- $dV_{b,i}$ = volume variation of i-th burned zone
- dV = chamber instantaneous volume variation

Subscript “i” refers to the i-th burned zone sequentially generated, while “n” refers to the last generated zone.

Applying mass conservation law, the following equation is obtained

$$dm = d\left(m_f + m_a + m_r\right) = dm_u + dm_{b,n} = 0$$

where:

- m_f = fuel mass

- m_a = air mass
- m_r = residuals mass
- m_u = unburned mass
- m_b = burned mass

Introducing the mass fraction burned equation

$$x_b = \frac{m_b}{m}$$

we get the following relationships

$$m_b = x_b m \qquad x_b = \sum_{i=1}^{n} x_{b,i};$$

$$m_u = (1 - x_b) \cdot m; \qquad m_{b,i} = m x_{b,i}$$

Applying energy conservation equation to burned and unburned zones we get

$$-q_u A_u \frac{d\theta}{\omega} + V_u dp = (1 - x_b) m di_u$$

$$-q_{b,i} A_{b,i} \frac{d\theta}{\omega} + V_{b,i} dp = m x_{b,i} di_{b,i}$$

where $q_u A_u$ and $q_{b,i} A_{b,i}$ represent the heat transfer rates from the considered region to adjacent gas zones and cylinder wall. Heat transfer between gas zone is then neglected respect to heat losses through walls, so heat transfer rates refer only to heat exchanged with the cylinder structure.

Applying this principle to the entire cylinder content, following equation can be obtained

$$-(q_u A_u + q_b A_b) \frac{d\theta}{\omega} + V dp = \left(i_{b,n} - i_u\right) m dx_{b,n} + (1 - x_b) m di_u + m \sum_{i=1}^{n} x_{b,i} di_{b,i}$$

and $q_b A_b$ expresses the global heat transfer rate from burned zones to cylinder walls.

In-cylinder pressure is given applying perfect gas law

$$p = \frac{m}{V} \left[(1 - x_b) R_u T_u + \sum_{i=1}^{n} x_{b,i} R_{b,i} T_{b,i} \right]$$

Finally, 'prompt-burning' approach (i.e. mixture entrained in the flame front promptly burns) is applied to evaluate the evolution of mass fraction burned with the aforementioned equation

$$dx_b = dx_{b,n} = \frac{1}{m}\rho_u A_{bf} S_b \frac{d\theta}{\omega}$$

To fully describe this equation, in the following chapters will be explained how to evaluate turbulent flame speed S_b.

1.4.2 Turbulent flame speed submodel

In order to predict heat-release rate, turbulent flame speed S_b must be computed considering, as said before, turbulence generation and interaction with flame. Turbulence generation in based on a zero-dimesional energy model that considers a cascade energy transfer from the mean flow to the smallest eddies where viscous effects dissipate energy. Rates of energy variation are described by the following equations, differentiating between kinetic energy at macroscopic level and energy dissipation at microscopic vortices level:

$$\frac{dK}{dt} = \frac{1}{2}\dot{m}_i v_i^2 - P - K\frac{\dot{m}_o}{m}$$

$$\frac{dk}{dt} = P - m\varepsilon - k\frac{\dot{m}_o}{m}$$

where:

- K, k = kinetic energy at macroscopic and microscopic level
- m = in-cylinder trapped mass
- $\dot{m}_i$ = mass flow rate entering the cylinder
- $\dot{m}_o$ = mass flow rate exiting the cylinder
- v_i = mean speed of air entering the cylinder
- P = rate of turbulent kinetic energy production
- ε = rate of turbulent kinetic energy dissipation per unit mass

ε can be obtained as follows:

$$\varepsilon \cong u'^3/L_i$$

and L_i, that represents the characteristic lenght of turbulence macro scales, is expressed as

$$L_i = \frac{V}{\pi B^2/4}$$

with B equal to the cylinder bore. V is the instantaneous chamber volume. L_i is always subjected to the restriction $L_i < B/2$.

P is empirically estimated according to the following relation

$$P = 0.3307 c_\beta \frac{K}{L_i}\left(\frac{k}{m}\right)^{1/2}$$

where c_β is the turbulent dissipation constant, adjusted to obtain experimental profiles of u' and U, namely Kolmogorov (microscopic) and integral (macroscopic) velocity scales. Thus, average turbulence levels can be estimated at combustion start applying the model to induction and compression phases and assuming angular momentum conservation for large scale eddies, following relations must hold after ignition

$$\frac{L_i}{L_0} = \left(\frac{\rho_{u0}}{\rho_u}\right)^{\frac{1}{3}}$$

$$\frac{u'}{u'_0} = \left(\frac{\rho_u}{\rho_{u0}}\right)^{1/3}$$

where ρ_u refers to unburned gas desity and subscript "0" to the conditions at combustion start.

Once turbulence has been characterized, the interaction between turbulence and flame can be evaluated applying the fractal approach, that includes the laminar flamelet concept. It is assumed that turbulent flame combustion is confined to asymptotically thin moving laminar flamelets embedded in the turbulent flow. Considering this laminar behaviour, turbulent burning speed is related to laminar burning speed, corrected taking into account stretch and curvature effects of the flame front, and flamelets surface area according to the fractal theory:

$$\frac{A_T}{A_L} = \frac{S_b}{S_L} = \left(\frac{\varepsilon_0}{\varepsilon_i}\right)^{D-2}$$

where:

- A_T = turbulent flame area
- A_L = laminar flame area
- S_b = turbulent burning speed
- S_L = laminar flame velocity
- ε_0 = outer turbulence cutoff lenghtscale
- ε_i = inner turbulence cutoff lenghtscale
- D = fractal dimension of flame front surface

Model application is strictly related to the correct evaluation of cutoff lenghtscale values and fractal dimension. Outer cutoff lenghtscale is evaluated by the following relation

$$\varepsilon_o = L_i = C_L(h_{min} + S_p)$$

where:

- h_{min} = minimum clearance at TDC
- S_p = instantaneous piston position respect to TDC
- C_L = calibration parameter, used to tune the model

Inner cutoff lenghtscale is instead evaluated as follows

$$\varepsilon_i = \eta = L_i \left(\frac{u' L_i}{\nu}\right)^{-\frac{3}{4}}$$

where η is the turbulence micro-scale and ν the unburned gas kinematic viscosity.

Once lenghtscales are defined, the relation between turbulent and laminar flame speeds can rewritten as follows

$$\frac{S_b}{S_L} = \left\{ \frac{C_L(h_{min} + S_p)}{C_L(h_{min} + S_p)\left[\frac{u' C_{L0}(h_{min} + S_p)}{\nu}\right]^{-3/4}} \right\}^{D-2}$$

The fractal dimension D is derived by the following correlation and is function of the non-dimensional turbulent velocity fluctuation u'/S_L

$$D = \frac{2}{1 + u'/S_L} + \frac{2.35}{1 + S_L/u'}$$

Equation defining $\frac{S_b}{S_L}$, after etensive investigations, appears not to be sufficient alone to accurately define the turbulent burning speed, regardless of the value assumed by the fractal dimension, because neglects that small-scale turbulence also enhances transfer of species and heat. A more refined equation has been introduced, taking into account the two following aspects:

- the wrinkling effect of turbulence on flame front must be function of the ratio between characteristic flame front and microscopic vortexes dimensions, in fact initially regular flame front surface is progressively corrugated as its dimension increases respect to turbulent eddies;
- effects of species and heat transfer must be function of charge density.

Therefore, the equation becomes

$$\frac{S_b}{S_L} = \left(\frac{\rho}{\rho_0}\right)\left\{\frac{C_{L0}\sqrt{A_{bf}}}{C_{L0}(h_{min} + S_p)\left[\frac{u' C_{L0}(h_{min} + S_p)}{\nu}\right]^{-3/4}}\right\}^{D-2}$$

where ρ represents the charge density at the considered crank angle, while ρ_0 is the charge density evaluated at a predefined crank angle named θ_0, which is characteristic of the engine considered. A_{bf} is the flame front surface, that can be evaluated coupling the combustion model to an accurate CAD model and considered as a portion of spherical surface centred in the spark plug electrodes. The model has been finally further improved by the addition of a calibrating exponent n which allows to modulate the effect of the density ratio, leading to the equation employed in this research project

$$\frac{S_b}{S_L} = \left(\frac{\rho}{\rho_0}\right)^n \left\{ \frac{C_{L0}\sqrt{A_{bf}}}{C_{L0}(h_{min} + S_p)\left[\frac{u' C_{L0}(h_{min} + S_p)}{\nu}\right]^{-3/4}} \right\}^{D-2}$$

The equation contains both thermodynamic, fluidodynamics and geometric quantities therefore demonstrating the physical correlation of the model with the actual phenomenon.

1.4.3 Laminar flame speed submodel

In order to compute the turbulent flame speed, previous equation requires the evaluation of laminar burning speed, that can be obtained applying the following power correlation

$$S_L = S_{L,0}\left(\frac{T_u}{T_0}\right)^{\alpha}\left(\frac{p}{p_0}\right)^{\beta}(1 - 1.5x_{res})$$

where:

- T_0 = reference temperature (298 K)
- p_0 = reference pressure (1 atm)
- T_u = unburned temperature
- p = chamber pressure
- x_{res} = residuals fraction

and $S_{L,0}$, α and β are parameters dependent on the type of fuel and Realtive Air-to-Fuel Ratio (RAFR). Considering a small exstimation error, α and β can be considered constant and defined as follows

$$\alpha = 2.18 - 0.8\left(\frac{1}{RAFR} - 1\right)$$

$$\beta = -0.16 + 0.22\left(\frac{1}{RAFR} - 1\right)$$

and $S_{L,0}$, considering the emplyment of NG, obtained as

$$S_{L,0} = 0.369 - 2.10\left(\frac{1}{RAFR} - 1.12\right)^2 - 3.35\left(\frac{1}{RAFR} - 1.43\right)^3$$

The last part of the combustion process, named wall combustion, is influenced by the fact that flame front reaches cylinder walls. Combustion speed then decreases. The combustion model implemented in GT-Power software takes into account also this aspect, introducing a parameter, cwc, that represents the mass fraction burned value at which the flame propagating encounters the walls, defining the switch between the rapid combustion phase model and wall combustion model.

1.5 Ringing and knocking

During the analysis performed on the experimental pressure cycles provided, cycles with high frequency content were detected; this is usually, for a SI engine, an indicator of knocking cycle. Pressure oscillations during detonation perturb the rather smooth pressure curve of non-knocking cycles and a pressure signal with the following appearance is collected by measuring instruments.

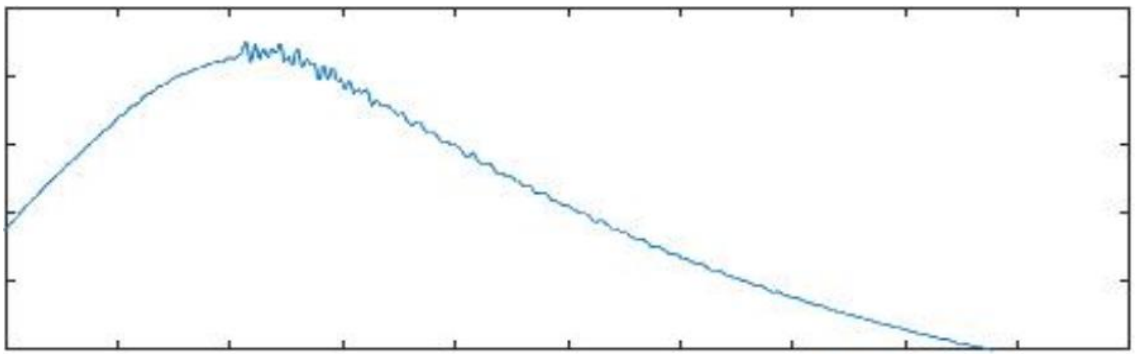

Figure 1.5 Knocking cycle pressure signal

Analysing more in detail the high frequency content cycles, some non-knocking cycles were observed. At such high compression ratios, natural gas, in the early stages of combustion, can show a behaviour similar to premixed diesel burning. It can produce pressure oscillations that propagate during combustion, denoted as “ringing”, that may be interpreted as knock occurrence by common detonation detection algorithms. In this research work a proper code has been developed, in order to evaluate the nature of pressure perturbations, coupling a traditional Knock Index computation approach to a refined frequency analysis of the pressure signals.

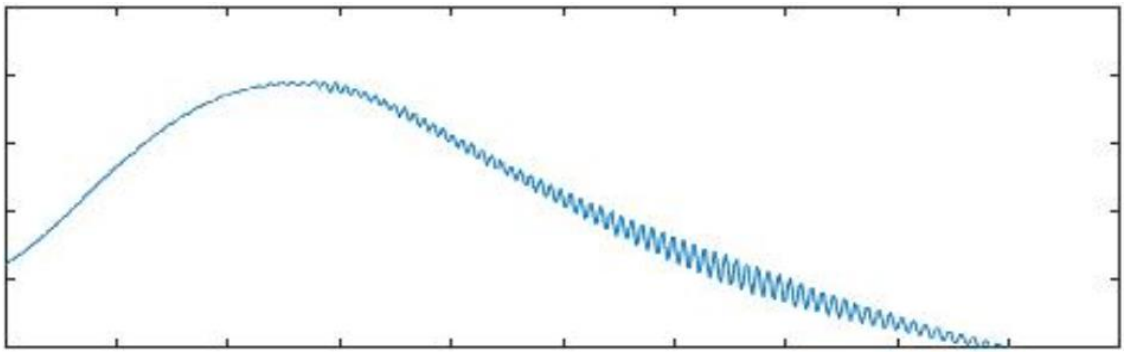

Figure 1.6 Ringing cycle pressure signal

1.6 GT-Power software

Simulations performed in this thesis work have been carried out with the GT-Power software. Widely employed in the engine research and development sector, it is able to simulate engine operation and performance in a computing environment. This represents a big advantage in the engine design and testing phases respect to bench testing, in terms of both time and cost savings.

Models built with this code provide a description of main engine performance parameters and operating variables. A monodimensional fludiodynamic analysis is performed by the software in order to evaluate the gas evolution through the ducts, for which pressure drops and heat exchanges are estimated. Combustion instead is addressed with a zero-dimensional approach, however satisfactory results are achieved even respect to CFD analyses, that provide a three-dimensional description and evolution of the mixture allowing to take into account charge inhomogeneities, but much more time consuming.

Models are built adding predefined templates included in the GT-Power library and modifying their parameters to reproduce the geometric configuration and working conditions of the engine under study. Parts are linked according to the actual engine layout. Models for the gas (air and fuel) running in the ducts and evolving through the engine cycles are included. Boundary conditions such as local pressures and temperatures measured by sensors are fixed, as well as information about valve lift and injection profiles.

The post-processor, named GT-Post, collects simulation results that can be gathered and further analysed to evaluate the effects on engine performance produced by different imposed input conditions.

2 Input data

In the following chapter, main engine features and experimental data provided will be shown.

2.1 Engine features

The engine under study is a prototype model made to explore NG application to a mono-fuelled, properly designed engine. It is a high-performance turbocharged engine, employing VVA (Variable Valve Actuation) and direct injection technologies. The use of NG as the only fuel supply allows to reach compression ratio values that could not be withstood by a conventional gasoline powered SI engine. Anyway, such a high CR (12.6), allowing to achieve greater combustion efficiency levels, could promote knock occurrence. It is therefore necessary to pay special attention to this aspect, in particular in the predictive model evaluation.

Following tables show the main engine and turbocharger features.

Engine data	
Denomination	Fire 1.4 C GDI ALPHA
N° cylinders	4 in-line
Bore	72 mm
Stroke	84 mm
Connecting rod length	128.95 mm
Displacement	1368 cm^3
Compression ratio	12.6
Air supply	Turbocharged
Fuel	CNG
Intake valve lift	Fire PFI Short Boot
Exhaust valve lift	PFI Mair 170cv
Valve actuation system	MultiAir Fi2

Table 2.1 Engine features

Turbocharger data	
Compressor denomination	C22(38)-60T-038AR
Compressor diameter	38 mm
Turbine denomination	T231(35.5)-81T-34AR
Turbine diameter	35.5 mm
Turbocharger inertia	$0.43 \cdot 10^5$ kg·m^2
RPM max	270000

Table 2.2 Turbocompressor features

2.2 Experimental pressure cycles processing

This analysis has been performed on experimental pressure cycle signals provided by AVL and carried out by means of a MatLab code. In particular, for each working point 200 cycles per cylinder are available.

Knock can be recognized analysing the frequency content of pressure cycle signals. High frequency oscillations are usually a marker for detonating combustion. Signal must be sampled and filtered. Remembering Nyquist-Shannon Theorem, it is important to consider a minimum sample frequency double respect to the maximum observable frequency. Considering the signals processed, no relevant components of frequency over 35 kHz are present, so it should be sufficient to sample the signal at a frequency equal to 70 kHz, but, to avoid aliasing effects, the best choice should be sampling at a frequency higher than the Nyquist one ($\cong 10\ f_N$).

In order to analyse the frequency content due to detonation, all the contributions not deriving from knocking must be removed from the signal. To highlight the combustion and detonation frequency contents, the signal is filtered by a passband filter, implemented in Matlab superimposing a high-pass and a low-pass filter, with cutoff frequencies 5 – 35 kHz. When applying a filter, it is important to verify that a possible ripple effect in correspondence of cutoff frequencies does not amplify the signal being processed, introducing an error. In this case, in correspondence of 5 and 35 kHz, the

absence of any noticeable component assures filtering correctness. Moreover, with the application of a sampling frequency higher than 70 kHz, it is assured that the filtered signal under half of the sampling frequency (35 kHz) is immune from aliasing effect.

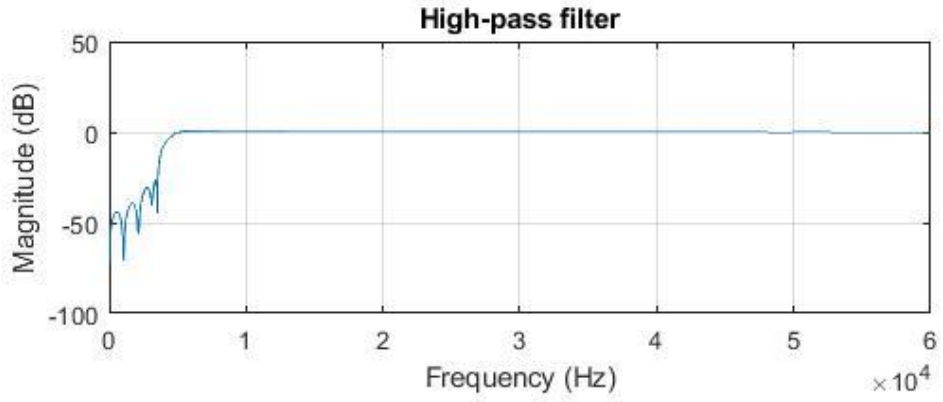

Figure 2.1 High-pass filter

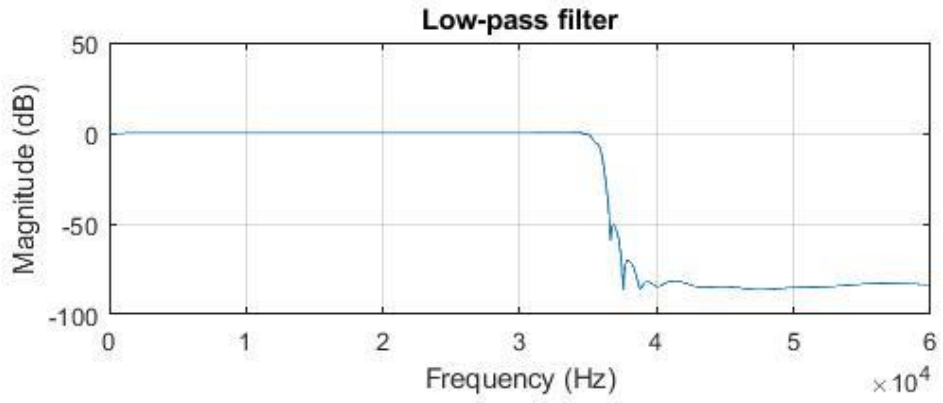

Figure 2.2 Low-pass filter

Once the filter is applied, the analysis of pressure signal is limited to the time interval in which combustion occurs, in this case from -30° to +90° respect to TDCF (top dead centre of firing) in order to exclude possible disturbances introduced by other phenomena not directly linked to combustion.

In the following figure an example of filtered pressure trend over 200 cycles is showed.

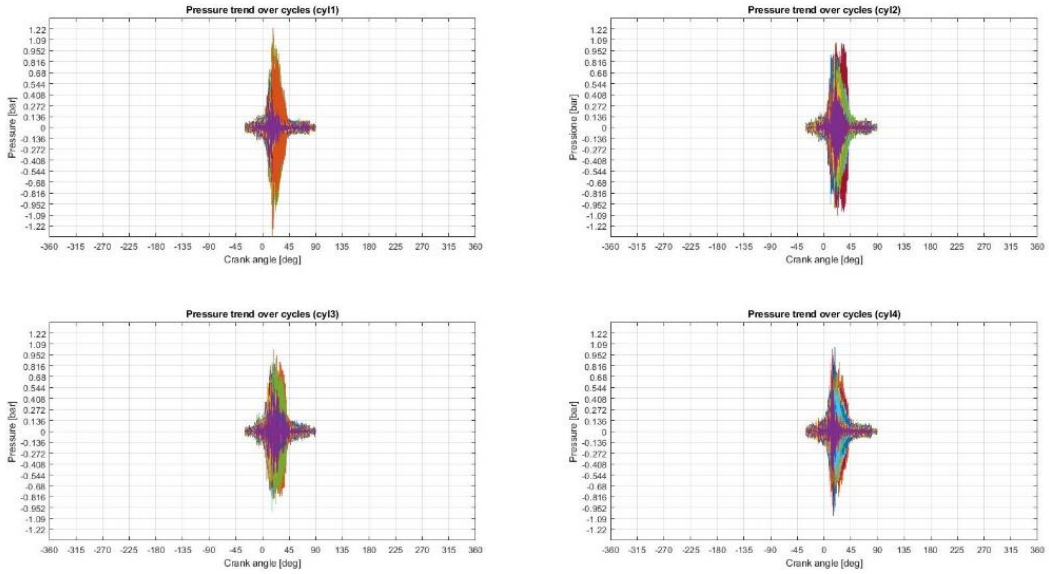

Figure 2.3 Filtered pressure trend over 200 cycles

The following step to analyse frequency content is switching from time domain to frequency domain obtaining the PSD (Power Spectral Density) of the signals, as shown in the following example.

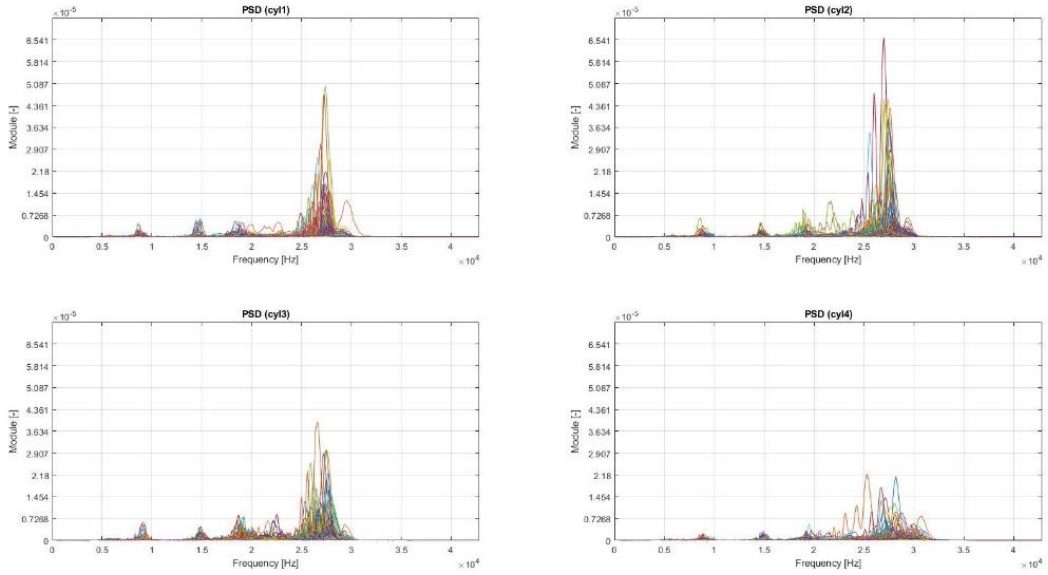

Figure 2.4 Power Spectra Density over 200 cycles

3 Analysis of experimental data and knock detection

Analysing experimental pressure cycles data, it is necessary to perform a frequency content evaluation in order to discriminate knocking and non-knocking cycles. Following figures highlight the presence of higher oscillations in case of knock onset.

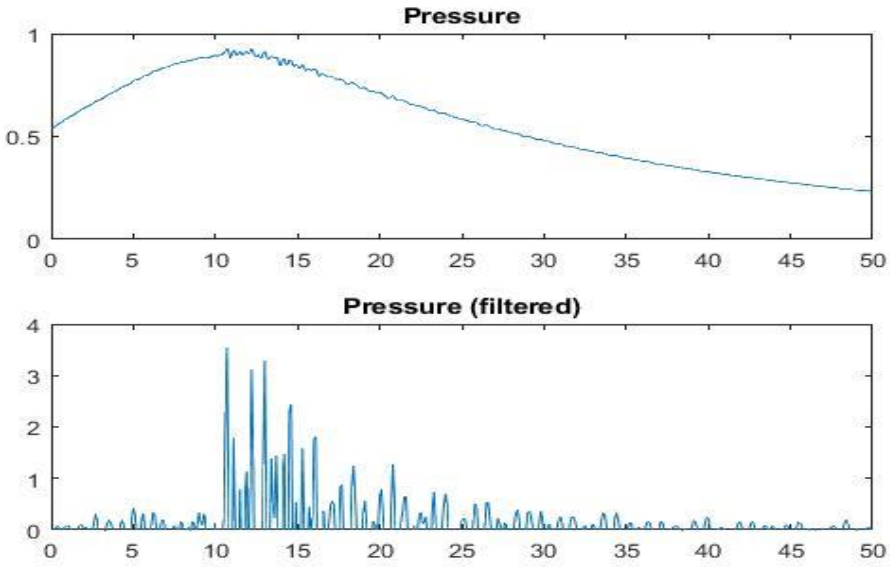

Figure 3.1 Detonating cycle – oscillation amplitude

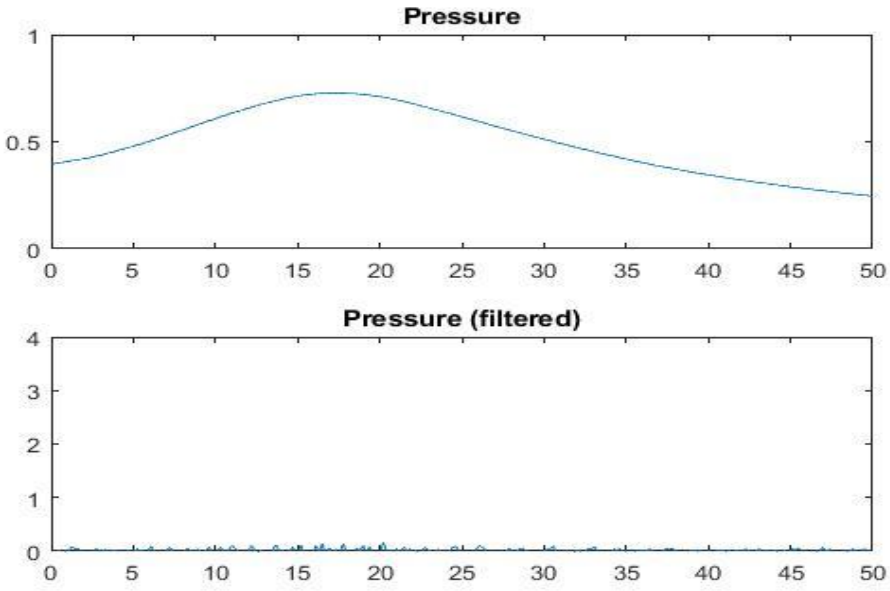

Figure 3.2 Non-detonating cycle – oscillation amplitude

3.1 Knock detection through Knock Index

Based on previous considerations, in order to define knocking cycles, a new parameter is introduced, the Knock Index, evaluated with the following expression

$$K.I. = \int \left| \frac{dP_{filt}}{dt} \right| dt$$

Where P_{filt} is the previously obtained filtered pressure signal.

$K.I.$ value for detonating cycles will be higher compared to non-detonating ones, that would however show a value ≠ 0 because of their non-null frequency content.

It is then defined a threshold value of $K.I.$ as the double of the mean value of Knock Index of the whole population ($K.I._{threshold} = 2\mathrm{K.I.}_m$). The detection criterion of knocking cycles is based on the overcoming of the predefined threshold, when $K.I._{cycle} > K.I._{threshold}$ the cycle is considered a detonating one. The following figure represents an example of the results obtained with this computation.

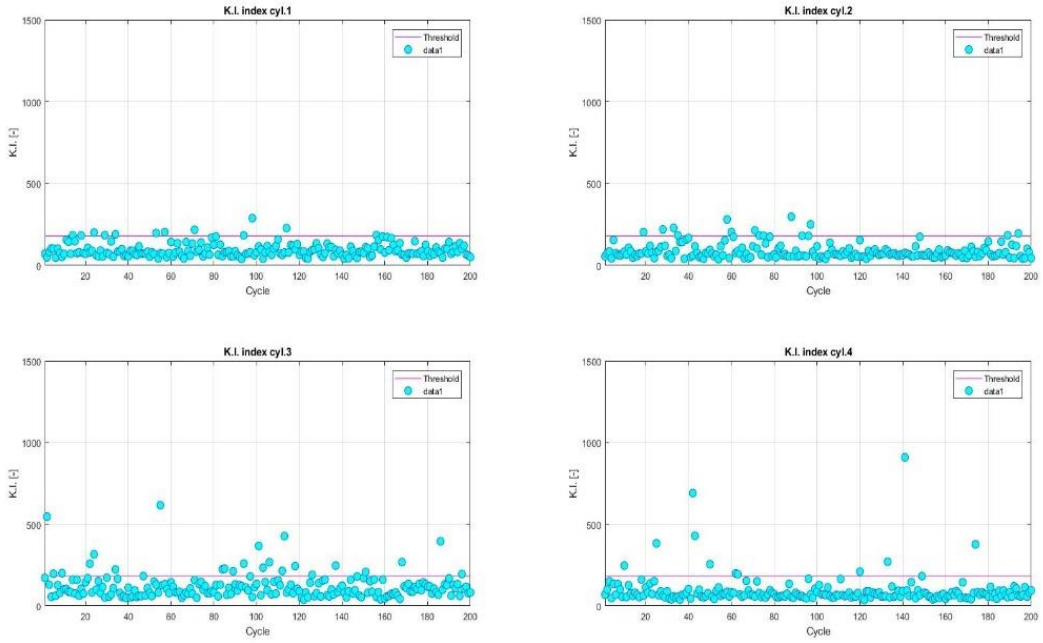

Figure 3.3 Knock Index

3.2 Knock and ringing submodel

With an accurate observation of the cycles denoted as knocking by the algorithm just described, it was possible to note that some non-detonating cycles were included because of their non-negligible frequency content. These cycles are the ringing ones, formerly described in a previous chapter.

Visually it is possible to discriminate knocking and ringing cycles by the observation of their pressure trend evolution, but it was necessary to conceive an analytical algorithm that could be implemented in a computing environment.

Therefore, a more refined code has been developed in order to further improve the detection model, analysing in more detail the signal frequency content with the application of the Fast Fourier Transform. Signals so processed show a different behaviour depending on their knocking or ringing nature.

Ringing phenomenon mostly excites a frequency band approximately included between 22 and 29 kHz. Taking this into account, the code computes the value of the integral of the FFT of the signal over this band and over the whole frequency band (5-35 kHz) and calculates their ratio (r_{cycle}). A second threshold is established (r). Now, if:

- $r_{cycle} > r$ the cycle is considered ringing;
- $r_{cycle} < r$ the cycle is considered knocking.

This means that, if most of the signal frequency content is found in the “ringing band”, the high value of Knock Index must be attributed to the ringing phenomenon occurrence, while, if a non-negligible part is located outside the band, it is caused by knock.

Following figures justify what has been outlined: in the first, it is evident the ringing nature of the cycle, and the FFT trend shows a well-defined band of interest; in the second one, detonation effect is prominent and frequency excitation is spread outside the aforementioned range.

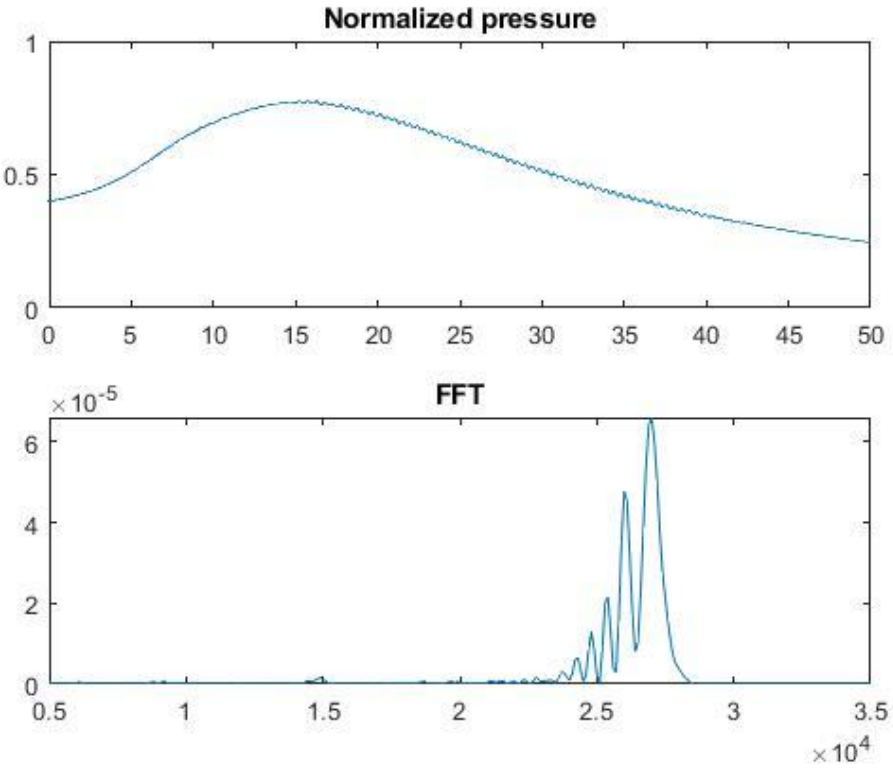

Figure 3.4 Ringing cycle

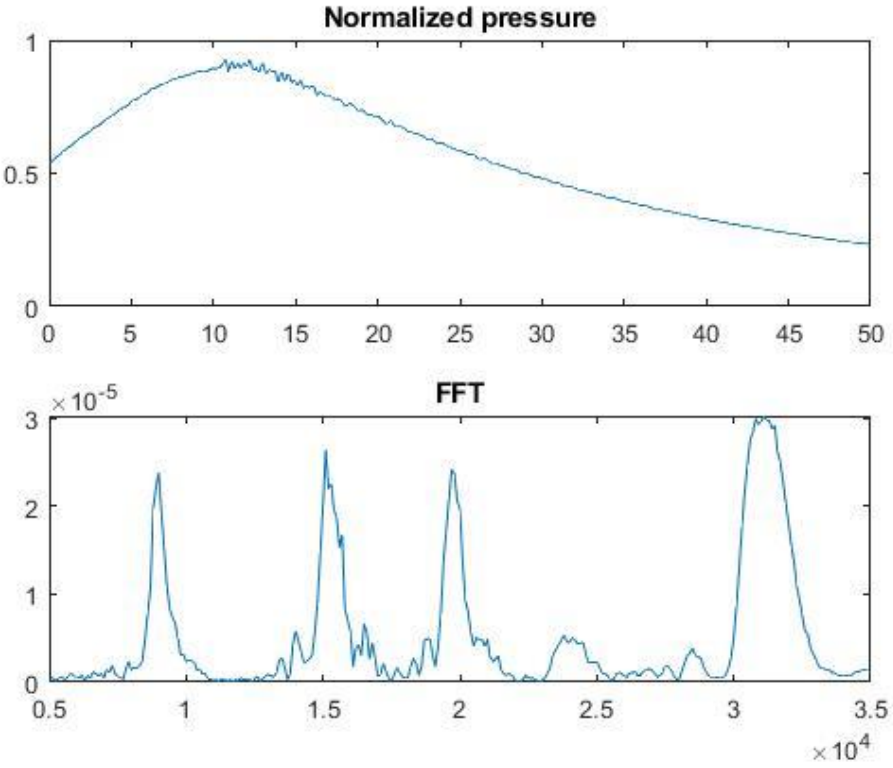

Figure 3.5 Knocking cycle

3.3 Analysis results

The procedure just outlined has been applied to analyse a number of detonation tests provided by AVL. All tests are carried out at 2000 rpm and same working conditions, except for the variation of the spark advance. Anticipating spark advance promotes knock onset. The following table resumes analysed tests.

TEST ID	SPEED [RPM]	P_{MAX} [kPa]	SPARK ADVANCE [°CA]	EXPERIMENTAL DETONATING CYCLES (%)
1977	2000	10800	7.00	0
1978	2000	11000	7.59	0
1979	2000	11200	8.16	0
1980	2000	11400	8.60	1.5
1981	2000	11600	9.14	5
1982	2000	11800	9.72	10
1983	2000	11900	10.01	15
1985	2000	11950	9.93	15

Table 3.1 Detonation tests

Following figures show the results obtained by Knock Index analysis; as expected, with the increase of the spark advance, more cycles overcome the threshold value of $K.I.$, experimentally set to 180, meaning an increasing tendency to detonation.

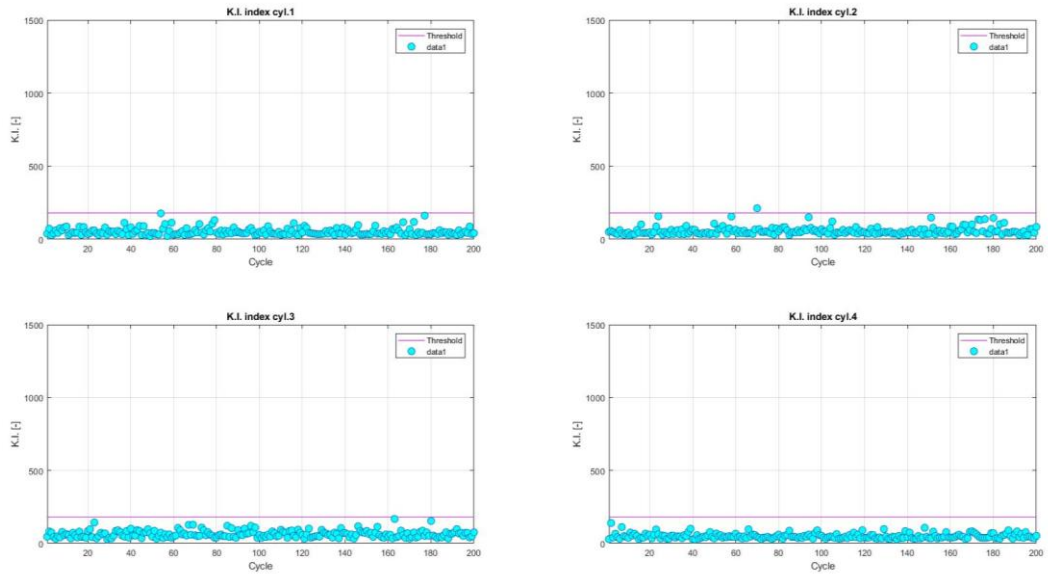

Figure 3.6 K.I. – 1977 (SA 7.00°)

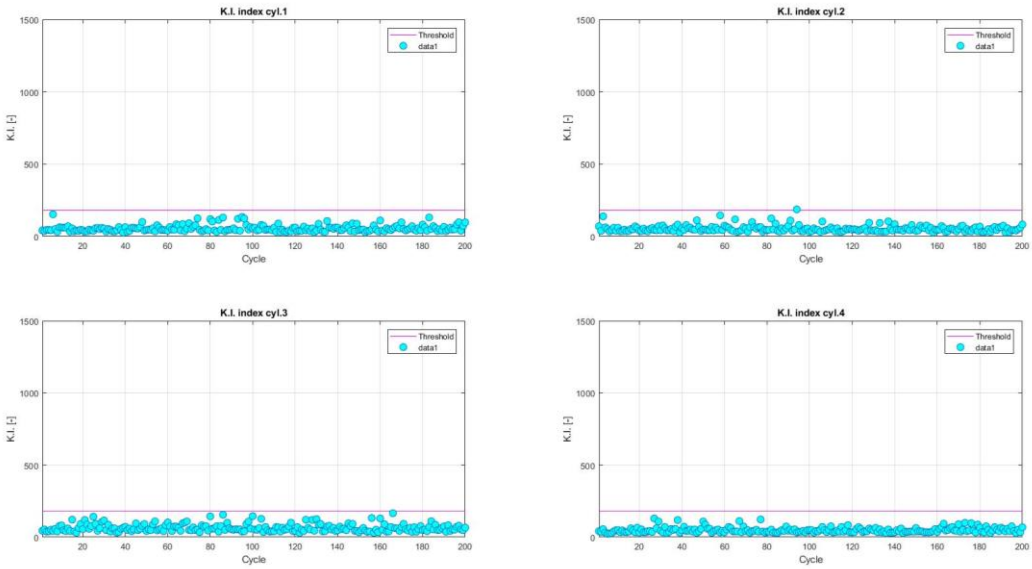

Figure 3.7 K.I. – 1978 (SA 7.59°)

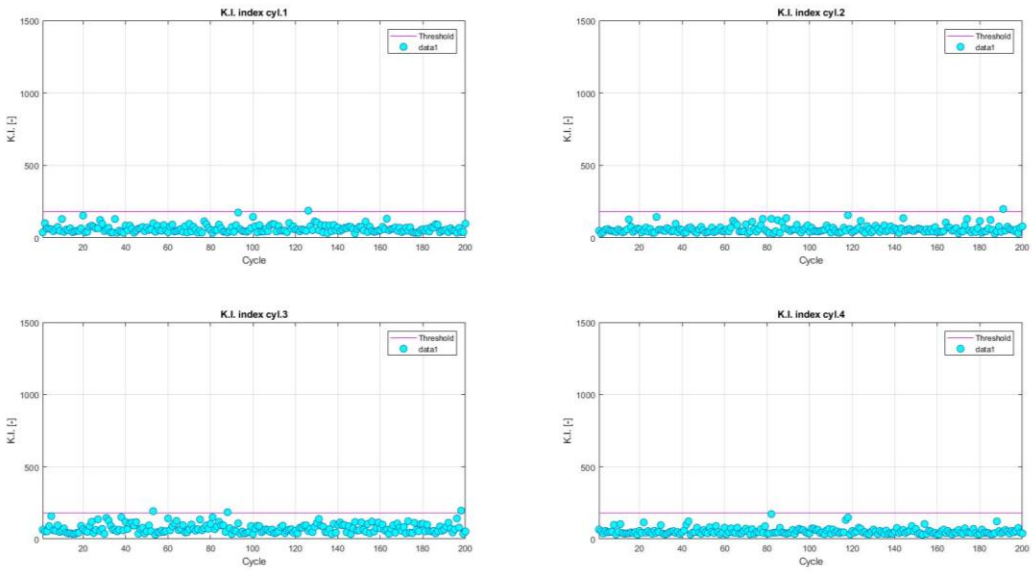

Figure 3.8 K.I. – 1979 (SA 8.16°)

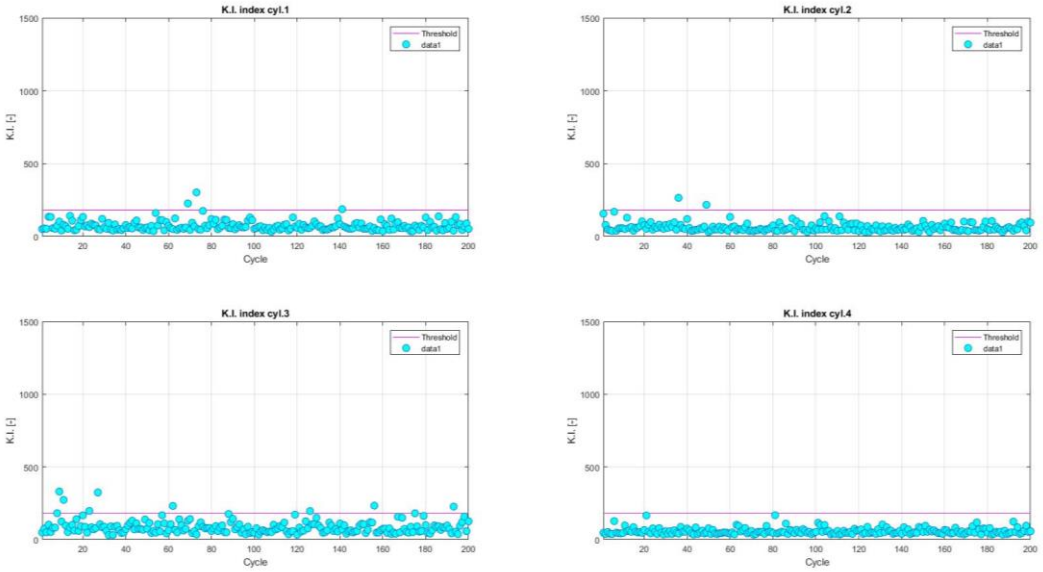

Figure 3.9 K.I. – 1980 (SA 8.60°)

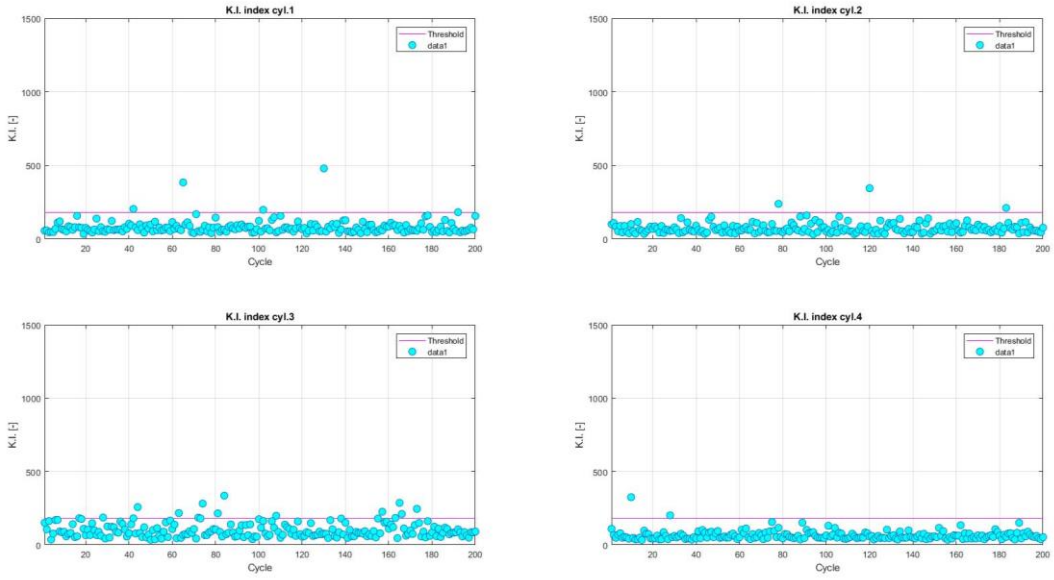

Figure 3.10 K.I. – 1981 (SA 9.14°)

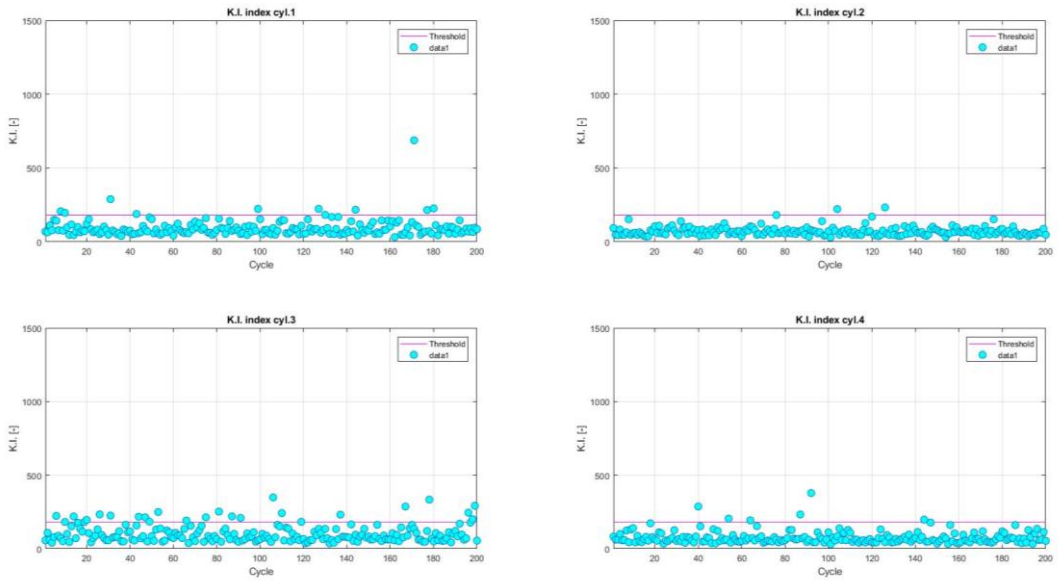

Figure 3.11 K.I. – 1982 (SA 9.72°)

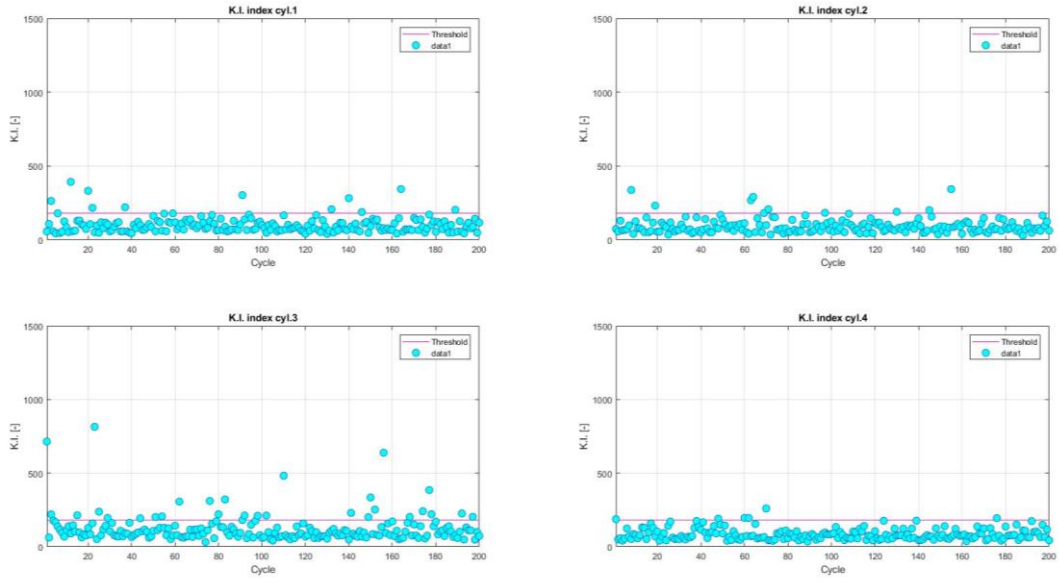

Figure 3.12 K.I. – 1983 (SA 10.01°)

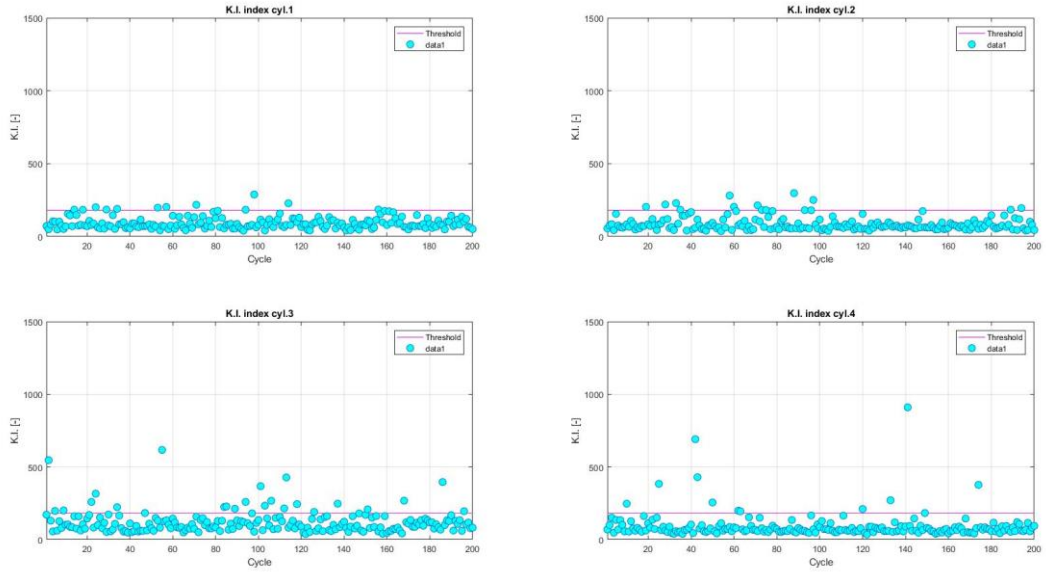

Figure 3.13 K.I. – 1985 (SA 9.93°)

Then the algorithm for ringing and knocking discrimination has been employed. This model has been subjected to a sensitivity analysis interesting cutoff frequencies of "ringing band" and parameter r.

In the following table and picture results are resumed.

TEST ID	1977	1978	1979	1980	1981	1982	1983	1985
Knock KI 180	0.1%	0.1%	0.6%	1.9%	3.3%	5.6%	7.0%	8.0%
Knock (22-29 KHz, r=0.9)	0.0%	0.0%	0.4%	0.6%	1.6%	3.8%	4.6%	5.9%
Knock (21-29 KHz, r=0.9)	0.0%	0.0%	0.4%	0.6%	1.4%	3.5%	4.3%	5.6%
Knock (22-30 KHz, r=0.9)	0.0%	0.0%	0.4%	0.6%	1.4%	3.4%	4.0%	4.9%
Knock (22-29 KHz, r=0.85)	0.0%	0.0%	0.4%	0.5%	0.9%	2.8%	3.2%	4.1%
Knock (22-29 KHz, r=0.95)	0.0%	0.0%	0.6%	1.4%	2.8%	5.3%	6.4%	7.4%
Knock (Experimental)	0.00%	0.00%	0.00%	1.50%	5.50%	10.00%	15.00%	15.00%

Table 3.2 Knock and ring model sensitivity analysis

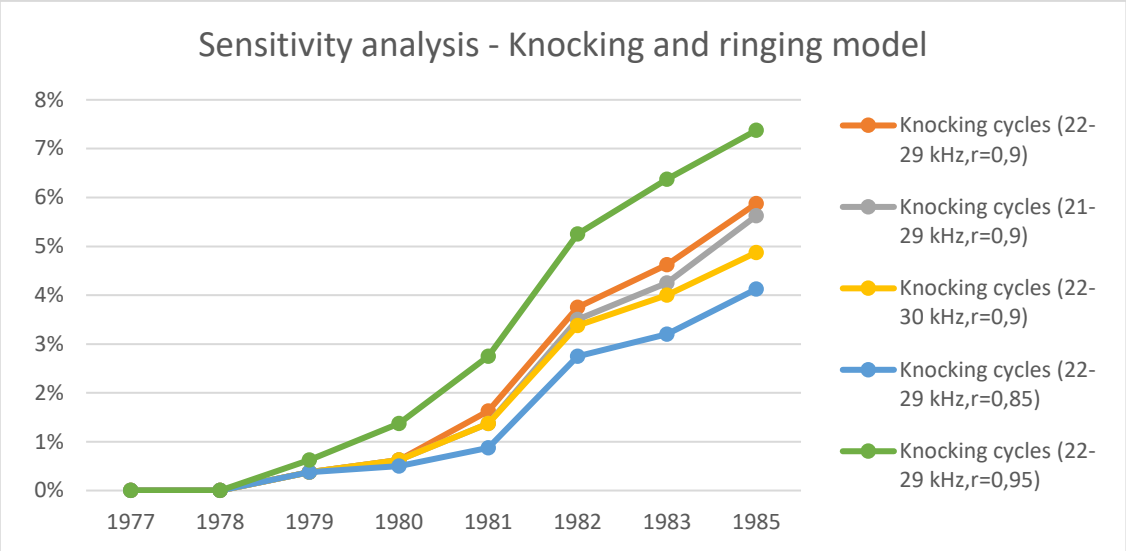

Figure 3.14 Knock and ring model sensitivity analysis

As shown by the last picture, the model is not much sensitive to ring window variation, while a small change in the threshold value r introduces non-negligeable differences, considering the precision required by this kind of investigation.

In many cases the algorithm is able to recognize correctly the nature of the cycles, as shown below.

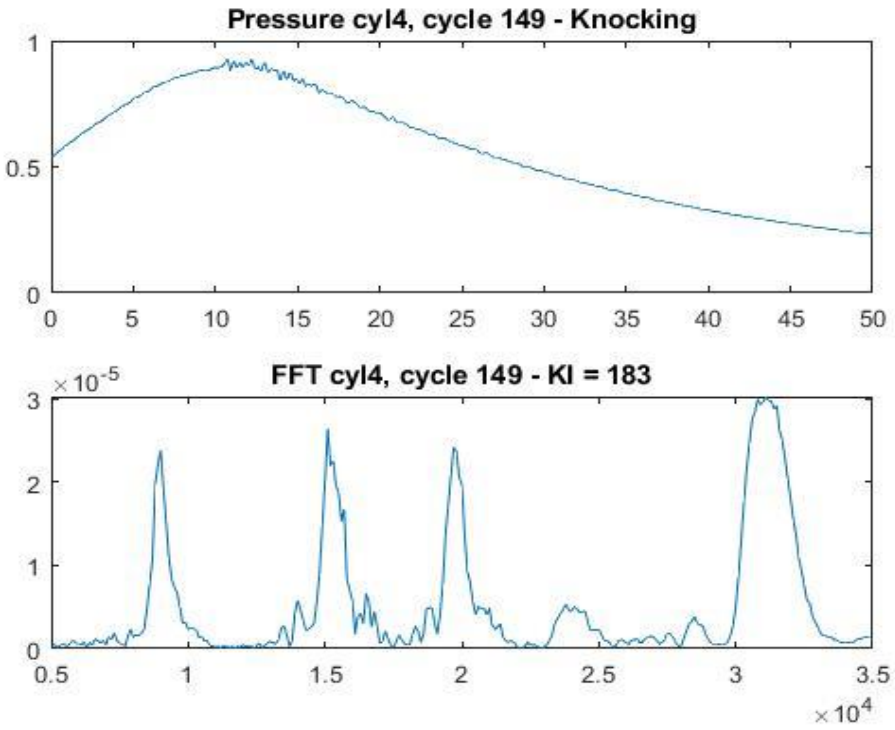

Figure 3.15 Well-recognized knocking cycle

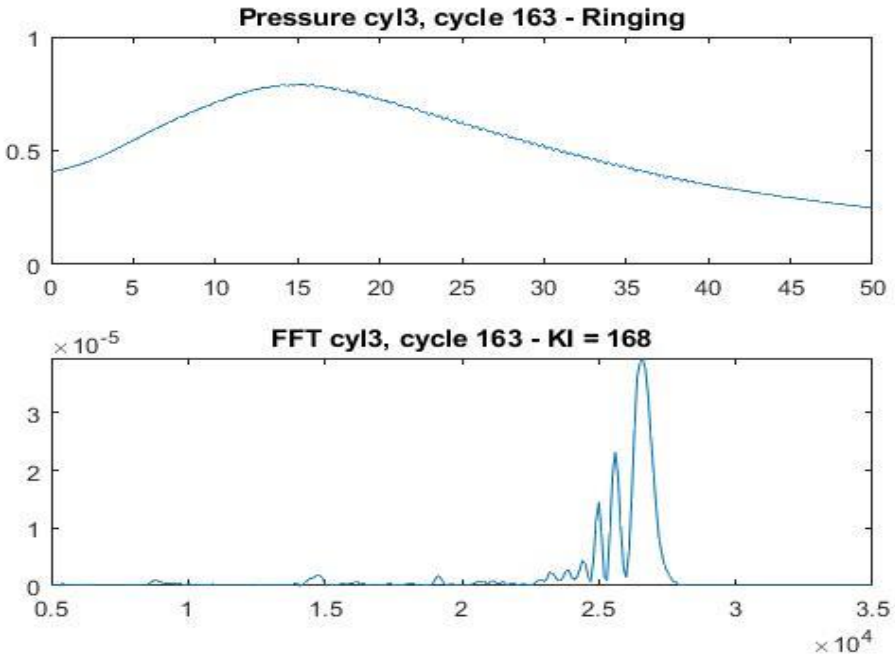

Figure 3.16 Well-recognized ringing cycle

In some cases, instead, it is not capable of providing the correct interpretation, such as in the following example: the cycle, visually showing mainly a ringing behaviour, is evaluated as a knocking one. The algorithm requires further refinement and calibration in order to perform an error-free discrimination.

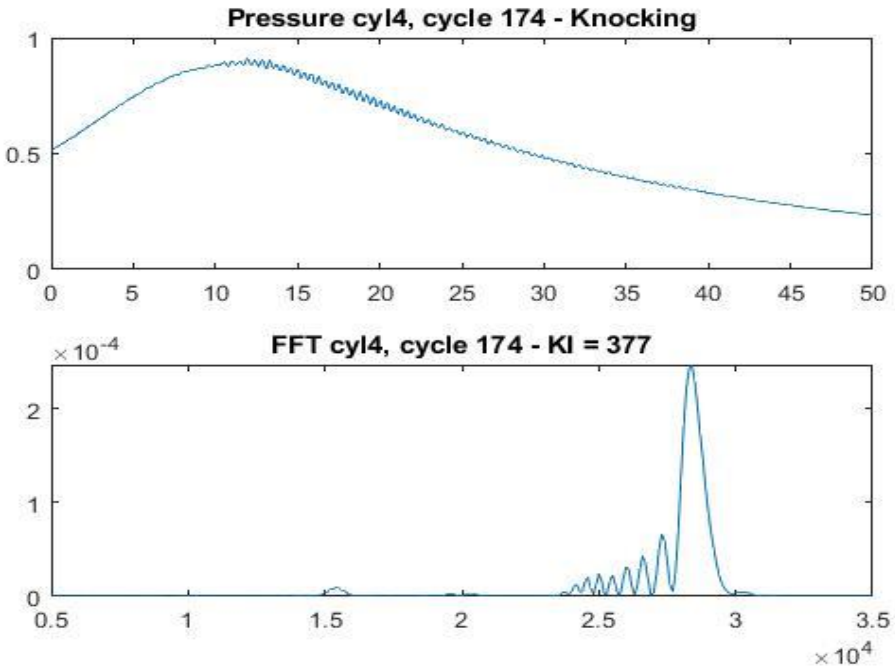

Figure 3.17 Ringing cycle interpreted as knocking

Considering the low value of percentage of knocking cycles obtained by the code respect to the experimental data provided, a further verification has been performed, trying to decrease the Knock Index value below 180. For this attempt, it has been fixed to 160. Some other detonating cycles have been detected, so a reduction of the $K.I.$ value must be considered to improve the model.

The following picture shows a pressure cycle with $K.I.$ under the pre-established threshold value.

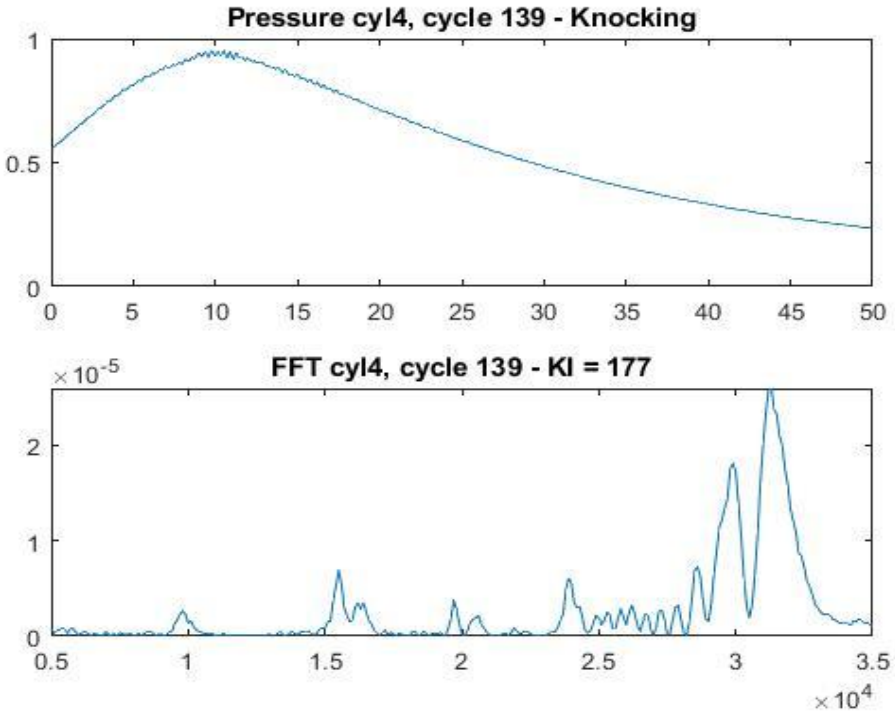

Figure 3.18 Knocking cycle with K.I. lower than threshold

In the following table results obtained imposing K.I. equal to 160 are shown.

TEST ID	1977	1978	1979	1980	1981	1982	1983	1985
Knock KI 180	0.1%	0.1%	0.6%	1.9%	3.3%	5.6%	7.0%	8.0%
Knock KI 160	0.5%	0.3%	0.9%	3.1%	5.1%	7.8%	10.6%	11.0%
Knock (22-29 KHz, r=0.9, KI=180)	0.0%	0.0%	0.4%	0.6%	1.6%	3.8%	4.6%	5.9%
Knock (22-29 KHz, r=0.9, KI=160)	0.0%	0.1%	0.4%	1.4%	3.3%	5.5%	8.1%	8.4%

Table 3.3 Knock percentage evaluation with lower K.I.

4 Engine simulation model

In this chapter, main steps followed in order to simulate and predict engine operation in a computing environment will be explained, with the evaluation of knock occurrence as the final target. Starting from an existing GT-Power model, based on the CRF test bench layout, the model has been modified according to AVL test bench configuration. Then, a TPA (Three Pressure Analysis), has been performed in order to check the fluidodynamic behaviour of the simulation model. After that, fractal combustion has been introduced, followed by the implementation of cyclical dispersion. This procedure has been applied to both some calibration points taken from the engine map and to the knock tests outlined in the previous chapter. Finally, for detonation tests, an algorithm for knock detection and counting has been included.

The engine behaviour is controlled by the wastegate valve opening, with the target of achieving the same pressure level experimentally measured in the intake manifold.

The following figure represents the simulation model in the AVL test bench configuration, obtained modifying intake and exhaust ducts geometry according to the new layout. For each test, boundary conditions (temperatures and pressures provided by sensors) have been set. Moreover, engine geometry and operating parameters for each test including information about valve lifting profiles, injection profile, target air-fuel ratio and spark advance have been set.

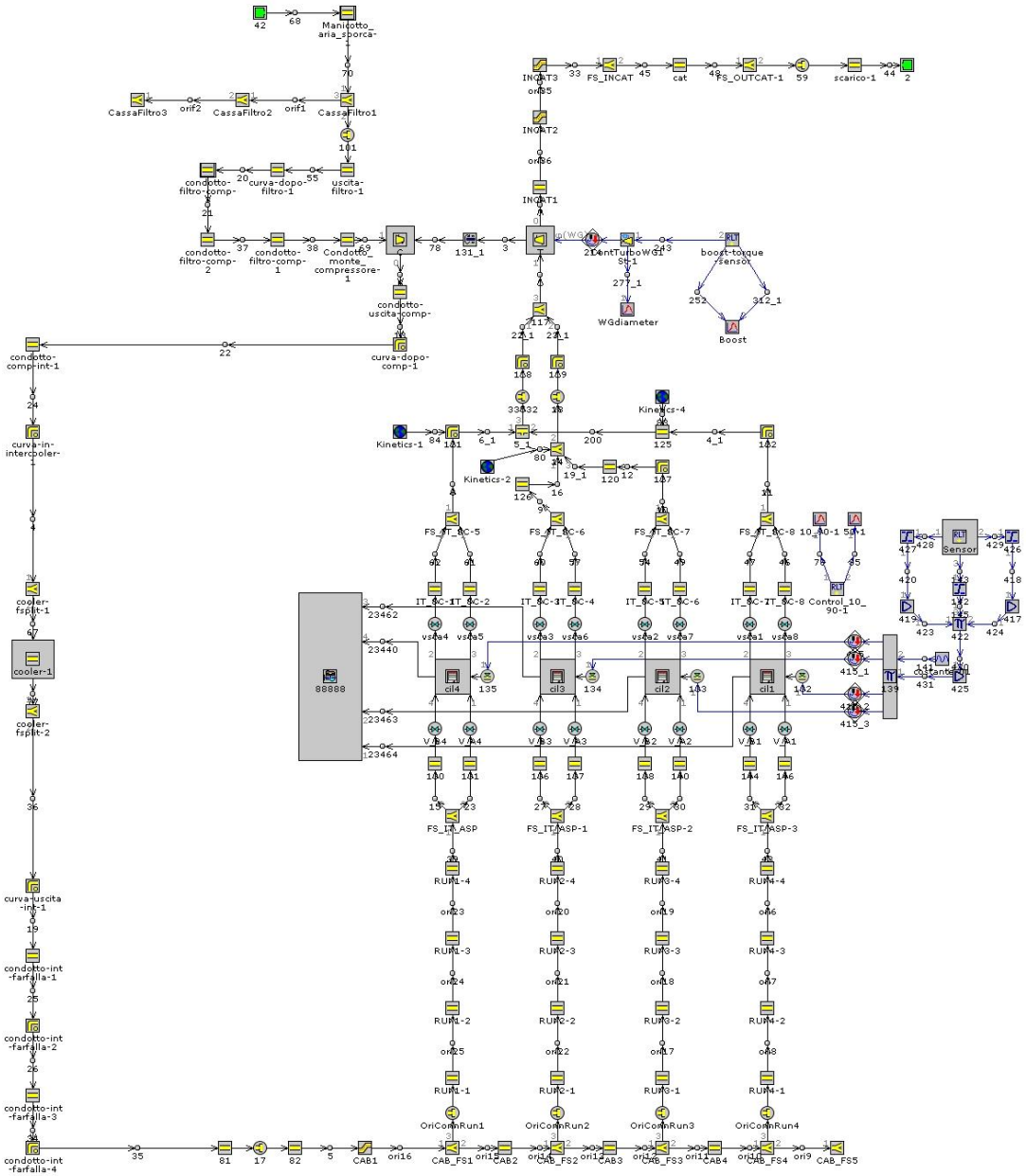

Figure 4.1 GT-Power model – AVL layout

4.1 TPA

A first verification of the fluidodynamic behaviour of the model must be performed before applying the fractal combustion model. This is done by means of a Three Pressure Analysis. TPA calculations are based on the imposition of combustion. Experimental mean pressure cycles are included in the computation code. TPA generates by iteration a burn rate, based on three measured pressures (intake, exhaust and cylinder pressure), that produces a pressure cycle as much similar as possible to the experimental one.

The convergence of the algorithm is reached when the simulated intake manifold pressure reaches the value of the experimental one acting on the opening of the turbocharger wastegate valve. In a turbocharged engine, intake manifold pressure is related to compressor boost pressure and, at WOT condition, turbocharger speed and consequently boost pressure would increase at values that could not be withstood by the engine. For this reason, a bypass valve, named wastegate, is included in the exhaust system. With the wastegate valve opening, a portion of the exhaust gases is discharged directly after the turbine avoiding a further rotational speed increase, limiting boost pressure in the intake manifold. For each simulation cycle, wastegate opening is modified in order to reach the target intake manifold pressure.

Output of the simulation is a burned mass fraction x_b that produces a simulated pressure cycle that can be superimposed to the actual one. In order to reach this correspondence, GT-Power software can correct the fuel Lower Heating Value. Anyway, in the considered cases, by tuning the heating exchange multiplier with cylinder walls, this correction remains within the range $\pm 5\%$ of the NG heating value, thus resulting in an acceptable error.

In the results chapter, comparisons between simulated and measured pressure cycles, intake manifold pressure and temperature and air and fuel mass flow rates will be provided.

4.2 Fractal combustion model

The following figure represents the model obtained after the implementation of fractal combustion and turbulence models outlined in the theory chapter. The aim of the model is to be able to simulate engine behaviour without the imposition of the actual combustion. The development of a predictive tool is promoted by the implementation of the fractal combustion model, which can reach a good predictive capability, if appropriately tuned. It is important to remember the strict physical correlation of the model: even if GT-Power software evaluates the combustion with a zero-dimensional approach, the introduced submodels allow to take into account also one-dimensional effects of flame front propagation and turbulence-flame front interaction.

In the following pictures, the obtained GT-Power model and related user sub-routines are showed.

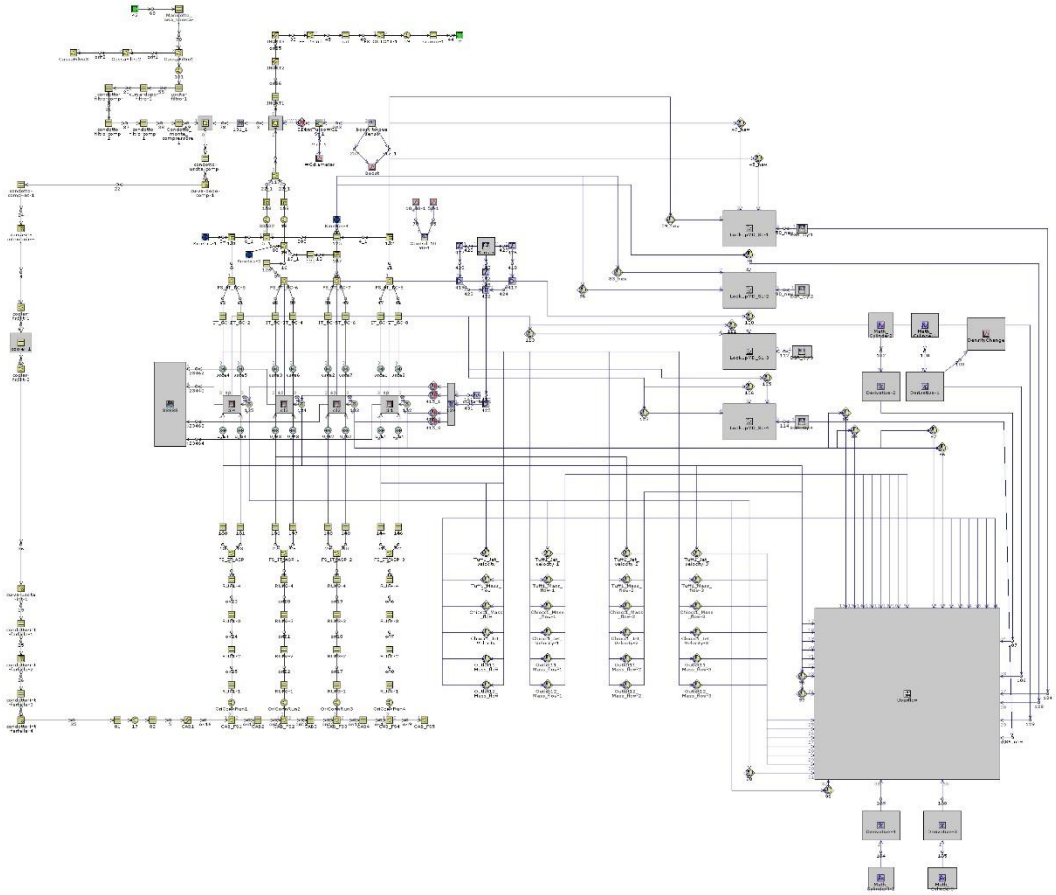

Figure 4.2 GT-Power model – fractal model implementation

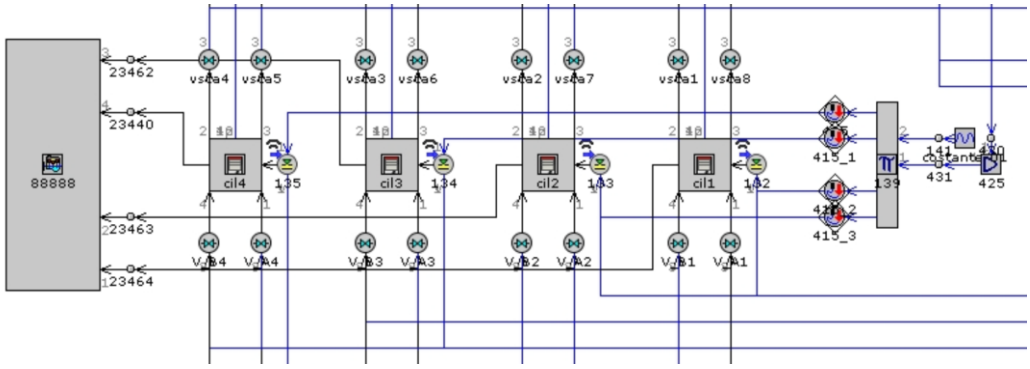

Figure 4.3 User-subroutine for implementation of combustion model

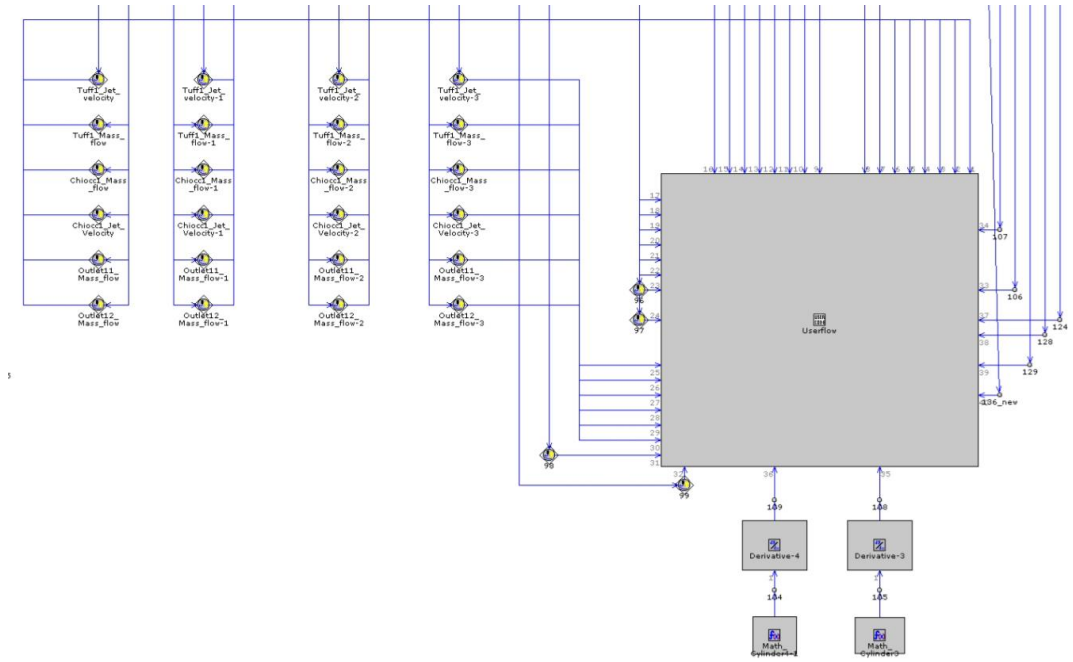

Figure 4.4 User-subroutine for implementation of turbulence model

Operating target of this phase is to model the mass fraction burnt trend simulated by the fractal model in order to be superimposed to the one generated by the TPA, which in turn is representative of the experimental one once the TPA model has been validated. This can be done by acting on the values of the following parameters, that are not constant but change depending on operating and thermodynamic conditions:

- $\Delta\theta_{0-1}$ defines the crank angle interval between spark discharge and the achievement of 1% of mass fraction burnt. Its evaluation is not included in the fractal theory because kernel growth is affected by different phenomena; some correlations are present in the literature, but, in this case, it has been evaluated observing the mass fraction burnt curve obtained from TPA and identifying the appropriate crank angle interval;
- Cl_0 describes the interaction between flame front and turbulence during the rapid combustion phase. A greater value corresponds to a more rapid combustion and, in terms of mass fraction burnt curve, a steeper slope. It has been manually tuned in order to fit experimental data provided by the Three Pressure Analysis;
- cwc defines the mass fraction burnt value at which the propagating flame front reaches the cylinder walls, determining a reduction in the burning rate. Also in this case, a manual tuning has been performed in order to fit TPA data.

4.2.1 Cyclical dispersion

In order to evaluate cyclical dispersion phenomenon, useful to develop a predictive algorithm for knock detection, cycle-to-cycle variability has been introduced in the model by means of the Coefficient of Variation previously outlined. The combustion variability has been imposed after the simulation code has reached convergence, through the dispersion of $\Delta\theta_{0-1}$ and Cl_0; cwc has not been included in the computation because of its minor influence on output results. Calculations are iterated for 100 cycles.

$$CoV_{\Delta\theta_{0-1}} = \frac{\sigma_{(\Delta\theta_{0-1})}}{\mu_{(\Delta\theta_{0-1})}}$$

$$CoV_{Cl_0} = \frac{\sigma_{(Cl_0)}}{\mu_{(Cl_0)}}$$

$CoV_{\Delta\theta_{0-1}}$ and CoV_{Cl_0} have been manually calibrated in order to reach the same experimental value of CoV_{PFP}, where PFP represents the peak firing pressure of the cycle.

In practice, $CoV_{\Delta\theta_{0-1}}$ has been fixed to 10% according to experimental analyses performed on the engine of Politecnico di Torino, while the only value of CoV_{Cl_0} has been actually tuned.

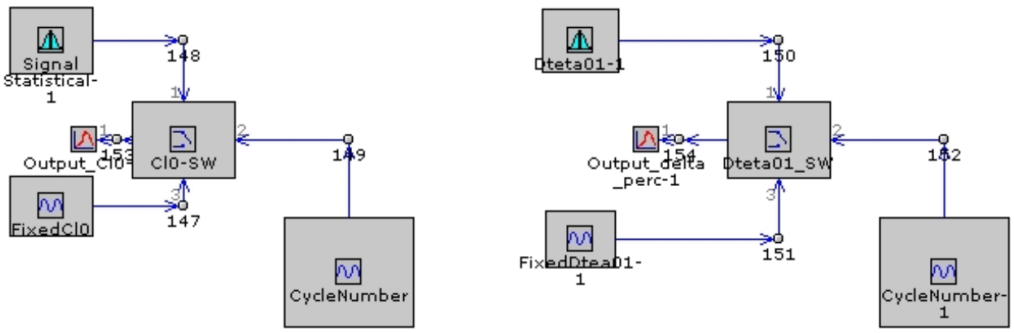

Figure 4.5 Model for cyclical dispersion introduction

The figure represents the model included to introduce the dispersion for $\Delta\theta_{0-1}$ and Cl_0.

4.2.2 Knock model

After cyclical dispersion definition, a knock detecting and counting code has been introduced in the GT-Power model of detonation tests. It is based on the previously described detonation algorithm

$$\int \frac{dt}{\tau} = 1 \qquad \text{with} \qquad \tau = c_1 p^{-c_2} e^{\frac{c_3}{T}}$$

When knock integral reaches the value 1 before the end of combustion, the cycle is considered as a knocking one. The number of detonating cycles is then stored and the percentage of knock is computed. Coefficient c_1 has been calibrated in order to match simulation results with experimental ones.

The following GT-Power model is then obtained.

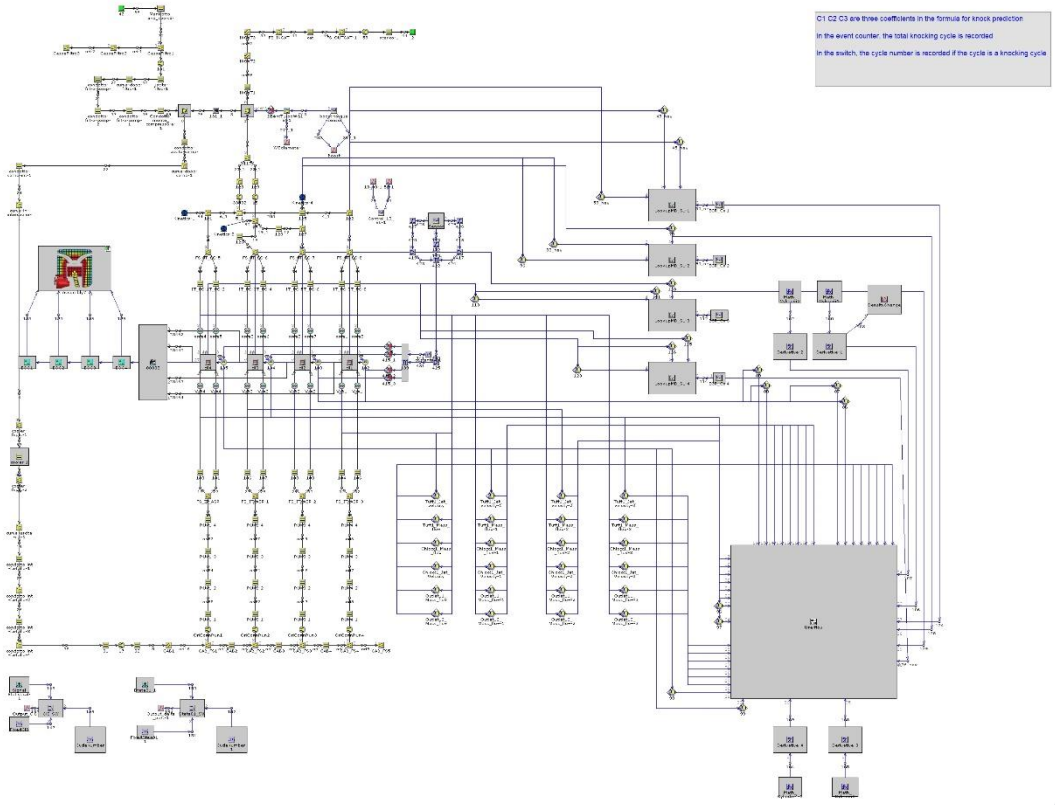

Figure 4.6 GT-Power model – knock detection implementation

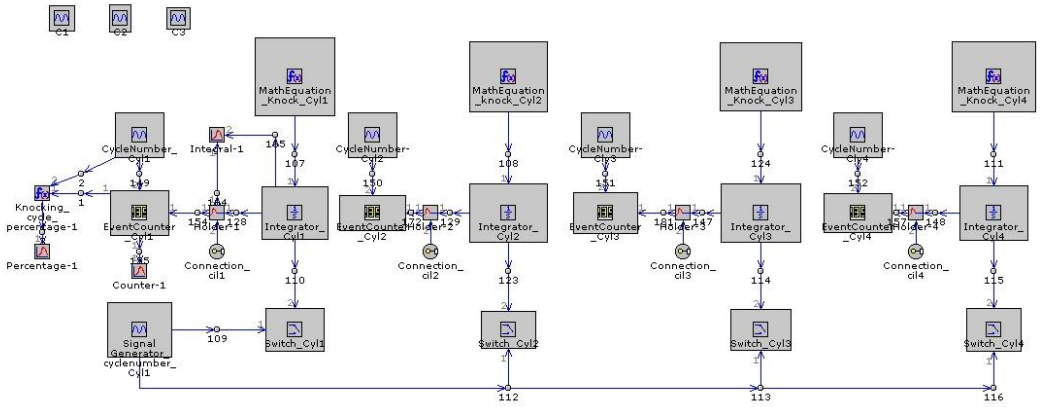

Figure 4.7 Knock detection and counting submodel

This last picture shows the submodel in care of computing the aforementioned integral and calculating the percentage of knocking cycles.

4.3 Calibration tests results

The whole above-mentioned procedure, except for knock algorithm implementation, has been applied to analyse the following tests, taken by the engine map. They are useful to characterize the engine and to calibrate and validate the model behaviour.

TEST ID	SPEED [RPM]	BMEP [bar]
0088	2000	4
0268	2000	8
1758	2500	13
0397	3000	3
0534	4000	5

Table 4.1 Calibration tests

4.3.1 TPA – calibration tests

Applying TPA to the model, fluidodynamic behaviour is verified. The following figures and tables show normalised simulated and experimental pressure cycles relative to cylinder #1, as well as intake manifold pressure and temperature and air and fuel mass flow rates. As can be observed, all the data computed by simulation and collected fit quite well experimental measurements.

Therefore, the model can be considered validated, and trend of burnt mass fraction x_b, which comes from it, plausibly true.

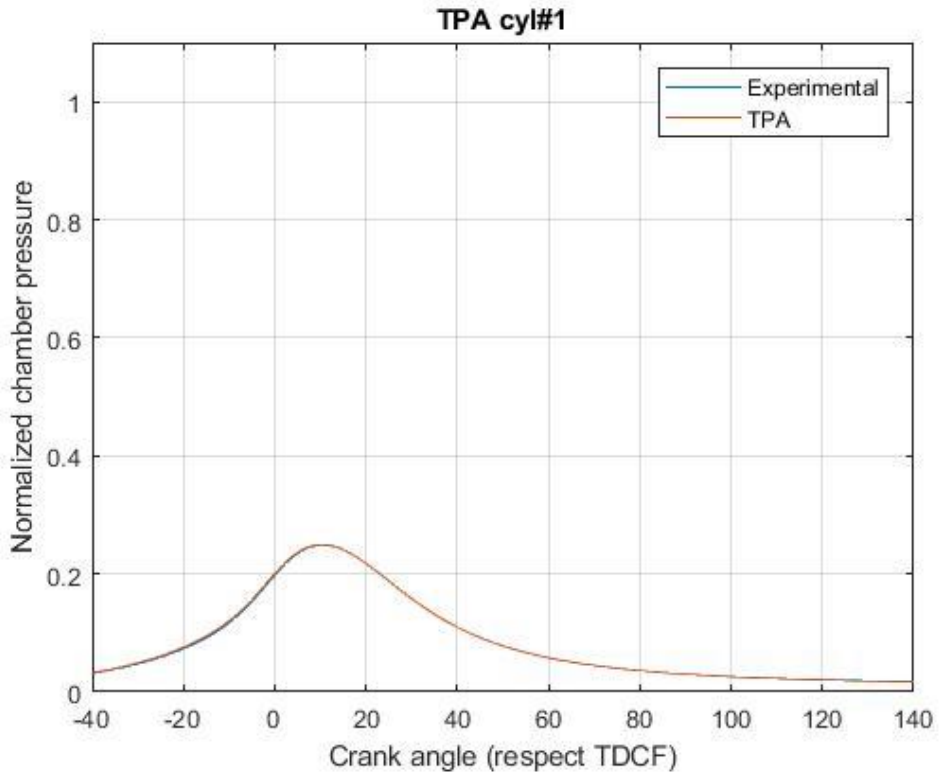

Figure 4.8 TPA 0088 – pressure cycle cyl#1

TEST ID 0088	[]	Experimental	Simulation result (TPA)
Intake manifold pressure	[bar]	1.024	1.024
Intake manifold temperature	[K]	311	309
Fuel mass flow rate	[kg/h]	2.28	2.14
Air mass flow rate	[kg/h]	39	37

Table 4.2 TPA 0088 – additional results

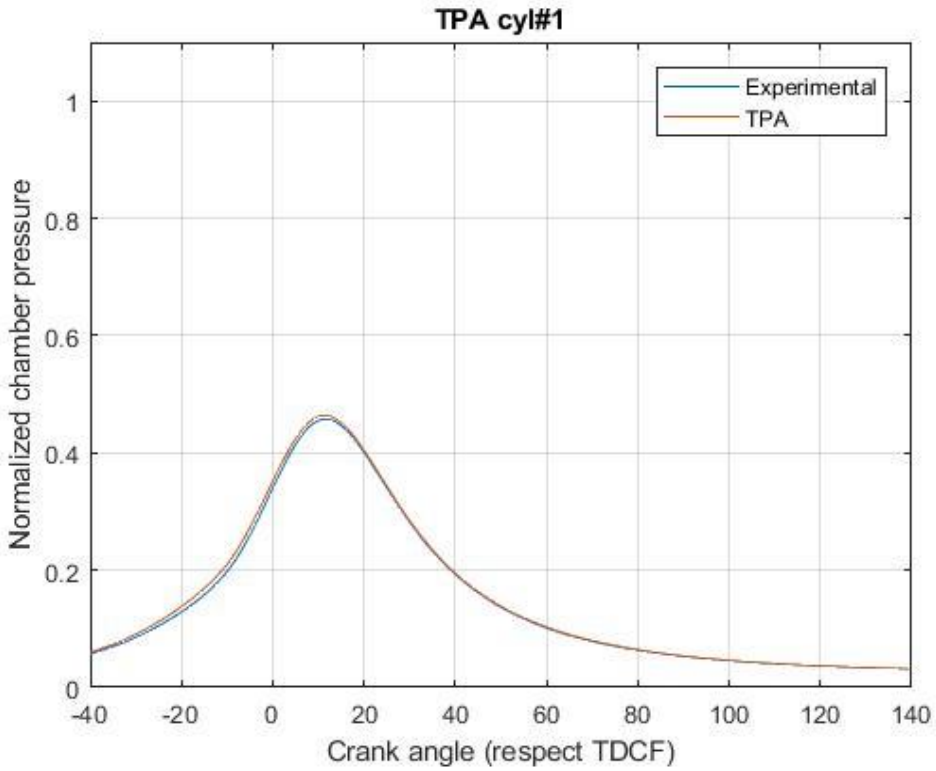

Figure 4.9 TPA 0268 – pressure cycle cyl#1

TEST ID 0268	[]	Experimental	Simulation result (TPA)
Intake manifold pressure	[bar]	1.147	1.147
Intake manifold temperature	[K]	311	310
Fuel mass flow rate	[kg/h]	3.91	3.86
Air mass flow rate	[kg/h]	67	66

Table 4.3 TPA 0268 – additional results

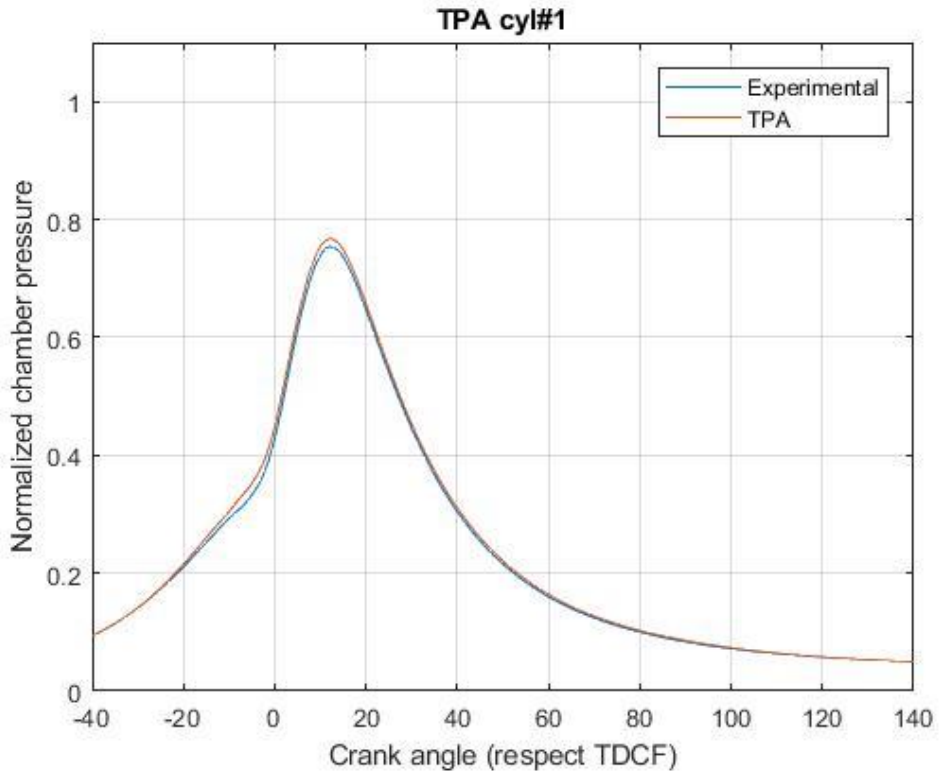

Figure 4.10 TPA 1758 – pressure cycle cyl#1

TEST ID 1758	[]	Experimental	Simulation result (TPA)
Intake manifold pressure	[bar]	1.279	1.279
Intake manifold temperature	[K]	313	310
Fuel mass flow rate	[kg/h]	7.68	7.56
Air mass flow rate	[kg/h]	131	129

Table 4.4 TPA 1758 – additional results

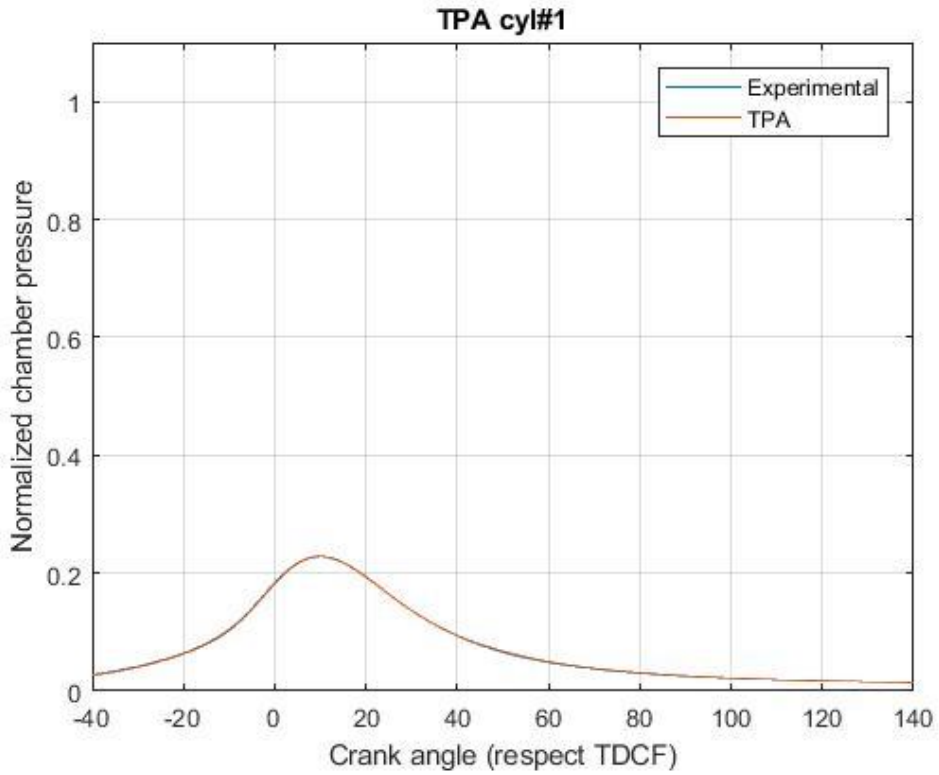

Figure 4.11 TPA 0397 – pressure cycle cyl#1

TEST ID 0397	[]	Experimental	Simulation result (TPA)
Intake manifold pressure	[bar]	1.058	1.058
Intake manifold temperature	[K]	313	312
Fuel mass flow rate	[kg/h]	2.93	2.73
Air mass flow rate	[kg/h]	50	47

Table 4.5 TPA 0397 – additional results

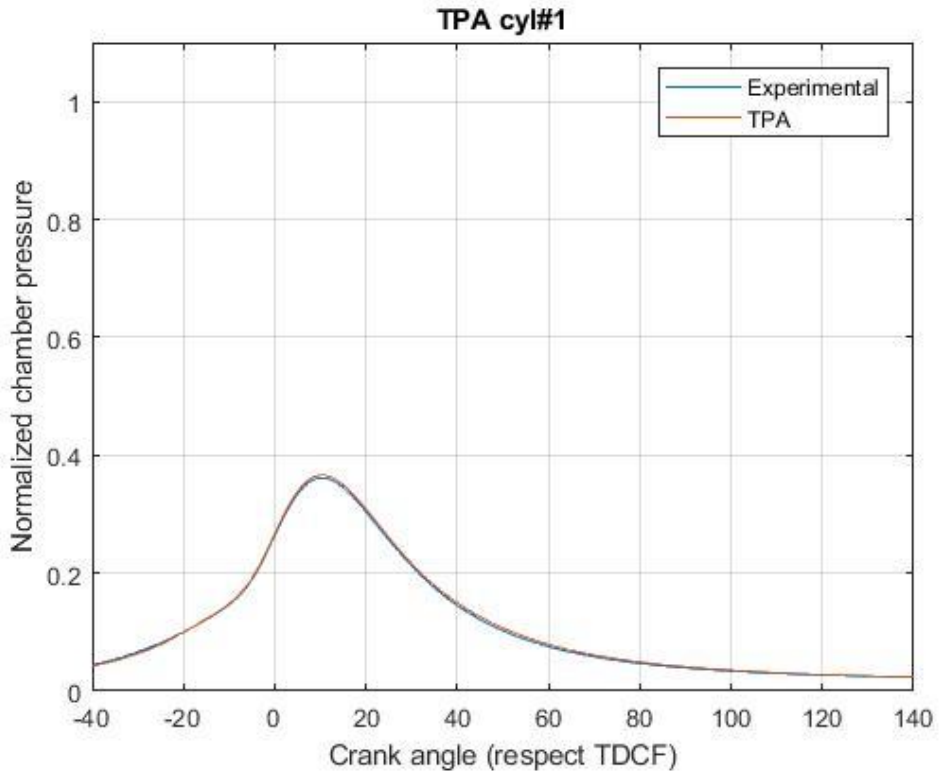

Figure 4.12 TPA 0534 – pressure cycle cyl#1

TEST ID 0534	[]	Experimental	Simulation result (TPA)
Intake manifold pressure	[bar]	1.225	1.225
Intake manifold temperature	[K]	316	315
Fuel mass flow rate	[kg/h]	5.97	5.71
Air mass flow rate	[kg/h]	103	99

Table 4.6 TPA 0534 – additional results

4.3.2 Fractal combustion model – calibration tests

In this chapter, results obtained applying fractal model to calibration tests are outlined, showing resulting simulated pressure cycle. In the following table, manually tuned values of $\Delta\theta_{0-1}$, Cl_0 and cwc are reported, remembering that their evaluation has been made by means of burn rate calibration on the basis of the one obtained through TPA, assuming this last representative of the actual one.

TEST ID	WORKING POINT	$\Delta\theta_{0-1}$	Cl_0	cwc
0088	2000x4	20.7	0.13	0.14
0268	2000x8	12.5	0.25	0.05
1758	2500x13	4.3	1.00	0.01
0397	3000x3	15.5	0.16	0.01
0534	4000x5	10	0.21	0.01

Table 4.7 Fractal model – characterisc parameters value – calibration tests

Following pictures prove the good fitting of simulated pressure, consequence of the appropriate tuning of mass fraction burnt curve. It is important that both incubation and rapid burning phases can be superimposed, while, for the last part of combustion, being heat release quite low, fitting is not fundamental. Moreover, some post-reactions are not evaluated by the model.

Next step should be the development of a regression model, able to compute the values of abovementioned parameters starting from the evaluation of engine geometry and its operating and thermodynamic conditions.

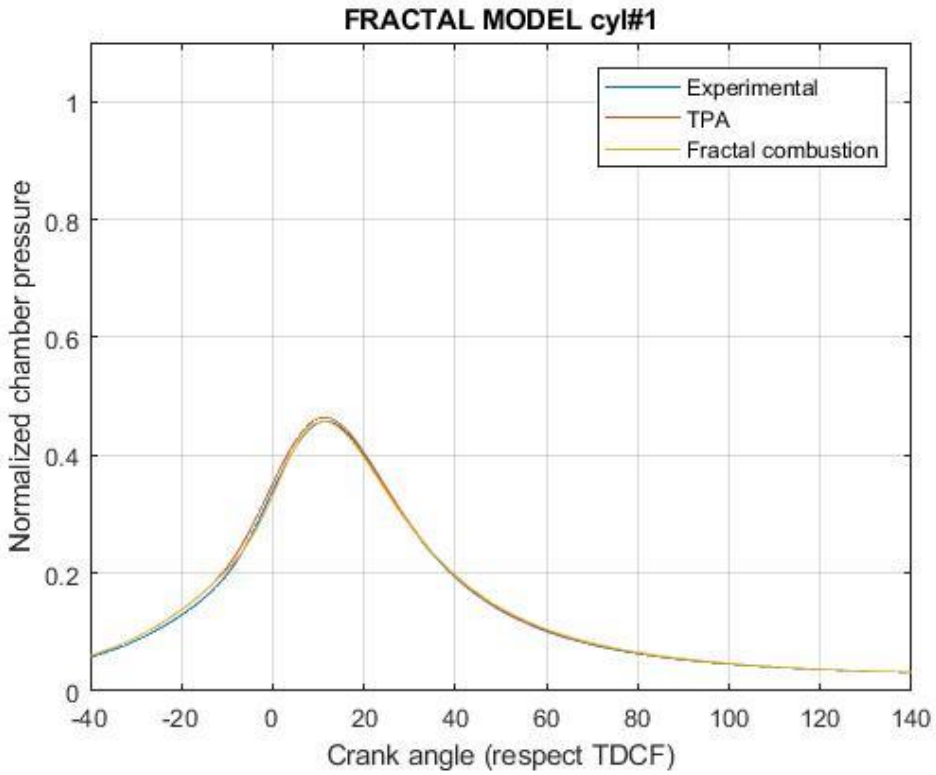

Figure 4.13 Fractal combustion 0088 – pressure cycle cyl#1

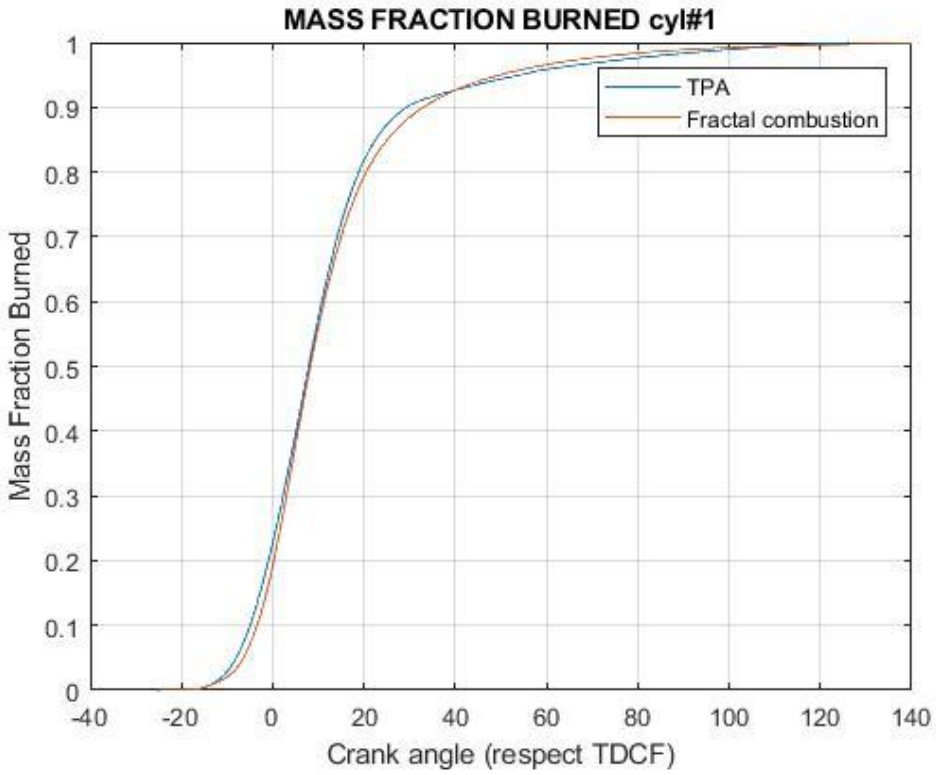

Figure 4.14 Fractal combustion 0088 – mass fraction burnt cyl#1

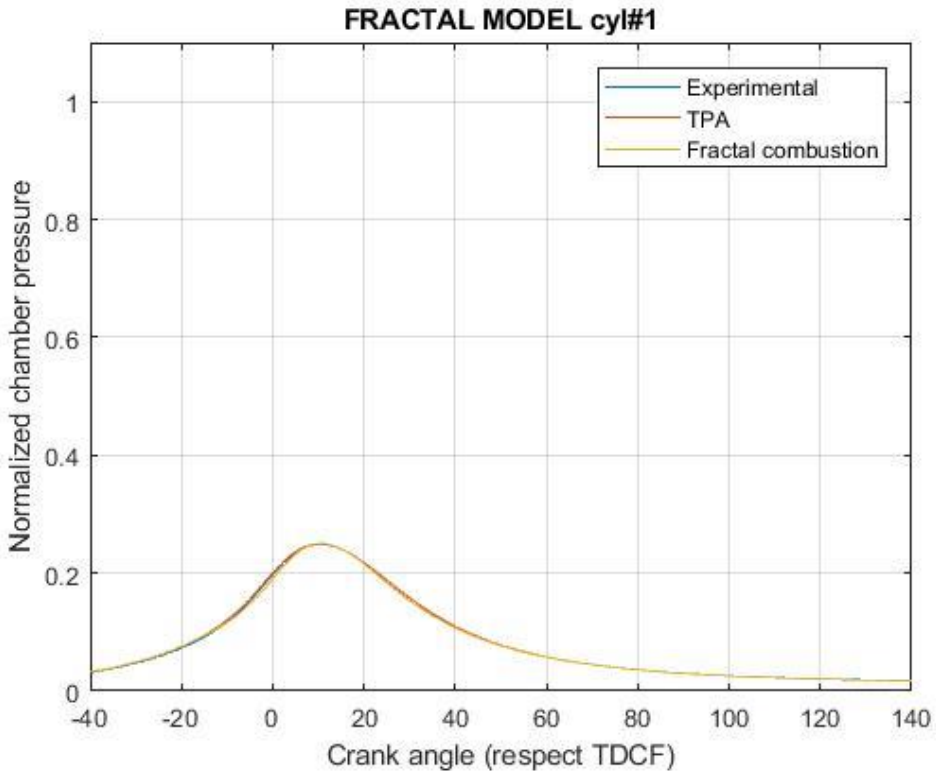

Figure 4.15 Fractal combustion 0268 – pressure cycle cyl#1

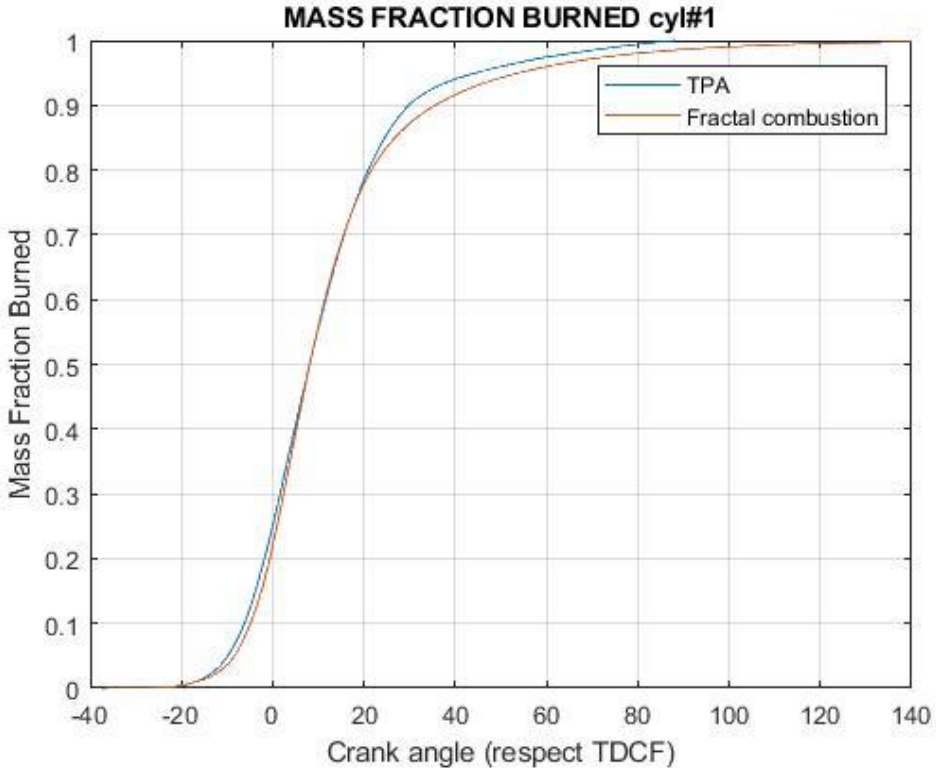

Figure 4.16 Fractal combustion 0268 – mass fraction burnt cyl#1

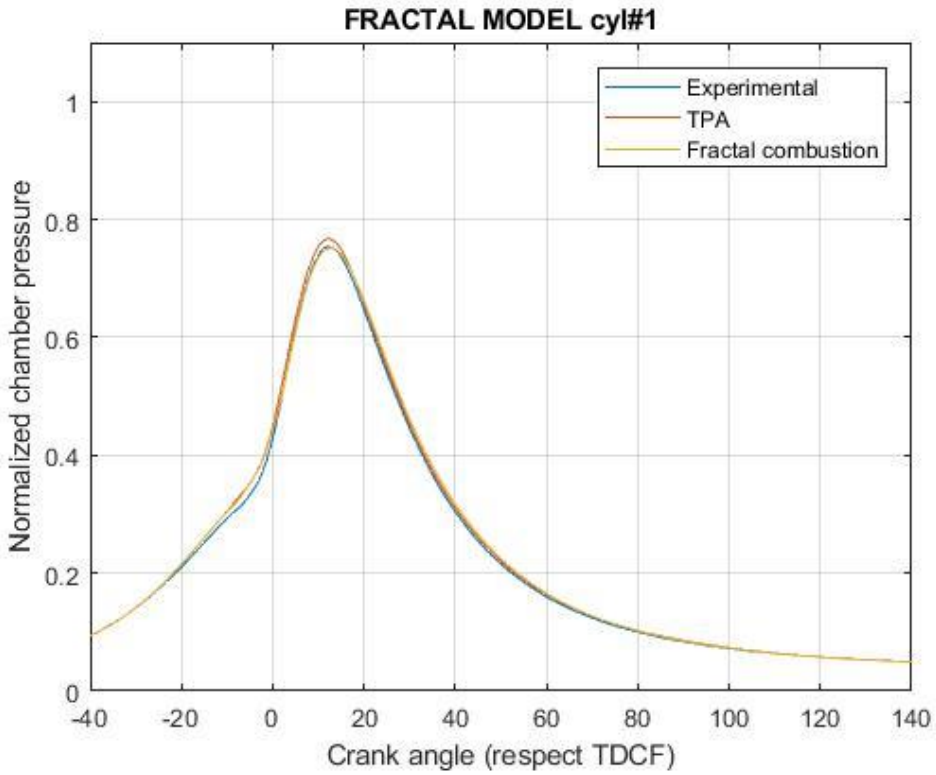

Figure 4.17 Fractal combustion 1758 – pressure cycle cyl#1

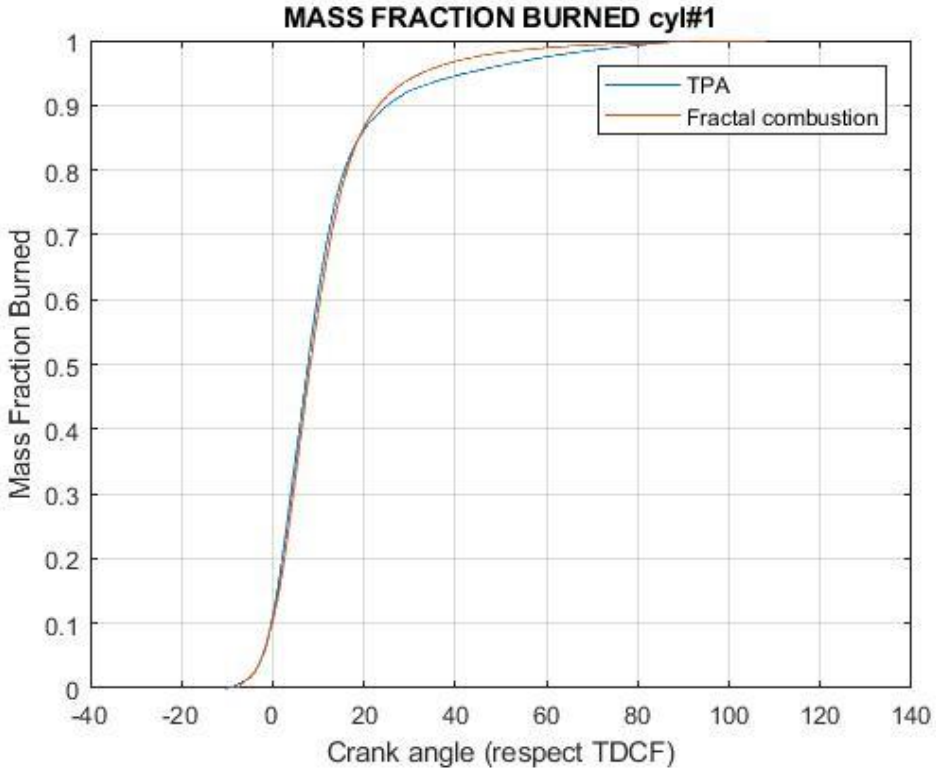

Figure 4.18 Fractal combustion 1758 – mass fraction burnt cyl#1

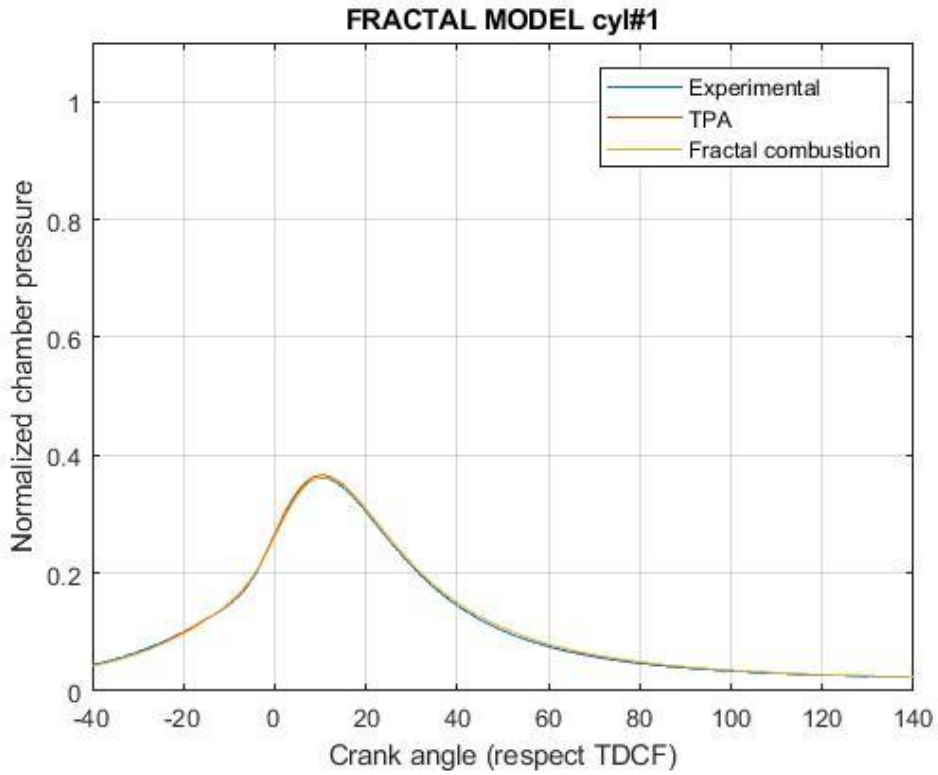

Figure 4.19 Fractal combustion 0397 – pressure cycle cyl#1

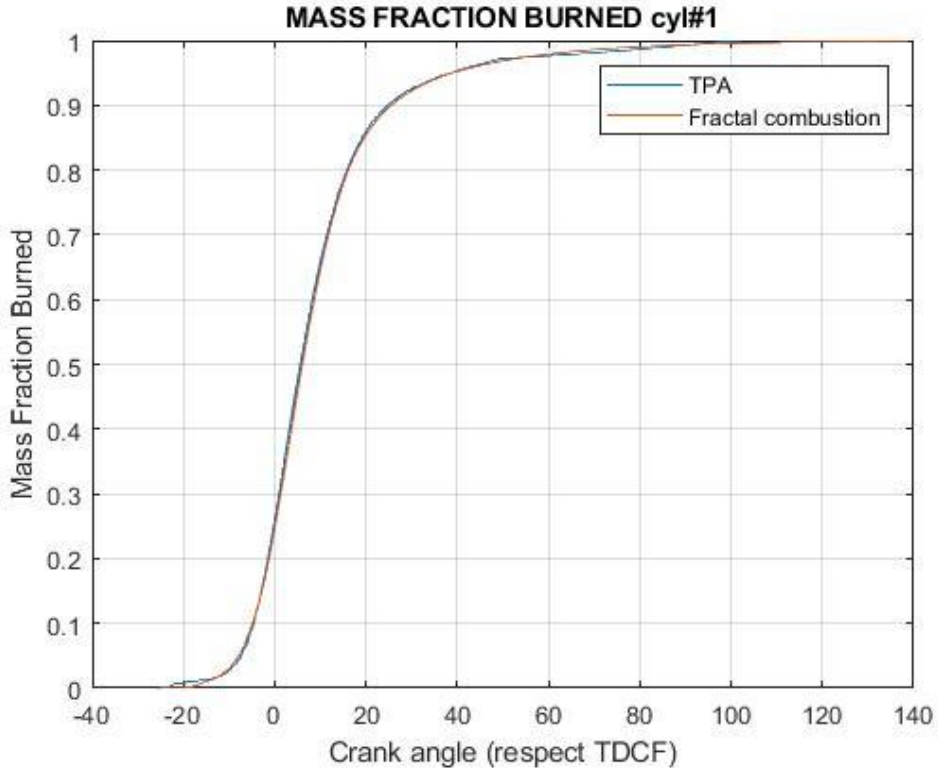

Figure 4.20 Fractal combustion 0397 – mass fraction burnt cyl#1

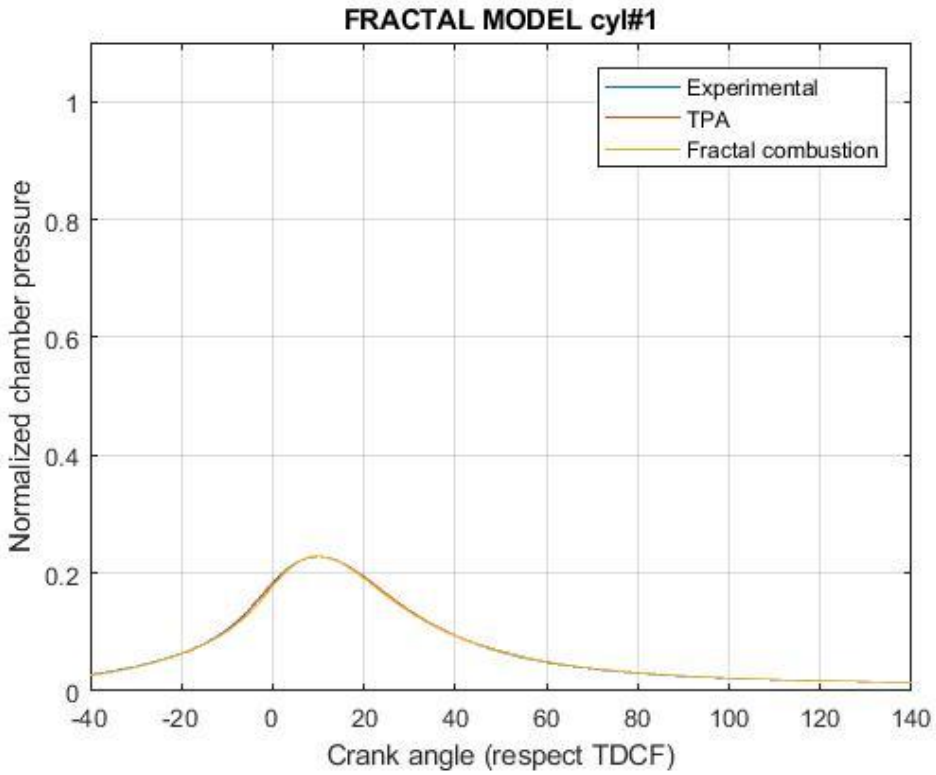

Figure 4.21 Fractal combustion 0534 – pressure cycle cyl#1

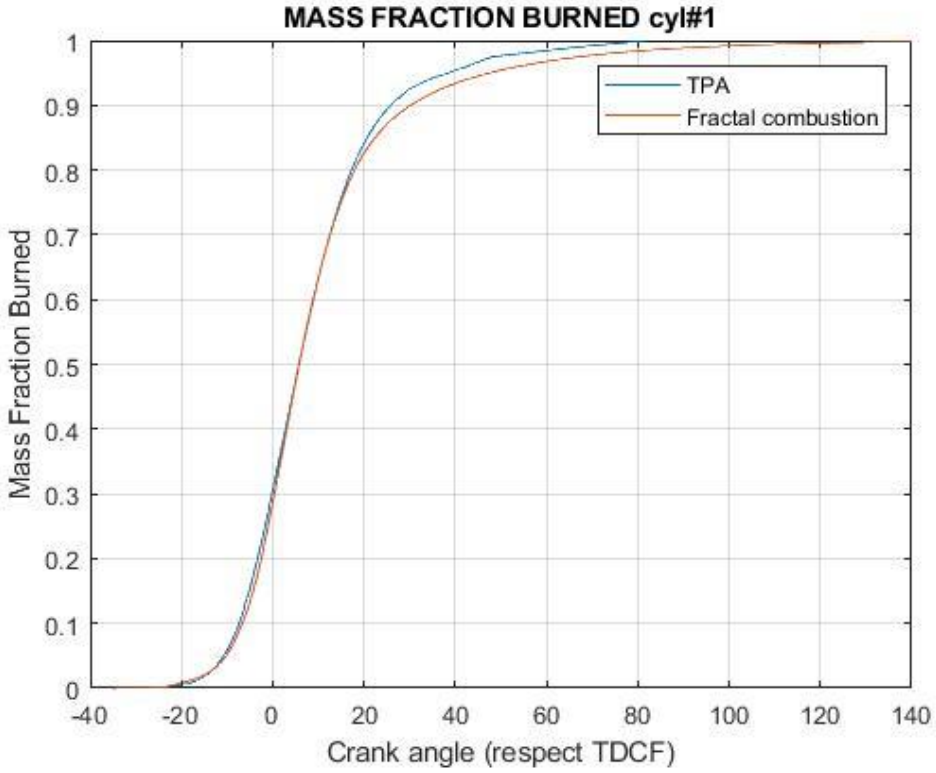

Figure 4.22 Fractal combustion 0534 – mass fraction burnt cyl#1

4.3.3 Cyclical dispersion model – calibration tests

In order to simulate cycle-to-cycle variability, a dispersion model has been included for the values of $\Delta\theta_{0-1}$ and a Cl_0, defining for each of them a Coefficient of Variation, manually calibrated, that would produce the same CoV_{PFP} experimentally observed.

The following table resumes obtained results. As mentioned before, $CoV_{\Delta\theta_{0-1}}$ value is kept constant and equal to 10% while CoV_{Cl_0} is varied in order to fit experimental data.

TEST ID	Working point	CoV_{Cl_0}	$CoV_{\Delta\theta_{0-1}}$	CoV_{PFP} (simulated)	CoV_{PFP} (experimental)
0088	2000x4	45%	10%	9.67%	9.97%
0268	2000x8	40%	10%	7.71%	7.87%
1758	2500x13	28%	10%	4.55%	4.56%
0397	3000x3	48%	10%	9.41%	9.22%
0534	4000x5	38%	10%	7.49%	7.38%

Table 4.8 Fractal model –coefficients of variation values - calibration tests

As for fractal combustion model parameters, also for cyclical dispersion evaluation a regression model should be required to correctly forecast CoV values.

4.4 Knock tests results – spark advance sweep at full load

The same procedure applied to calibration tests has been performed on a group of knock tests. All these working points share the same operating conditions except for the spark advance. Increasing its value enhances knock tendency.

The following table summarizes tests working conditions.

TEST ID	SPEED [RPM]	P_{MAX} [kPa]	SPARK ADVANCE [°CA]	EXPERIMENTAL DETONATING CYCLES (%)
1977	2000	10800	7.00	0
1978	2000	11000	7.59	0
1979	2000	11200	8.16	0
1980	2000	11400	8.60	1.5
1981	2000	11600	9.14	5
1982	2000	11800	9.72	10
1983	2000	11900	10.01	15
1985	2000	11950	9.93	15

Table 4.9 Detonation tests

Moreover, an increase in the spark advance will anticipate the occurrence of peak firing pressure and will increase its value, as shown in the following picture.

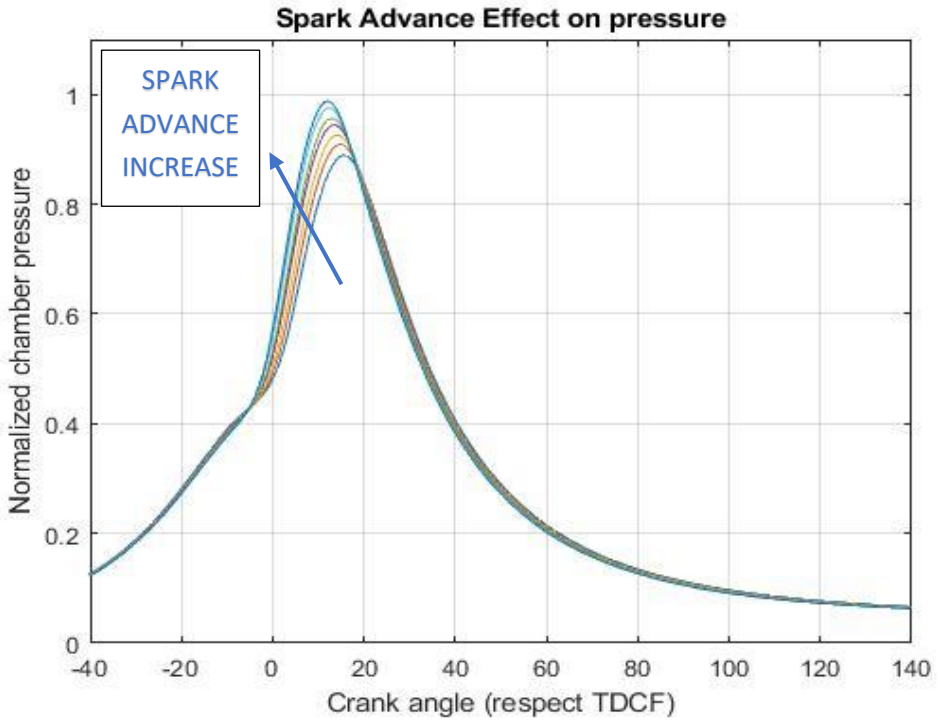

Figure 4.23 Spark advance effect on pressure cycle

4.4.1 TPA – knock tests

Also in these tests, fluidodynamics of the model are verified. Following pictures represent TPA results. Pressure cycle trends, as well as intake manifold pressure and temperature and air and fuel mass flow rates are compared.

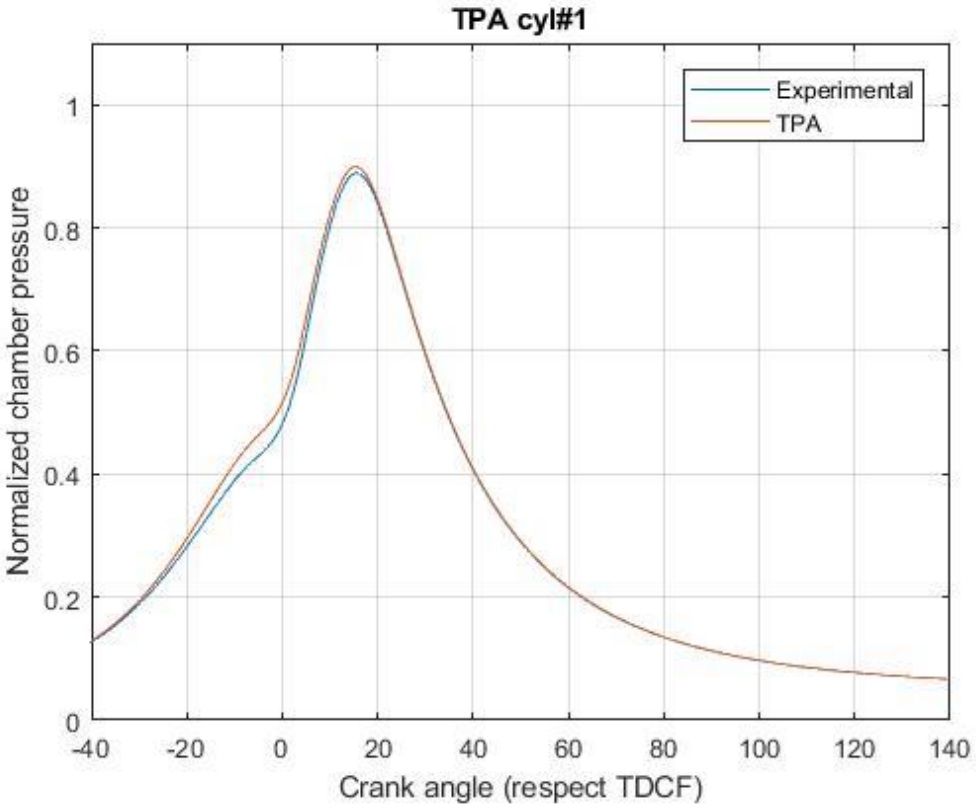

Figure 4.24 TPA 1977 – pressure cycle cyl#1

TEST ID 1977	[]	Experimental	Simulation result (TPA)
Intake manifold pressure	[bar]	1.741	1.741
Intake manifold temperature	[K]	349	354
Fuel mass flow rate	[kg/h]	8.01	7.77
Air mass flow rate	[kg/h]	136	132

Table 4.10 TPA 1977 – additional results

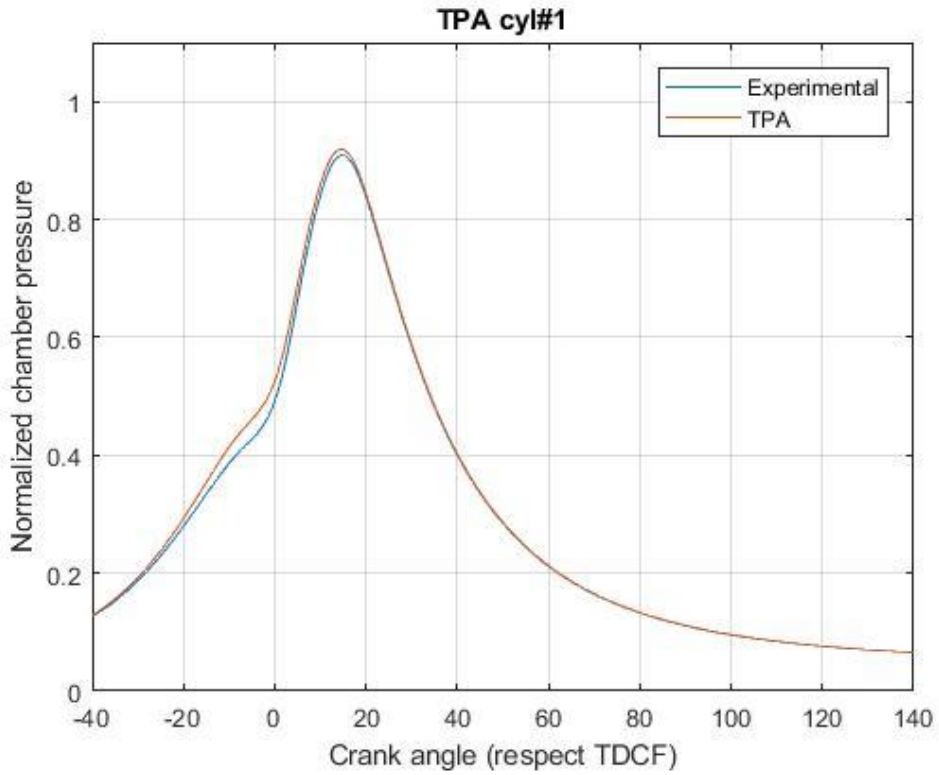

Figure 4.25 TPA 1978 – pressure cycle cyl#1

TEST ID 1978	[]	Experimental	Simulation result (TPA)
Intake manifold pressure	[bar]	1.728	1.728
Intake manifold temperature	[K]	350	354
Fuel mass flow rate	[kg/h]	7.94	7.71
Air mass flow rate	[kg/h]	135	131

Table 4.11 TPA 1978 – additional results

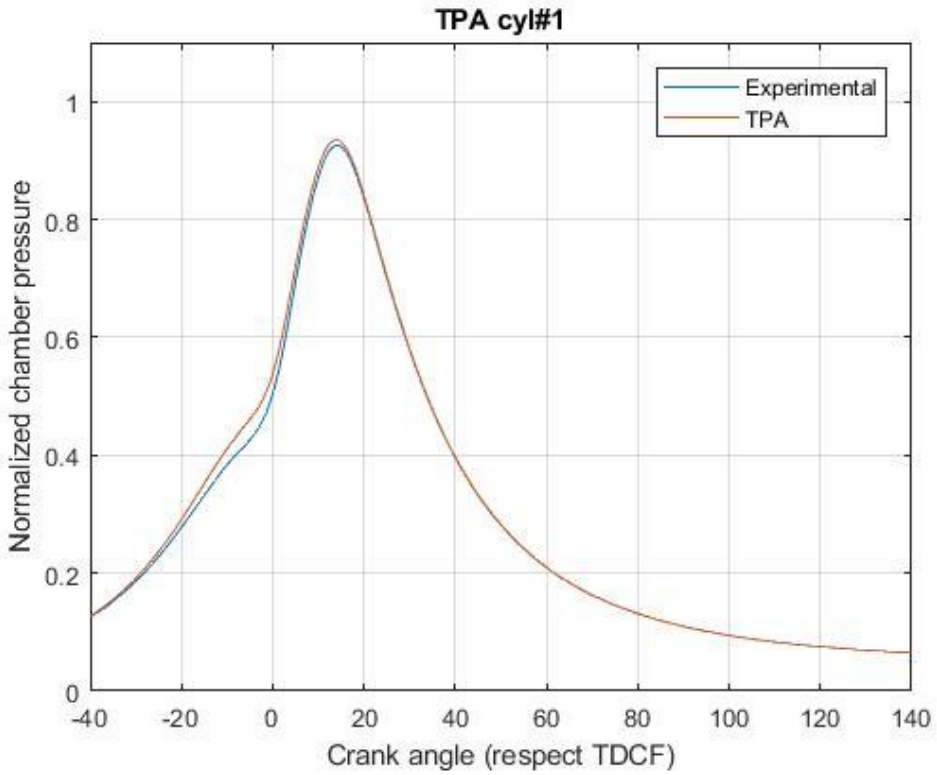

Figure 4.26 TPA 1979 – pressure cycle cyl#1

TEST ID 1979	[]	Experimental	Simulation result (TPA)
Intake manifold pressure	[bar]	1.717	1.717
Intake manifold temperature	[K]	350	354
Fuel mass flow rate	[kg/h]	7.88	7.66
Air mass flow rate	[kg/h]	133	130

Table 4.12 TPA 1979 – additional results

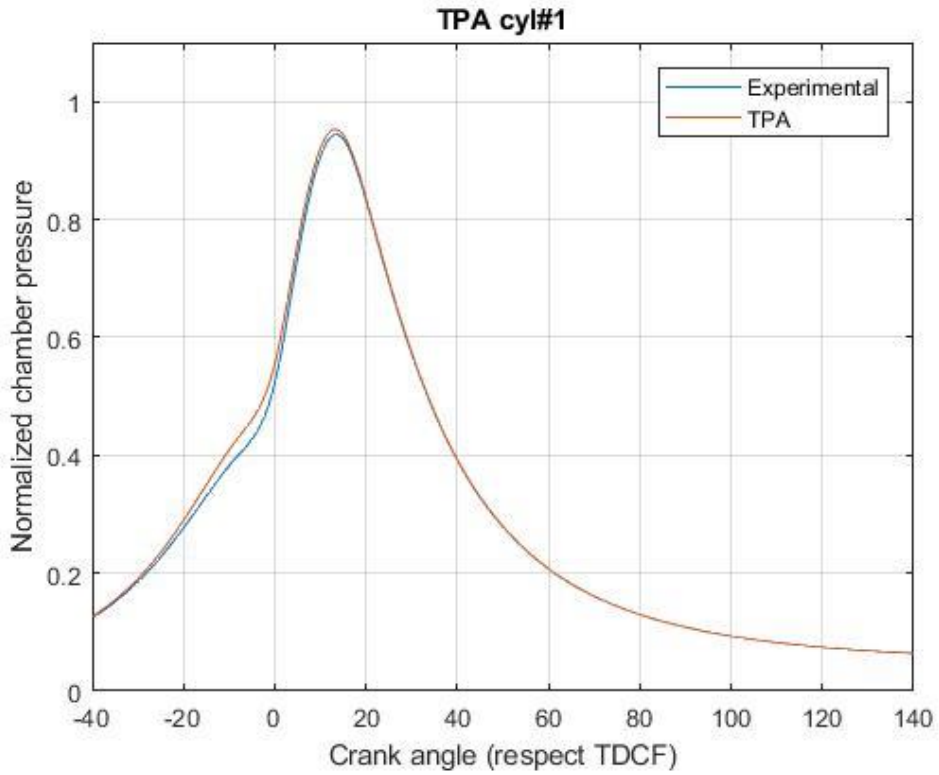

Figure 4.27 TPA 1980 – pressure cycle cyl#1

TEST ID 1980	[]	Experimental	Simulation result (TPA)
Intake manifold pressure	[bar]	1.708	1.708
Intake manifold temperature	[K]	350	354
Fuel mass flow rate	[kg/h]	7.82	7.61
Air mass flow rate	[kg/h]	133	129

Table 4.13 TPA 1980 – additional results

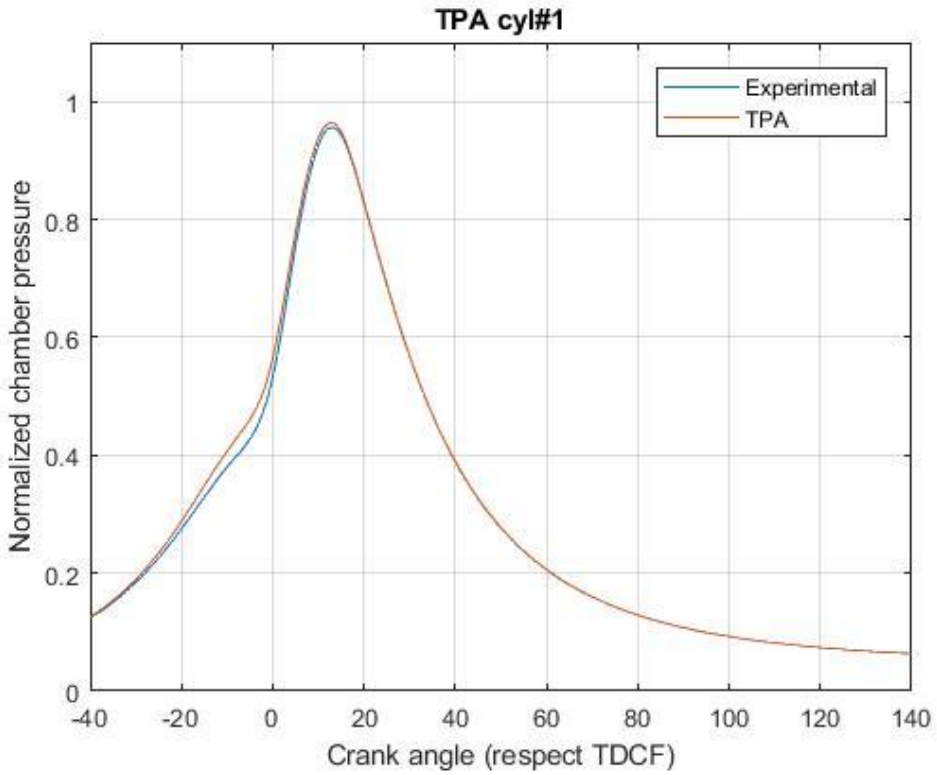

Figure 4.28 TPA 1981 – pressure cycle cyl#1

TEST ID 1981	[]	Experimental	Simulation result (TPA)
Intake manifold pressure	[bar]	1.700	1.700
Intake manifold temperature	[K]	350	354
Fuel mass flow rate	[kg/h]	7.78	7.58
Air mass flow rate	[kg/h]	132	129

Table 4.14 TPA 1981 – additional results

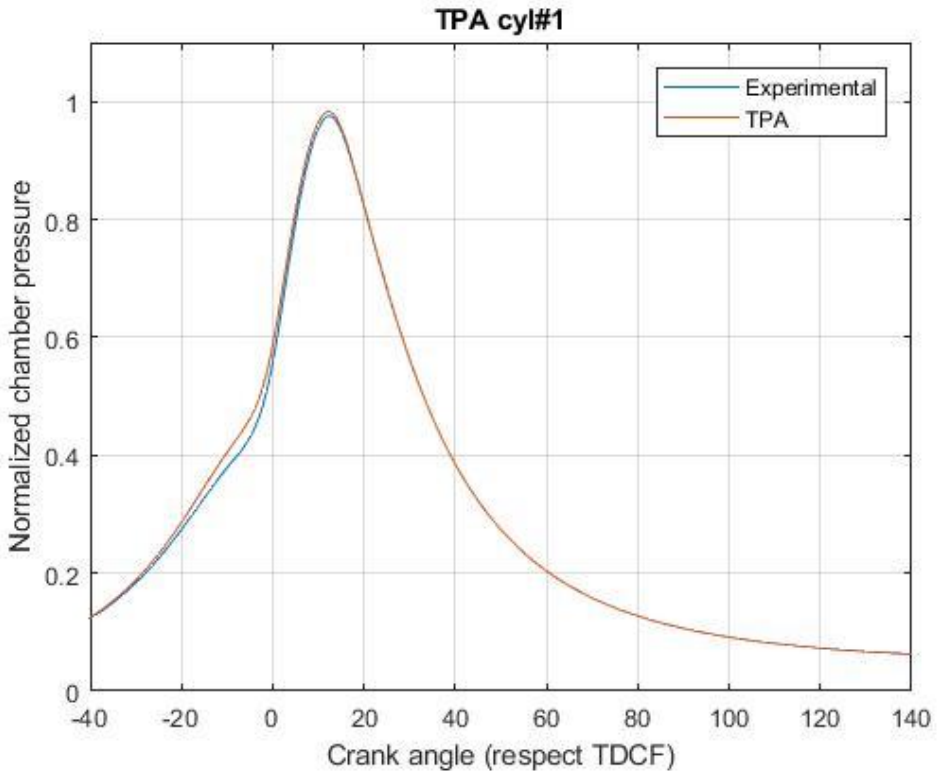

Figure 4.29 TPA 1982 – pressure cycle cyl#1

TEST ID 1982	[]	Experimental	Simulation result (TPA)
Intake manifold pressure	[bar]	1.689	1.689
Intake manifold temperature	[K]	350	354
Fuel mass flow rate	[kg/h]	7.71	7.53
Air mass flow rate	[kg/h]	131	128

Table 4.15 TPA 1982 – additional results

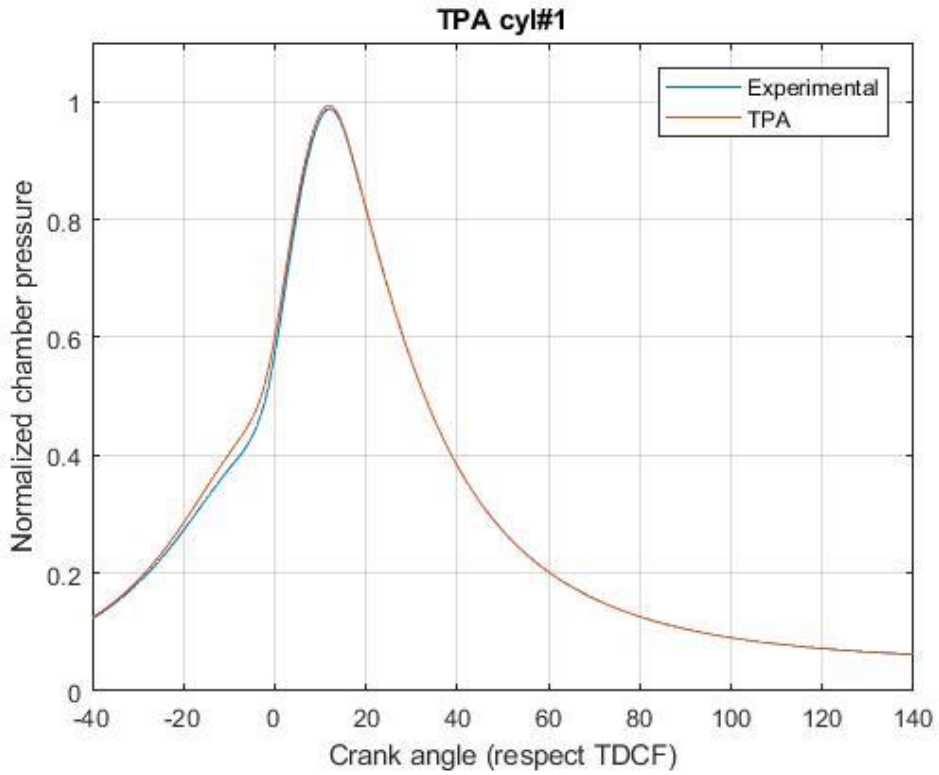

Figure 4.30 TPA 1983 – pressure cycle cyl#1

TEST ID 1983	[]	Experimental	Simulation result (TPA)
Intake manifold pressure	[bar]	1.683	1.683
Intake manifold temperature	[K]	351	355
Fuel mass flow rate	[kg/h]	7.69	7.50
Air mass flow rate	[kg/h]	130	127

Table 4.16 TPA 1983 – additional results

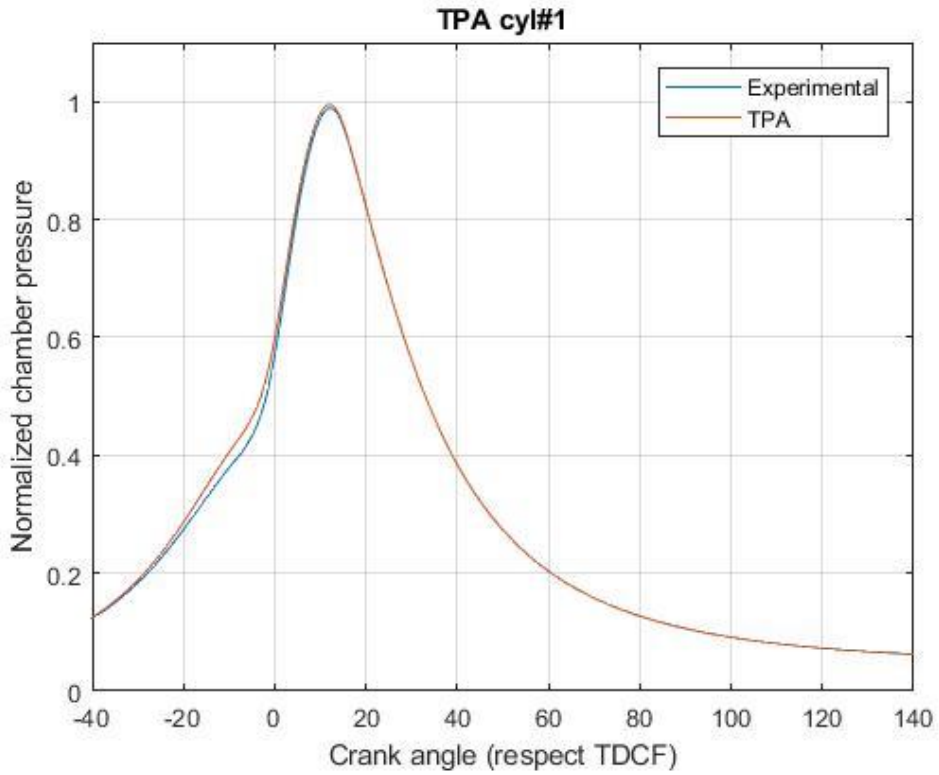

Figure 4.31 TPA 1985 – pressure cycle cyl#1

TEST ID 1985	[]	Experimental	Simulation result (TPA)
Intake manifold pressure	[bar]	1.690	1.690
Intake manifold temperature	[K]	350	354
Fuel mass flow rate	[kg/h]	7.72	7.53
Air mass flow rate	[kg/h]	131	128

Table 4.17 TPA 1985 – additional results

4.4.2 Fractal combustion model – knock tests

The same procedure applied to calibration points has been performed on knock tests in order to evaluate characteristic fractal combustion parameters. The following results have been obtained, also in this case by means of a manual tuning, trying to reproduce mass fraction burnt curve obtained by TPA.

TEST ID	SPEED [RPM]	P_{MAX} [kPa]	SA [°CA]	$\Delta\theta_{0-1}$	Cl_0	cwc
1977	2000	10800	7.00	4.8	1.30	0.1
1978	2000	11000	7.59	4.9	1.25	0.1
1979	2000	11200	8.16	4.5	1.10	0.1
1980	2000	11400	8.60	4.3	1.00	0.1
1981	2000	11600	9.14	4.3	0.90	0.1
1982	2000	11800	9.72	4.3	0.85	0.1
1983	2000	11900	10.01	4.5	0.85	0.1
1985	2000	11950	9.93	4.3	0.85	0.1

Table 4.18 Fractal model – characterisc parameters value – knock tests

It should be necessary to introduce a regression model in order to be able to predict combustion parameters, avoiding manual tuning.

Following pictures show the comparison between simulated and measured pressure cycles and burn rates for detonation tests, both well fitted.

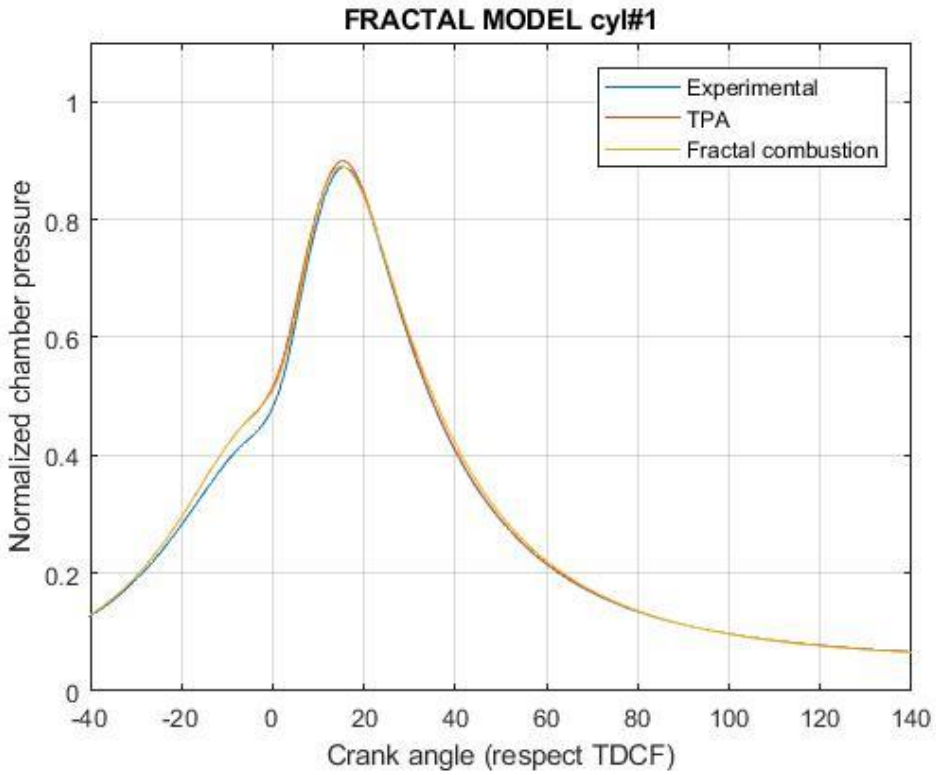

Figure 4.32 Fractal combustion 1977 – pressure cycle cyl#1

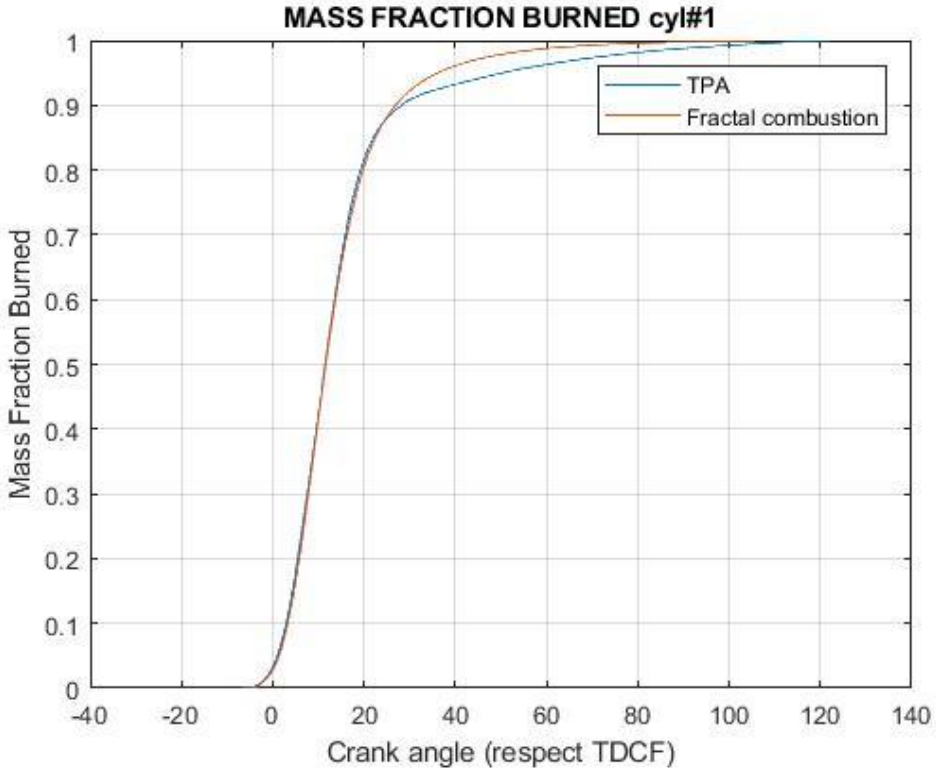

Figure 4.33 Fractal combustion 1977 – mass fraction burnt cyl#1

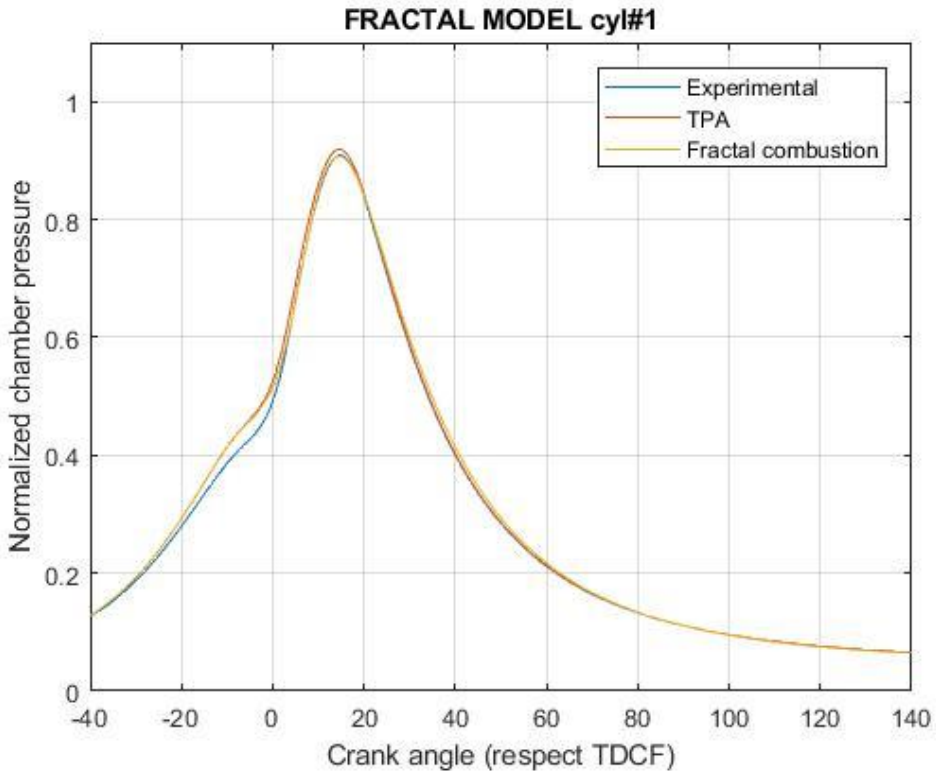

Figure 4.34 Fractal combustion 1978 – pressure cycle cyl#1

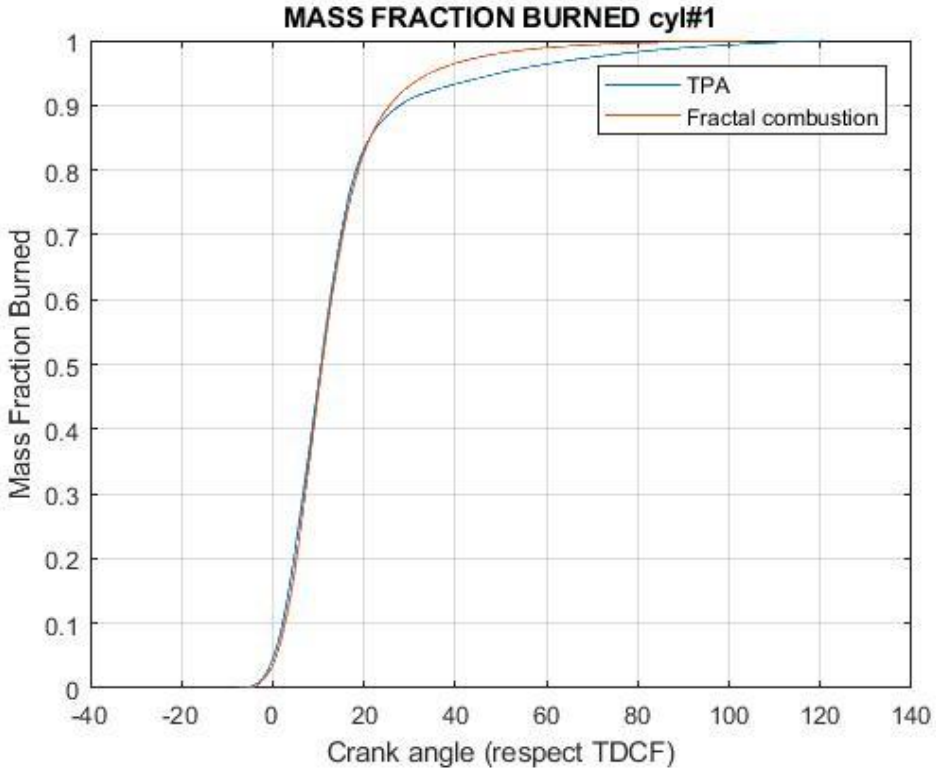

Figure 4.35 Fractal combustion 1978 – mass fraction burnt cyl#1

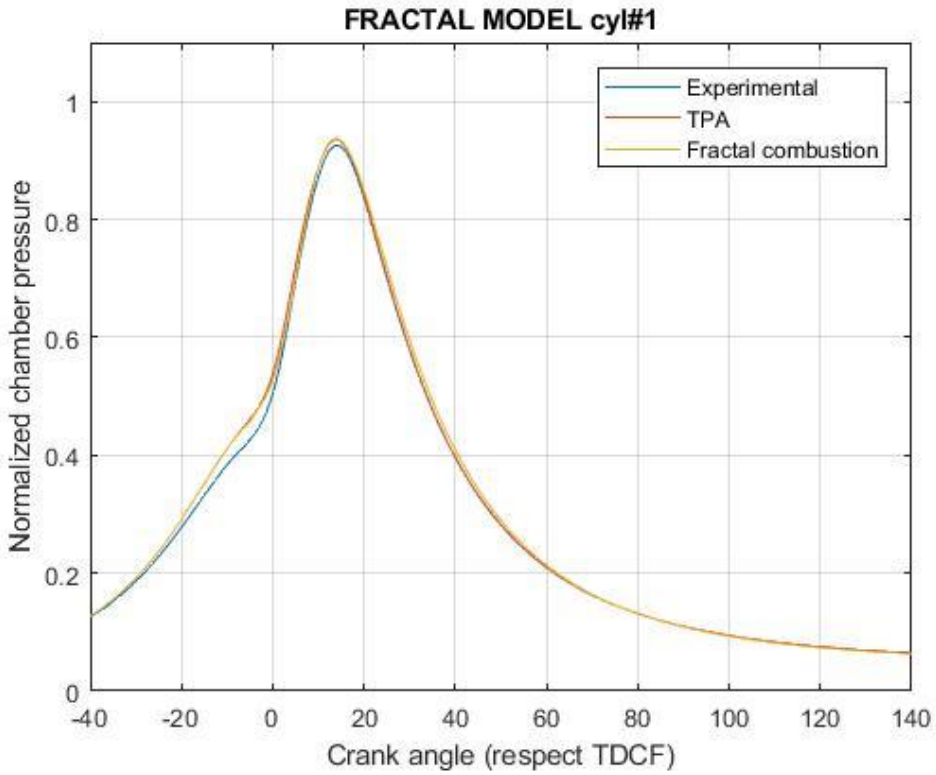

Figure 4.36 Fractal combustion 1979 – pressure cycle cyl#1

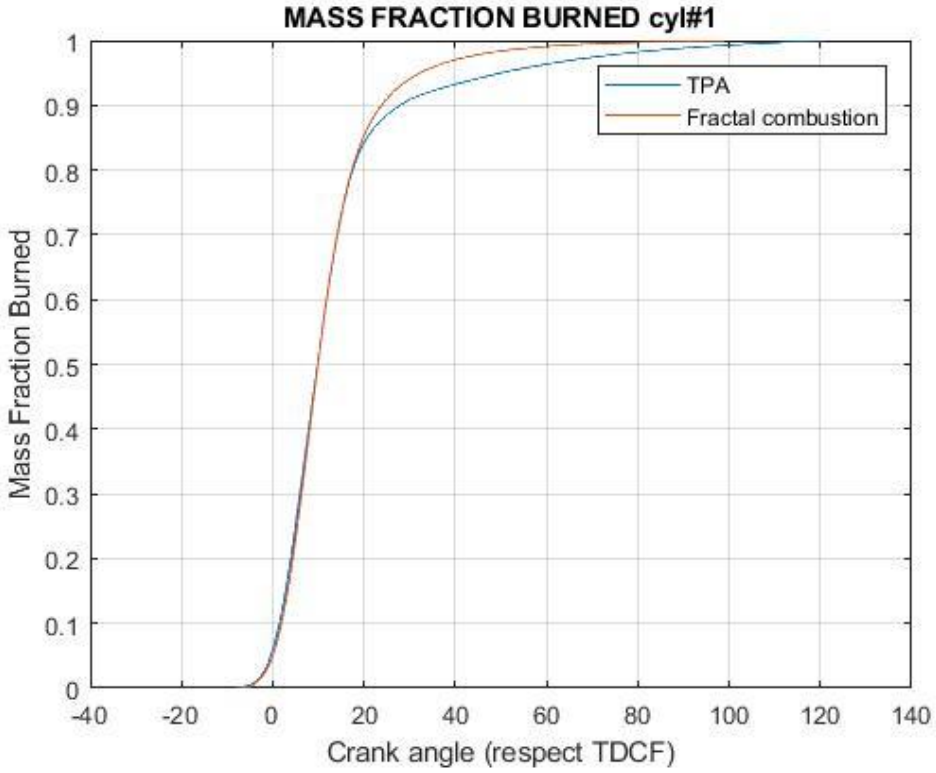

Figure 4.37 Fractal combustion 1979 – mass fraction burnt cyl#1

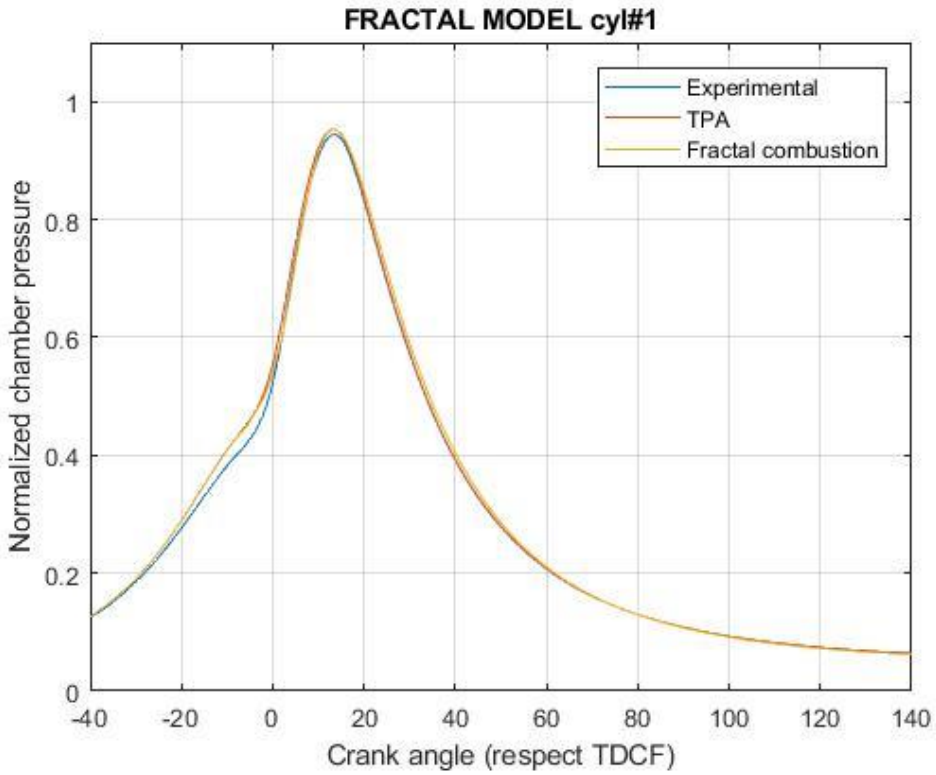

Figure 4.38 Fractal combustion 1980 – pressure cycle cyl#1

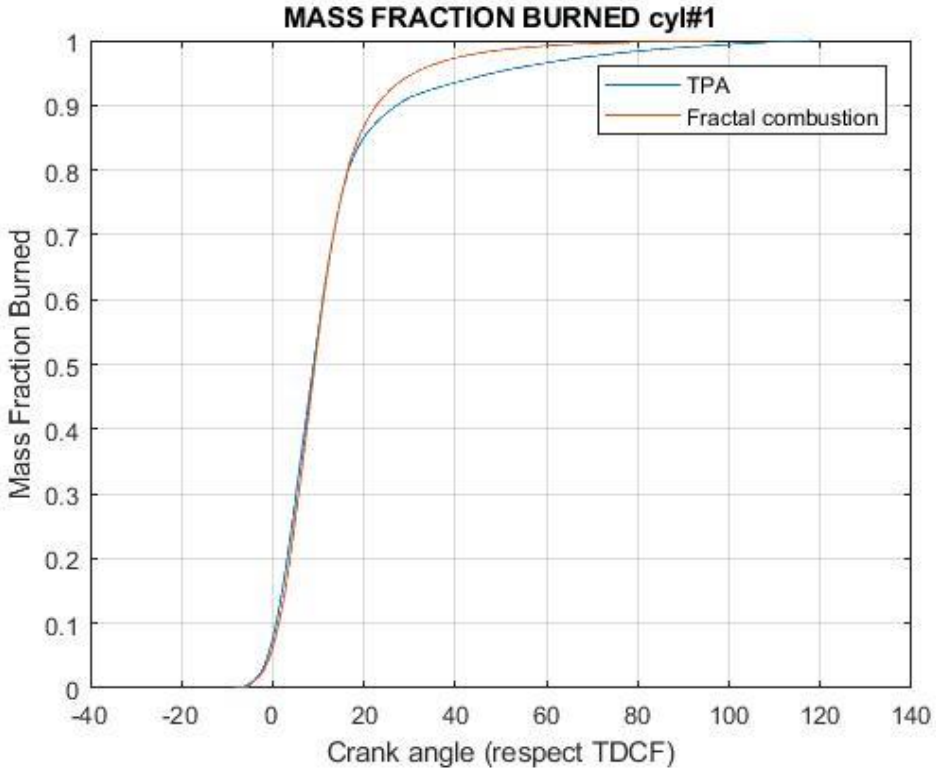

Figure 4.39 Fractal combustion 1980 – mass fraction burnt cyl#1

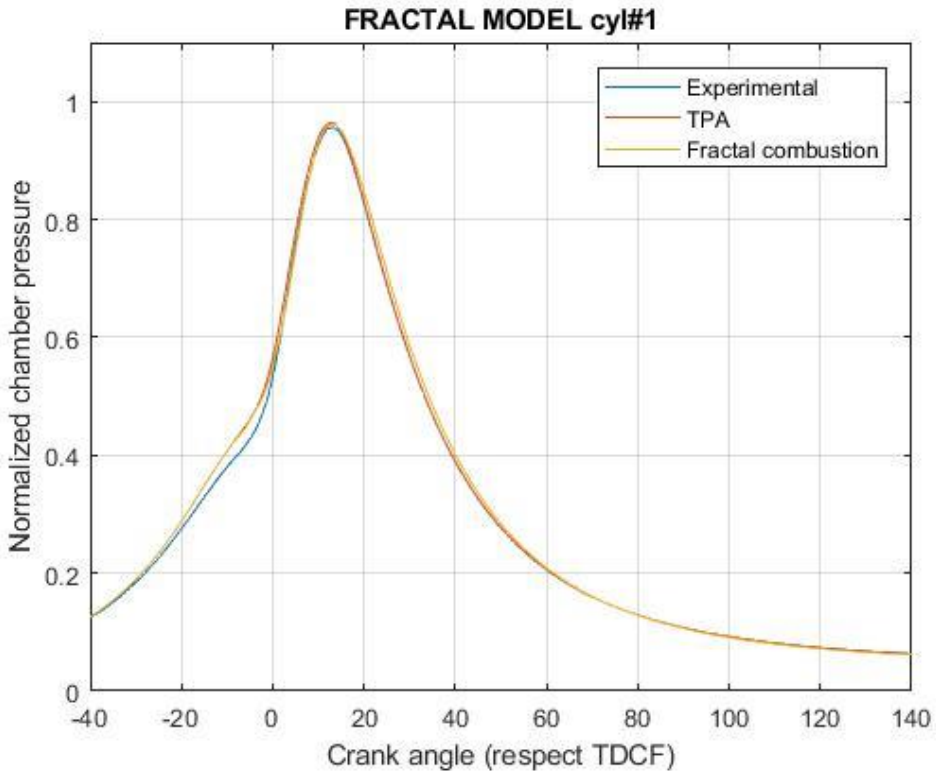

Figure 4.40 Fractal combustion 1981 – pressure cycle cyl#1

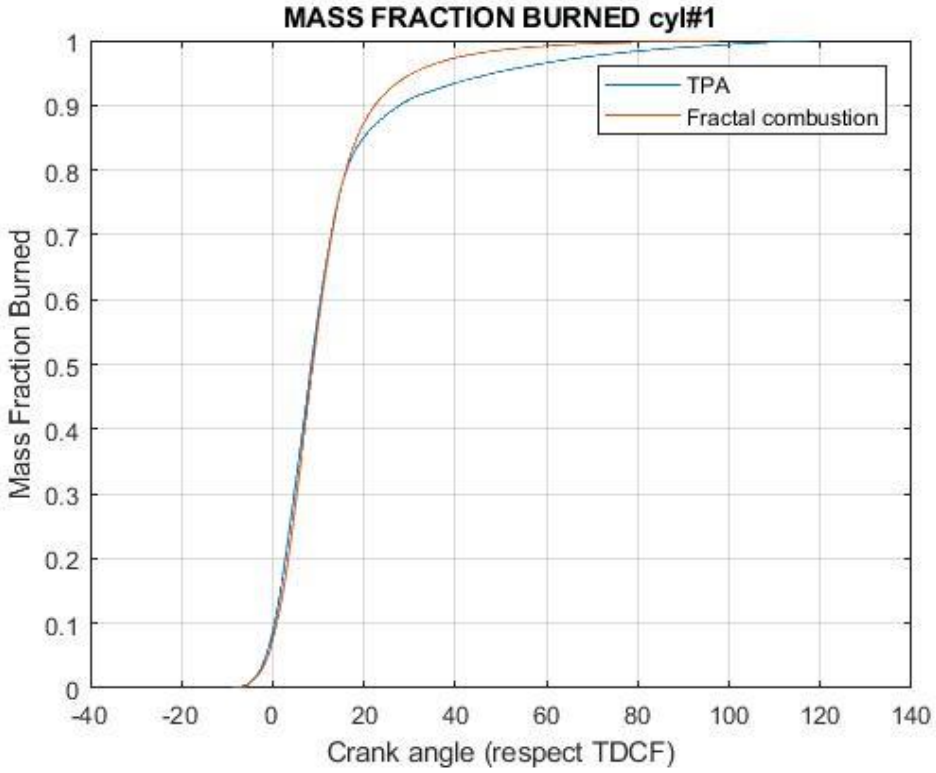

Figure 4.41 Fractal combustion 1981 – mass fraction burnt cyl#1

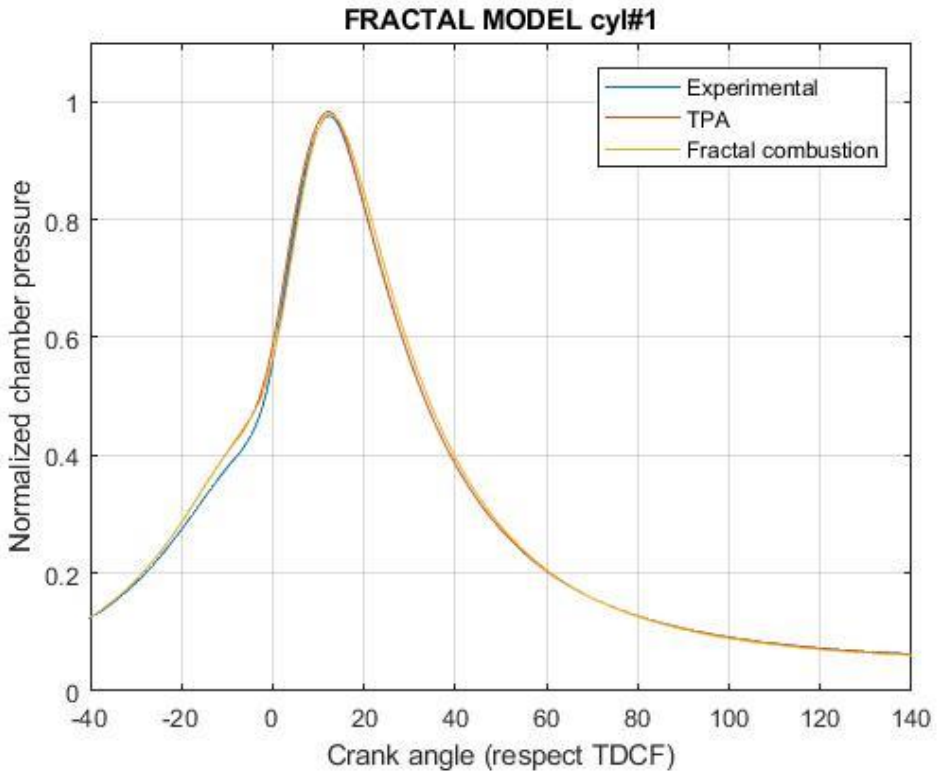

Figure 4.42 Fractal combustion 1982 – pressure cycle cyl#1

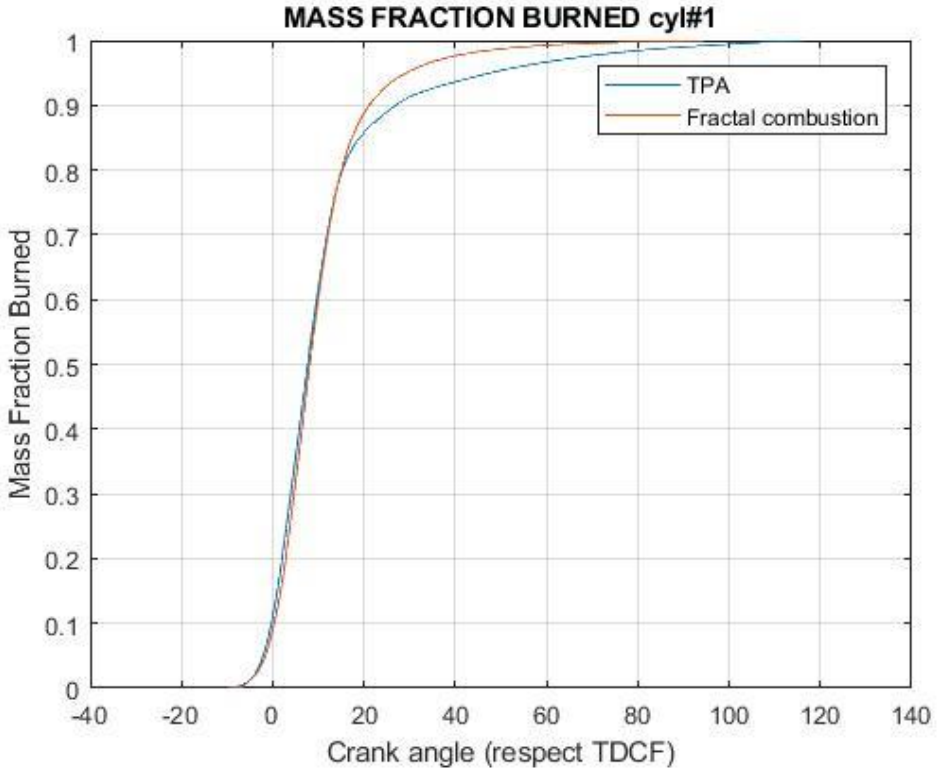

Figure 4.43 Fractal combustion 1982 – mass fraction burnt cyl#1

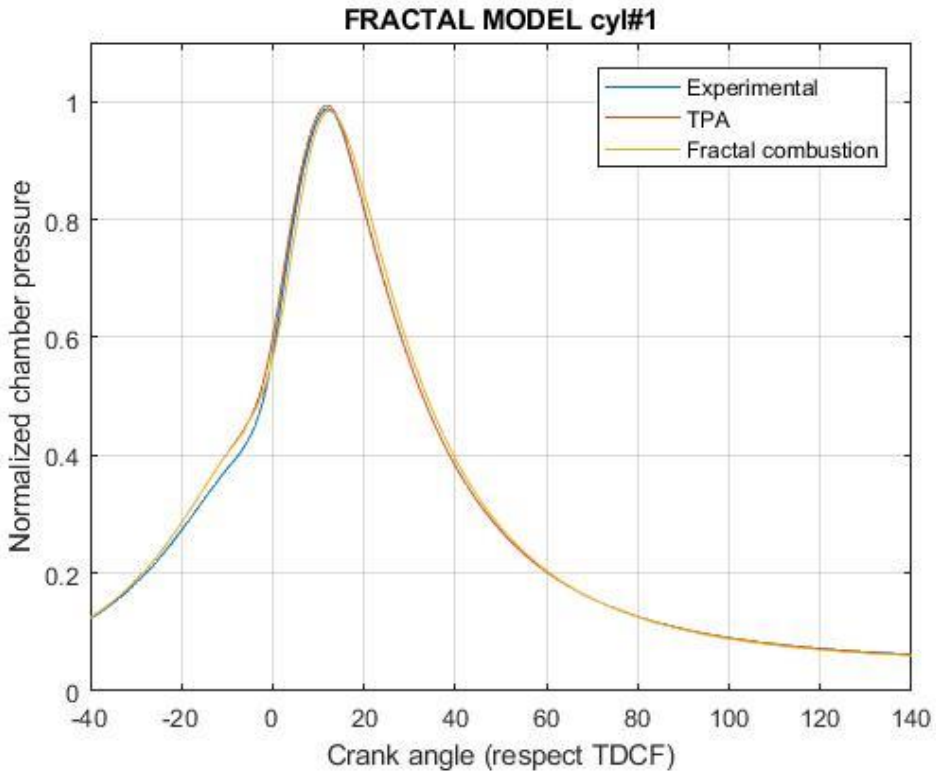

Figure 4.44 Fractal combustion 1983 – pressure cycle cyl#1

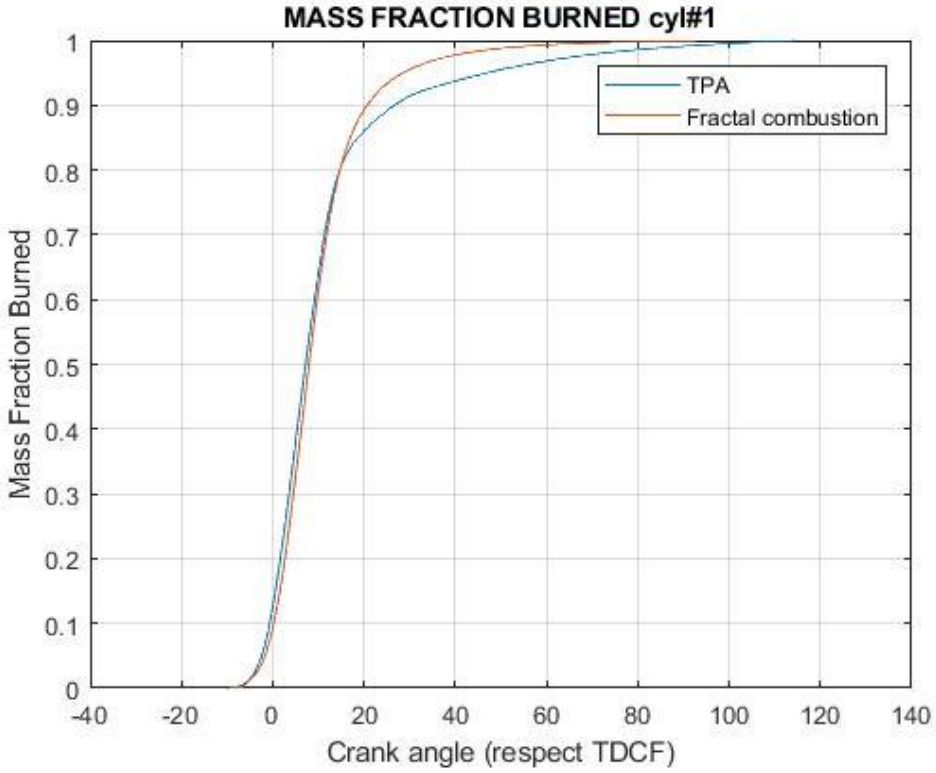

Figure 4.45 Fractal combustion 1983 – mass fraction burnt cyl#1

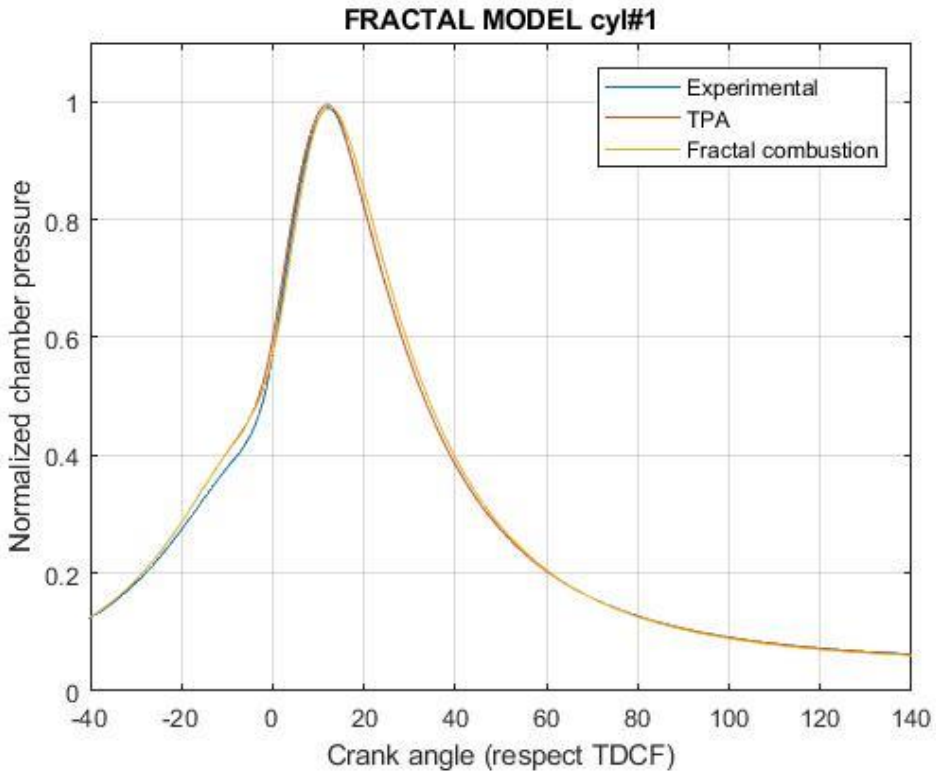

Figure 4.46 Fractal combustion 1985 – pressure cycle cyl#1

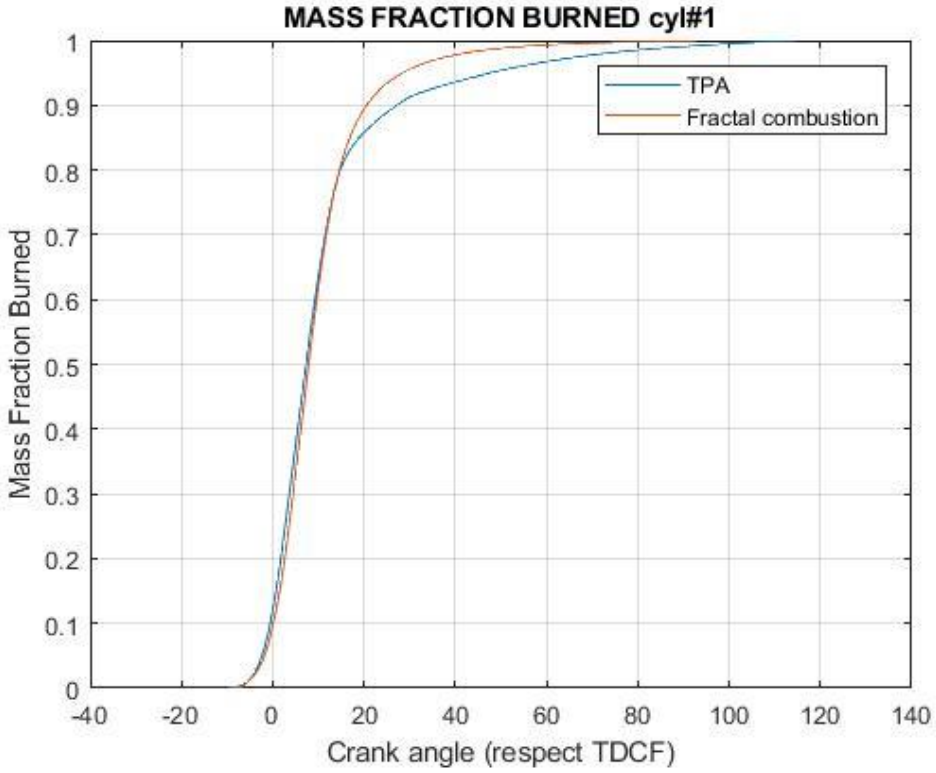

Figure 4.47 Fractal combustion 1985 – mass fraction burnt cyl#1

4.4.3 Cyclical dispersion model – knock tests

Cyclical dispersion is introduced in the simulation model to the parameters $\Delta\theta_{0-1}$ and Cl_0 in order to reproduce PFP dispersion effect. In the following table, obtained results are outlined. For knock tests, this analysis is required in order to be able to simulate and compute knock occurrence.

TEST ID	SPEED [RPM]	P_{MAX} [kPa]	SA [°CA]	CoV_{Cl_0}	$CoV_{\Delta\theta_{0-1}}$	CoV_{PFP} (simulated)	CoV_{PFP} (experimental)
1977	2000	10800	7.00	22.0%	10.0%	4.30%	4.29%
1978	2000	11000	7.59	18.0%	10.0%	3.83%	3.85%
1979	2000	11200	8.16	20.0%	10.0%	3.87%	3.87%
1980	2000	11400	8.60	21.0%	10.0%	3.87%	3.86%
1981	2000	11600	9.14	21.0%	10.0%	3.86%	3.86%
1982	2000	11800	9.72	23.0%	10.0%	4.14%	4.14%
1983	2000	11900	10.01	22.5%	10.0%	4.06%	4.06%
1985	2000	11950	9.93	19.5%	10.0%	3.61%	3.61%

Table 4.19 Fractal model –coefficients of variation values – knock tests

By manual tuning, CoV_{PFP} values are almost perfectly fitted. Observing that obtained values of CoV_{Cl_0} does not show significant variations in the various tests, a common value of 22% has been adopted obtaining the results resumed in the following table and plot.

TEST ID	CoV_{PFP} (CoV_{Cl_0} variable)	CoV_{PFP} (CoV_{Cl_0} fixed 22%)	CoV_{PFP} (experimental)
1977	4.30%	4.30%	4.29%
1978	3.83%	4.31%	3.85%
1979	3.87%	4.11%	3.87%
1980	3.87%	4.00%	3.86%
1981	3.86%	3.99%	3.86%
1982	4.14%	3.97%	4.14%
1983	4.06%	3.98%	4.06%
1985	3.61%	3.94%	3.61%

Table 4.20 Fractal model – CoV_{PFP} approximation 22% - knock tests

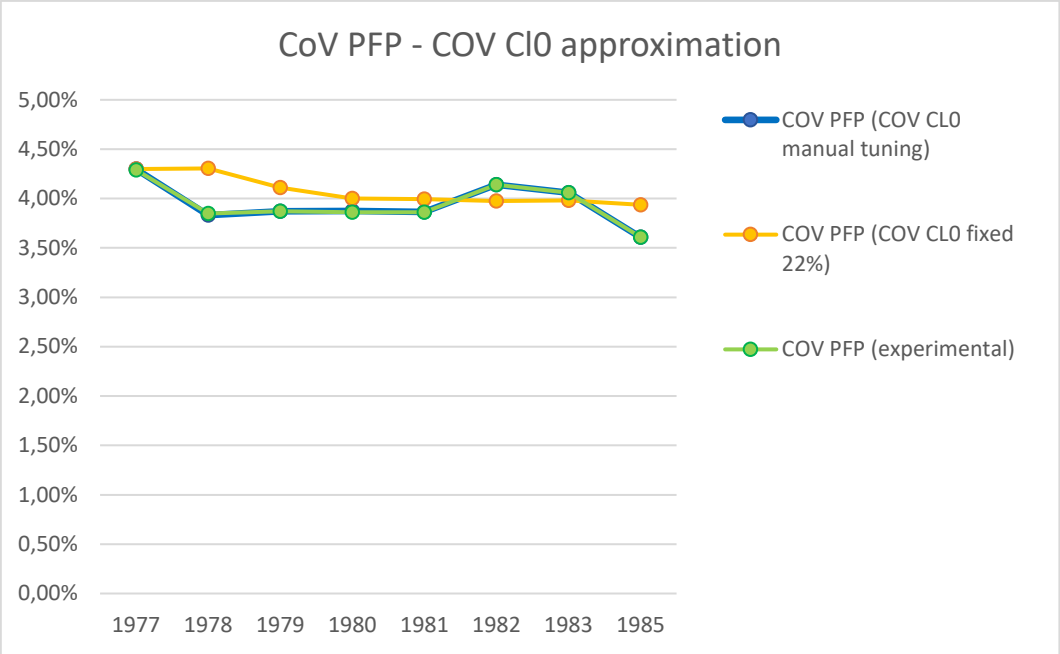

Figure 4.48 Fractal model – CoV_{PFP} approximation 22% - knock tests

As shown by both table and plot, an approximation of the CoV_{Cl_0} value to 22% leads to a maximum estimation error of CoV_{PFP} lower than 0.5%, therefore this value can be accepted.

4.4.4 Knock detection model – knock tests

Knock model has been finally implemented in the GT-Power simulation code including the evaluation of the integral $\int \frac{dt}{\tau} = 1$. τ value, evaluated at each crank angle interval, takes into account instantaneous pressure and temperature values inside the combustion chamber during combustion.

$$\tau = c_1 p^{-c_2} e^{\frac{c_3}{T}}$$

The initial values of calibration parameters c_1, c_2 and c_3 are taken from experimental analyses carried out on the engine of Politecnico di Torino.

Calibration parameter	Value
c_1	0.000935
c_2	1.11
c_3	17767.68

Table 4.21 Knock model calibration parameters – initial values

The first simulations showed inadequacy of the abovementioned values. Parameter c_1 has therefore been calibrated in order to simulate the actual knocking occurrence. The following table and plot represent the tuning work carried out to obtain a suitable value for c_1.

TEST ID	Knocking Cycles ($c_1 = 0.0030$)	Knocking Cycles ($c_1 = 0.0032$)	Knocking Cycles ($c_1 = 0.0028$)	Knocking Cycles ($c_1 = 0.00305$)	Knocking Cycles ($c_1 = 0.00295$)	Knocking Cycles (experimental)
1977	0.00%	0.00%	0.00%	0.00%	0.00%	0.00%
1978	0.00%	0.00%	0.00%	0.00%	0.00%	0.00%
1979	0.00%	0.00%	2.00%	0.00%	0.00%	0.00%
1980	1.00%	0.00%	5.00%	1.00%	2.00%	1.50%
1981	3.00%	0.00%	9.00%	2.00%	5.00%	5.50%
1982	9.00%	2.00%	30.00%	9.00%	11.00%	10.00%
1983	14.00%	6.00%	38.00%	10.00%	20.00%	15.00%
1985	15.00%	5.00%	38.00%	11.00%	21.00%	15.00%

Table 4.22 Knock model -c_1 calibration

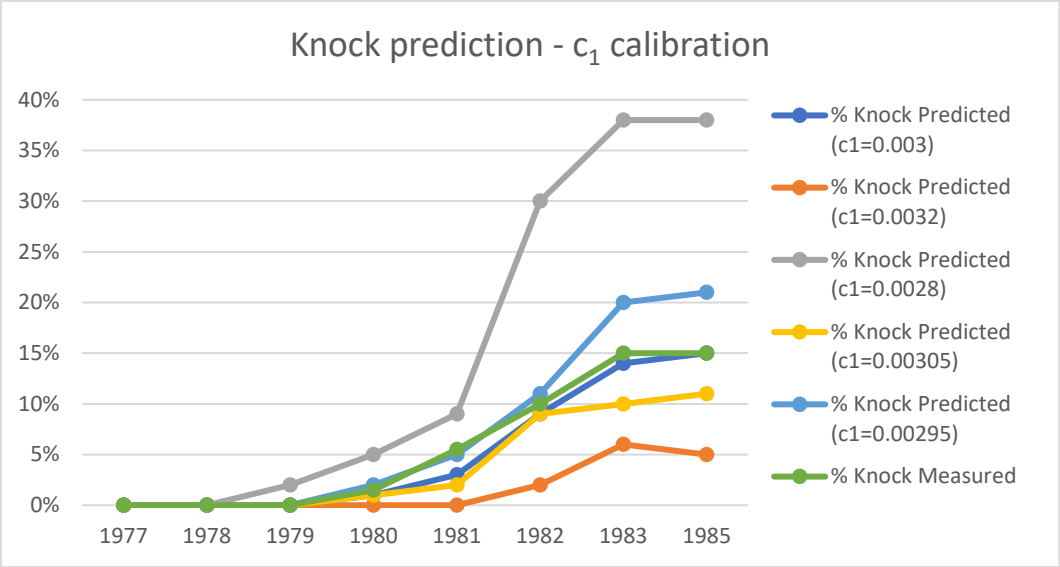

Figure 4.49 Knock model -c_1 calibration

From the previous figure, it is possible to observe that the value of c_1 that best fits experimental data is c_1= 0.00295, at least for tests in which a detonating tendency starts appearing. They are the most important concerning engine calibration; points with higher knock occurrence, around 10% and more, being affected by the autoignition effect (different combustion heat transfer) more and more frequently, cannot be correctly evaluated by this model.

The following table resumes the final parameter values adopted.

Calibration parameter	Value
c_1	0.00295
c_2	1.11
c_3	17767.68

Table 4.23 Knock model calibration parameters – final values

5 Conclusion and future steps

This work of thesis aims at developing and refining a predictive combustion model adapting it to a prototype NG fuelled turbocharged engine, starting from the analysis of experimental data provided by AVL partner.

Special care has been devoted to the characterization of knocking phenomenon, developing both an algorithm able to analyse and correctly interpret actual measurements and a predictive tool capable of simulating in a computing environment the engine operation forecasting its behaviour.

Concerning the model in charge of the analysis of experimental data and knock and ringing phenomena distinction, a more refined calibration is required in order to optimise the algorithm behaviour and correctly interpret cycle nature.

Fractal combustion and cyclical dispersion models instead require the application to a wider spectrum of working points of the engine map, in order to collect more data necessary to develop reliable regression correlations able to forecast parameters values and fully exploit the predictive potential. It is important to remember the strong point of this approach, represented by the involvement of actual physical, geometrical and thermodynamic quantities employed to predict combustion behaviour.

Finally, the application of the presented models to different engine configurations and working conditions is necessary to assess their validation.

6 Figures index

7 Tables index

Bibliography

Baratta, M., Catania, A. E., Spessa, E., & Vassallo, A. (2006). Development and Assessment of a Multizone Combustion Simulation Code for SI Engines Based on a Novel Fractal Model. *SAE*.

Baratta, M., Catania, A., Spessa, E., & Vassallo, A. (2005). Flame Propagation Speed in SI Engines: Modelling and Experimental Assessment. *ASME*.

Blizzard, N., & Keck, J. (1974). Experimental and Theoretical Investigation of Turbulent Burning Model for Internal Combustion Engines. *SAE*.

Catania, A., Misul, D., Spessa, E., & Vassallo, A. (2004). Analysis of Combustion Parameters and Their Relation to Operating Variables and Exhaust Emissions in an Upgraded Multivalve Bi-Fuel CNG SI Engine. *SAE*.

Gulder, O., & Smallwood, G. (1995). Inner Cutoff Scale of Flame Surface Wrinking in Turbulent Premixed Flames. *Combustion and Flame*.

Heywood, J. (1988). *Internal Combustion Engine Foundamentals.*

Mantzaras, J., Felton, P., & Bracco, F. (1989). Fractal and Turbulent Premixed Engine Flames. *Combust. Sci. and Tech.*

Metghalchi, M., & Keck, J. (1982). Burning Velocities of Mixtures of Air with Methanol, Isoctane and Indolene at High Pressure and Temperature. *Combust. Flame*.

Poulos, S., & Heywood, J. (1983). The Effect of Chamber Geometry on Spark-Ignition Engine Combustion. *SAE*.

Acknowledgements

I would like to express my gratitude to my supervisors Daniela Misul and Mirko Baratta, giving me the opportunity to work at this interesting project. Special thanks to Danilo Laurenzano, always helpful and available to clarify all my doubts.

To my family, especially my father and my mother, that always supported me and allowed to undertake and complete this academic path, spurring me whenever I need and giving me the chance to pursue the dreams that I had since I was a child.

To my friends, that I met during these academic years, with whom I have spent moments of study, but mostly of fun.

Finally, last but not least, to Veronica, that knows exactly what I need and when, my reference point, that always helped me to face any difficulty and shared her joy with me.

All these people made me what I am today.